LIQUID CRYSTAL FORMATION IN AQUEOUS SOLUTIONS OF SCHIZOPHYLLAN, A TRIPLE-HELICAL POLYSACCHARIDE

A Doctoral Thesis

by

Kazuo Van

Submitted to the Faculty

of Science, Osaka University

1984

APPROVALS

November, 1984

This thesis is approved
as to style and content
by

藤田博

Member-in-chief

小高忠男

Member

小林雅通

Member

幸本明夫

Member

ACKNOWLEDGMENTS

This work was performed at Fujita's Laboratory of the Department of Macromolecular Science, Osaka University. I thank Professor Hiroshi Fujita, Associate Professor Akio Teramoto, Dr. Takashi Norisuye, and Dr. Yoshiyuki Einaga for their guidance, advice, and encouragement throughout the course of this study. I also thank Dr. Yasuhiro Takahashi of the Department of Macromolecular Science, Osaka University for small-angle X-ray scattering measurements and his valuable comments on the conformation of polysaccharides.

The schizophyllan samples used were provided by Taito Co. to which my thanks are due.

I am indebted to Mr. Takashi Itou and Mr. Toshiaki Asakawa for their contributions to this study. Thanks are extended to all the members of Fujita's Laboratory for their friendship.

伴 和夫

Kazuo Van

November, 1984

CONTENTS

Chapter 1

INTRODUCTION

1-1 Mesomorphic Order and Liquid Crystal

Late in the nineteenth century, Reinitzer and Lehmann[1,2] found a new state of matter having properties between liquid and solid.[3] A substance in this state is as anisotropic as a crystal but has a fluidity comparable to liquids. For this unique nature, it is referred to as a liquid crystal or more properly a mesophase.

Friedel[4] was the first to recognize the liquid crystal as an independent thermodynamic state of matter. On the basis of optical properties, Friedel classified liquid crystals into three major types, i.e., smectics, nematics, and cholesterics, although he regarded cholesterics as a special member of nematics. Nematics and smectics are optically positive, namely, the direction of the largest refractive index coincides with the direction of orientation. On the other hand, cholesterics are optically negative and

exhibit such remarkable optical properties as strong optical rotation and selective reflection of circularly polarized light in a narrow range of wavelength.

Until now many organic compounds capable of forming mesophases, mesogens, have been found.[5,6] The structural feature common to these compounds is that they are geometrically anisotropic, usually long and relatively thin, e.g., rodlike or disklike. The name "liquid crystal" usually refers to a mesophase consisting of highly elongated molecules. When such molecules are chiral, they give a cholesteric liquid crystal.

Alternatively, liquid crystals are classified into thermotropic or lyotropic depending on how they become liquid crystalline. Thus, a thermotropic liquid crystal is obtained by heating a substance and a lyotropic one by dissolving a substance in a certain solvent. As is well known, liquid crystals, mostly of thermotropic type, have already found widespread and still increasing applications in display devices and sensors.[7-9] It is also known that the liquid crystal order, lyotropic and thermotropic, can be found in a variety of biological systems.[10-12]

1-2 Polymer Liquid Crystals

As low molecular weight mesogens do, rigid rodlike polymers form liquid crystals when dissolved in suitable solvents or heated. Synthetic helical polypeptides are typical of such polymers. Indeed, the first systematic study of polymer liquid crystals was performed on synthetic polypeptides by Robinson,[13-16] who found that a solution of a polypeptide, e.g., poly(γ-benzyl L-glutamate) (PBLG), became anisotropic above a certain concentration. The isotropic phase became unstable above another concentration higher than this critical concentration and the mixture became completely anisotropic. Robinson examined the structure and optical properties of the anisotropic phase in great detail and found the phase to be cholesteric. He referred to the critical concentration for the incipience of an anisotropic phase as the A-point and that for the disappearance of an isotropic phase as the B-point, and showed how these critical concentrations varied with the molecular weight of the sample.

This pioneering work has motivated a vast amount

of subsequent work on polymer liquid crystals, both theoretical and experimental. Thus, a variety of mesogenic polymers have been found; those include rodlike particles such as certain viruses and phages,[17-20] and such stiff-chain polymers as nucleic acids,[15] polypeptides,[13-16,21-41] aromatic polyamides,[42-47] aromatic polyesters,[48,49] main-chain heterocyclic polymers,[50,51] polyisocyanates,[52-54] and polysaccharides and their derivatives.[55-67] Polymers with mesogenic side chains also become liquid crystalline under appropriate conditions.[68] In addition to their thermodynamic[13,21,24-30] and optical properties,[32-34, 57,64,66,67] rodlike polymers have called considerable interest because of their interactions with magnetic and electric fields[35-39] and because of their characteristic rheological properties.[21,40,41,45,63,70]

Mesophase-forming polymers are also of practical interest. A typical example is ultra-high modulus fiber Kevlar produced by liquid crystal spinning.[47,71] Various kinds of polymers, e.g., main-chain heterocyclic polymers, thermotropic polyesters, etc., have been developed for more or less similar purposes.[48,58] However, in this thesis, we confine ourselves to a

basic study on rodlike polymers forming lyotropic liquid crystals.

1-3 Theoretical Basis for Liquid Crystal Formation

Onsager[72] was the first to show that molecular asymmetry alone is sufficient to produce a phase transition from isotropic to anisotropic (actually nematic). He dealt with an imperfect gas of cylindrical particles and predicted that the phase boundary concentrations, i.e., the A-point ϕ_A and B-point ϕ_B, should vary with the axial ratio x of the particle as

$$\phi_A \approx 3.3/x, \qquad \phi_B \approx 4.5/x \tag{1.1}$$

Essentially the same theory was developed independently by Ishihara.[73]

The Onsager theory should be used at relatively low concentrations, because it makes use of a free energy equation correct up to the term linear in concentration. Subsequent attempts[74-77] extended the Onsager theory to higher concentration; for example, Cotter used a scaled particle theory. Cotter's theory[76] is exact both at the large and small limits of x.

Using a lattice model, Flory[78] developed a statistical thermodynamic theory for solutions of inpenetrable rods in a solvent. In this theory, each rod is divided into submolecules or segments of the volume equal to that of the solvent, and the volume of the rod relative to that of the solvent is defined as the axial ratio. A rod inclining at an angle ψ to a director is divided into y submolecules, each containing x/y segments (Figure 1.1). Thus, y can be

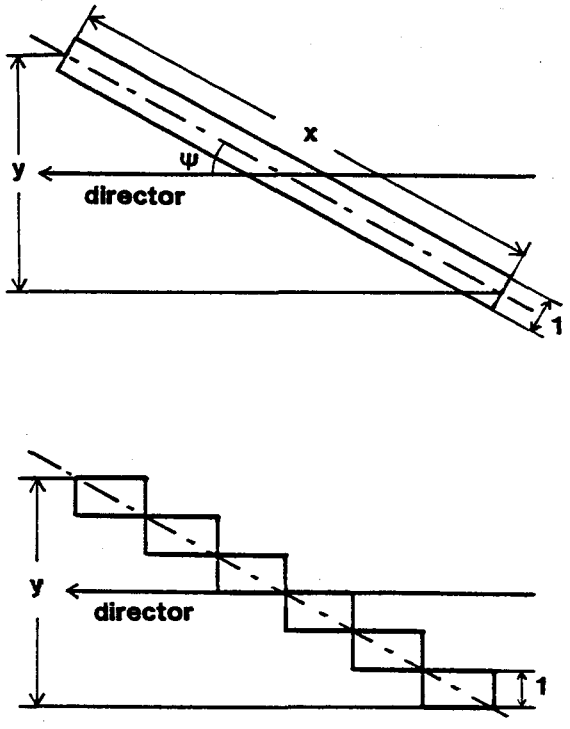

Figure 1.1
Lattice model treatment of a rod inclining at an angle ψ to the director.[78]

regarded as a parameter for the degree of disorientation of the rod and may be referred to as the disorientation index; $y = 1$ for a rod aligned parallel to the director and $y = x$ for a rod oriented randomly. As in the Flory-Huggins theory of flexible polymers, polymer-solvent interactions are taken into account by the interaction parameter χ. The theory predicts that, in the absence of polymer-solvent interaction, the phase boundary concentrations should vary with x approximately as

$$\phi_A \approx 8/x, \qquad \phi_B \approx 12.5/x \tag{1.2}$$

Two attractive features of the Flory theory are the following. First, it gives an exact partition function when all the rods are aligned parallel and hence should be useful at high concentrations. Second, effects of polymer-solvent interaction on phase behavior can be estimated easily by the interaction parameter. Figure 1.2 shows the theoretical phase diagram calculated for $x = 100$, which can be transformed to the temperature-composition phase diagram if χ is given as a function of temperature.[78] Under good-solvent conditions, i.e., for small or negative χ values,

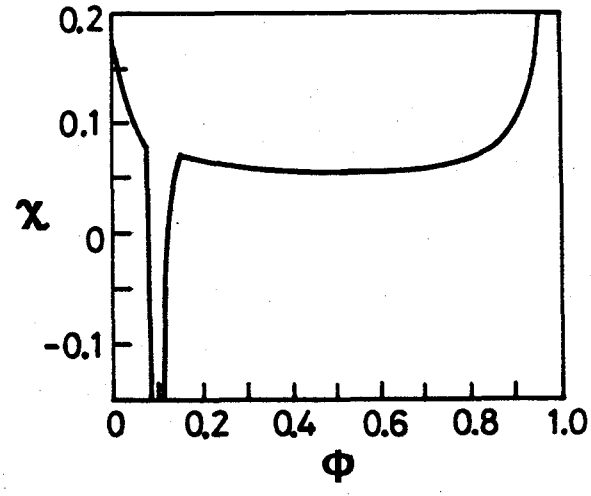

Figure 1.2
Theoretical phase diagram calculated by the Flory theory[78] for the axial ratio x = 100.

the Flory theory gives a narrow biphasic gap separating isotropic and anisotropic regions. When the solvent becomes poorer than a certain limit, the biphasic gap suddenly widens, and the system becomes biphasic almost over the entire composition.

1-4 Comparison of Experimental Data with Theory

As noted in Section 1-2, polyglutamates in certain solvents give cholesteric liquid crystals. Robinson[15] showed that the A- and B-points for PBLG in dioxane and methylene chloride varied approximately linearly with inverse molecular weight, confirming for the first time the prediction of the Flory theory.[29] However, this finding should be taken with reservation, since PBLG in the solvents studied is known to

associate intermolecularly even at high dilution.

Miller and coworkers[21,24,28] investigated PBLG and poly(ε-carbobenzoxy L-lysine) (PCBL) in dimethylformamide (DMF), in which these polymers disperse molecularly at room temperature. Figure 1.3 shows their temperature-composition phase diagram for PBLG, which consists of an almost vertical narrow biphasic gap between isotropic and cholesteric regions

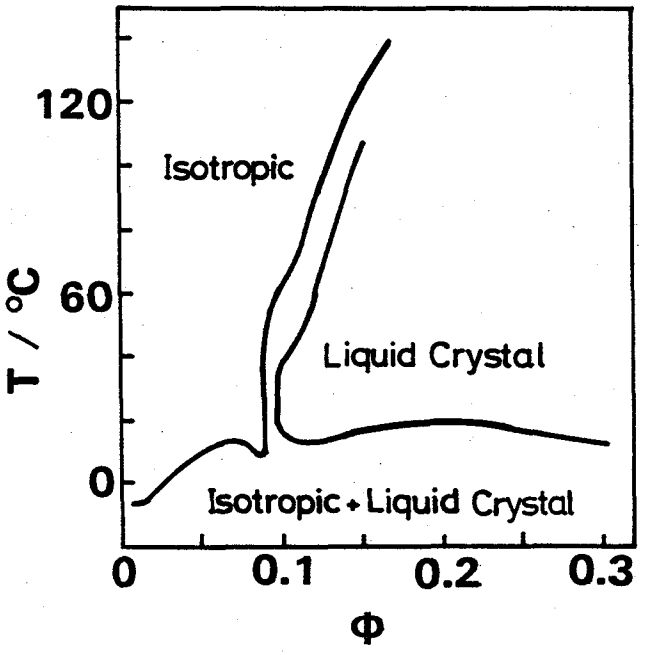

Figure 1.3 Temperature - composition phase diagram for the system PBLG - DMF, obtained by Miller et al.[21]

and a broad biphasic region at lower temperature. This phase diagram is very similar to the theoretical diagram shown in Figure 1.2, substantiating the validity of the Flory prediction.

The dependence of the phase boundary concentrations ϕ_A and ϕ_B on axial ratio x for the PBLG - DMF system was investigated by Miller and coworkers,[23,24] Kubo and Ogino,[26] and Funada et al.[30] It was found that the experimental ϕ_A and ϕ_B were higher and lower than the values predicted by the Flory theory at higher and lower molecular weights, respectively. The former disparity may be attributed to a greater flexibility of longer α-helix, but the latter disparity still finds no reasonable explanation.

Recently, Kubo and Ogino[26] obtained extensive osmotic pressure data for the system PBLG + DMF. At least for lower molecular weights, the osmotic pressure and ϕ_A and ϕ_B data were comparable to the prediction of the Cotter theory,[76] but the data for higher molecular weights were not. As previous authors,[23,24] they attributed the latter to the flexibility of the α-helix. However, dilute solution data show that the PBLG helix should be rigid and

straight except for the highest molecular weight sample examined.[79] Furthermore, Kubo and Ogino found for any samples no discontinuous change in solvent chemical potential to occur in crossing the biphasic gap. This suggests that their samples were considerably polydisperse in molecular weight.

Similar but less extensive studies on phase behavior have been reported for other polymer-solvent systems.[45-47] In many cases, the polymers used were poorly soluble in ordinary solvents, making it difficult to carry out molecular characterization. In addition to poor solubility and, in some cases, unknown rigidity, no imformation about polydispersity has been given on the samples in most cases. This point is very crucial, because polydispersity should have an appreciable effect on phase separation behavior.[80-83] Thus, we must conclude that the existing data for isotropic-liquid crystal phase equilibrium are not sufficient to test theoretical predictions.

1-5 Scope and Purposes of the Present Thesis

Because of the unsatisfactory experimental

situations as mentioned above, it is significant to carry out a study on another system better defined than the previously treated ones. In this doctral work, we chose the system schizophyllan + water for the reason given below.

Schizophyllan, a water-soluble polysaccharide produced by a fungus schizophyllum commune, consists of a repeating unit shown in Figure 1.4. Norisuye et al.[84] found that in aqueous solution schizophyllan exists as a rigid helical trimer. They showed from dilute solution studies that this trimer can be well modeled by a wormlike cylinder with a large persistent length of 200 nm.[85,86] Solubility of schizophyllan in aqueous media facilitates various physical

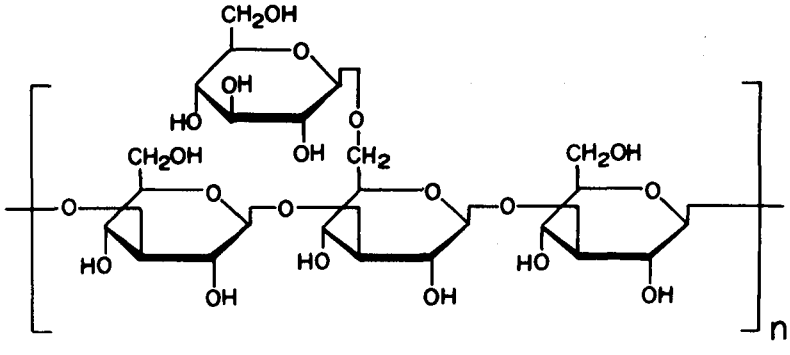

Figure 1.4 Repeat unit of schizophyllan.

measurements. Further, samples of this polymer are available in a wide range of molecular weight. Thus, we considered schizophyllan to be pertinent for investigating concentrated solutions of rodlike polymers.

Because of its high rigidity comparable to collagen, which is more rigid than any other stiff-chain polymers known to date, schizophyllan in aqueous solutions should form a liquid crystal at concentrations above a certain value. This polymer is optically active, and hence its triple helix should have a definite sense. Thus, its liquid crystal, if formed, should be cholesteric. As far as we aware, the mesophase formation of a rodlike polysaccharides is as yet not reported.

This thesis was undertaken mainly to elucidate optical and thermodynamic properties including the formation of a mesophase of rodlike polymer solutions, using aqueous schizophyllan as a model system. The most crucial question was whether aqueous schizophyllan gives a liquid crystal under relevant conditions. Fortunately, the answer to this question was "yes" as will be shown in Chapter 3.

Chapter 2 describes the molecular characterization of schizophyllan samples and the experimental procedures employed in the present study. Chapter 3 presents the experimental results leading to the conclusion that a cholesteric liquid crystal is formed from aqueous schizophyllan. Chapter 4 discusses extraordinary optical rotatory dispersion of the schizophyllan liquid crystal; this property is common to cholesterics. Chapter 5 is concerned with the excess chemical potential of water in aqueous schizophyllan. The data obtained are compared with theoretical predictions for solutions of rodlike polymers. Chapter 6 describes isotropic-liquid crystal phase diagrams for aqueous schizophyllan and their comparisons with relevant theories. Chapter 7 describes the results from a preliminary examination of the optical properties of an isotropic solution near the isotropic-biphasic boundary. Chapter 8 summarizes the results and conclusions obtained in the present study.

Chapter 2

EXPERIMENTAL DETAILS

2-1 Schizophyllan Samples

Sonicated schizophyllan samples supplied by Taito Co. were purified or separated to many fractions from aqueous solutions with methanol or acetone as the precipitant. Eight fractions were chosen and designated as SPG-01, E-4, SPG-3', U-1, R23, D-4, V-1, and D40. Their molecular weights were determined from sedimentation equilibrium and viscosity measurements on dilute aqueous solutions at 25°C; the intrinsic viscosity [η] - molecular weight relationship of Yanaki et al.[85] was used. The results are summarized in Table 2.1, where M_v, M_w, and M_z are the viscosity-average, weight-average, and z-average molecular weights, respectively, and A_2 is the second virial coefficient. The values of M_z/M_w for D40, R23, and SPG-3' are fairly close to unity, indicating that these samples are moderately narrow in molecular weight distribution.

Table 2.1

Molecular Characterization of the Schizophyllan Samples

Samples	$[\eta]$ / $100\ cm^3 g^{-1}$	M_v / $10^4\ g\ mol^{-1}$	M_w / $10^4\ g\ mol^{-1}$	M_z/M_w	A_2 / $10^{-4}\ cm^3\ mol\ g^{-2}$
SPG-01	0.41_6	10.5	-	-	-
E-4	0.85_0	15.0	-	-	-
SPG-3'	0.90_0	15.6	15.9	1.2	0.9_6
U-1	0.97_0	17.0	-	-	-
R23	1.7_3	23.0	24.5	1.2	0.9_0
D-4	4.0_0	38.0	-	-	-
V-1	4.3_1	40.0	-	-	-
D40	4.7_0	42.0	47.8	1.2	1.0_5

Samples U-1, R23, D-4, V-1, and D40 were used for microscopy and/or laser light diffraction, U-1 and V-1 for optical rotatory dispersion (ORD) measurement, D40, SPG-3', and R23 for thermodynamic measurement, and D40 for phase separation experiment. Sample R23 was used to examine optical properties near the A-point, and E-4 and SPG-01 were used for refractive

index and density measurements, respectively.

2-2 Solution Preparation

A known amount of a schizophyllan sample was dried in vacuo overnight and mixed with water in a stoppered flask or a small weighing bottle (except for phase separation measurement) or a calibrated glass tube (phase separation measurement, Chapter 6). The mixture became transparent within two days. Dissolution was ensured by slowly rotating the container or by stirring the mixture by a magnetic bar.

In most cases, the polymer weight fraction w was determined gravimetrically. The polymer mass concentration c (g cm^{-3}) was calculated from w and the specific volume v (cm^3 g^{-1}) of aqueous schizophyllan solutions at 25°C. The polymer volume fraction ϕ was calculated from w by

$$\phi = wv_p/[wv_p + (1 - w)v_0] \qquad (2.1)$$

where v_p is the partial specific volume of schizophyllan in water at infinite dilution (0.619 cm^3 g^{-1})[84] and v_0 is the specific volume of water at 25°C.

2-3 Microscopy and Laser Light Diffraction

2-3-1 Experimental Procedures

Polarizing light microscopic observations were performed on a Union Mec-3 microscope equipped with a thermostatting cell holder.

Laser light diffraction was performed on an apparatus schematically shown in Figure 2.1. A glass cell was placed in the cell holder fixed on the stage of a traveling microscope. Thus, the cell was movable along the direction of laser beam and its position could be determined as accurately as $\pm$ 0.002 cm. Diffraction patterns projected on a screen were measured by another traveling microscope.

Drum-shaped glass cells (diameter = 10 mm, thickness = 1 or 2 mm) with a thin inlet tube were used for both microscopy and laser light diffraction. A cell was filled with an appropriate volume of the solution and sealed at the inlet tube. Magnification was determined by photographing a microscope scale.

2-3-2 Analysis of Diffraction Data

Let a solution consist of a system of diffraction

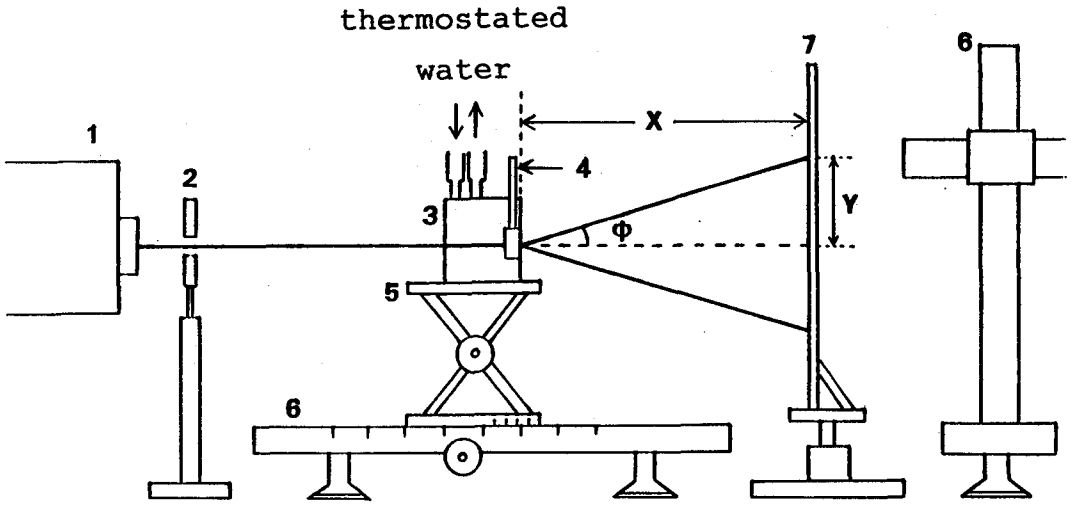

1. He-Ne laser
2. slit
3. cell holder
4. drum-shaped cell
5. stage of a traveling microscope
6. traveling microscope
7. screen

Figure 2.1 Arrangement of parts in the apparatus for laser light diffraction measurements.

gratings which have a constant spacing S but are randomly oriented. When this solution is illuminated by laser light, a diffraction ring (or rings) may be projected on the screen. The spacing S is related to the diffraction angle 2θ in the solution by the Bragg equation

$$2S\sin\theta = \lambda_0/n \qquad (2.2)$$

where λ_0 is the wavelength of light in vacuo and n the refractive index of the solution.[13] As shown in Appendix, S is related to the angle ϕ between the direction of incident light and that of diffracted light in air by

$$S = \lambda_0 \cos \theta / \sin \phi \qquad (2.3)$$

with

$$\cos \theta = \cos[(1/2)\sin^{-1}(n^{-1}\sin \phi)] \qquad (2.4)$$

The angle ϕ can be determined from the distance x between the screen and the outer cell wall and the radius y of the ring using the relation (Figure 2.4)

$$\tan \phi = (y_2 - y_1)/(x_2 - x_1) \qquad (2.5)$$

where y_1 and y_2 are the y values at different cell positions, x_1 and x_2, respectively. The correction factor cos θ given in Eq. (2.4) is not very different from unity nor sensitive to n. Therefore, in actual application to aqueous schizophyllan solutions, n was

assumed to be 1.35.

2-4 Optical Rotatory Dispersion

Optical rotatory dispersion measurement was made on a JASCO Model ORD/UV-5 spectropolarimeter in the range of wavelength between 210 and 600 nm. Glass cells were used down to 300 nm, whereas quartz ones were used down to 210 nm. Quartz cells 1 and 20 mm thick were used for isotropic solutions.

Quartz and glass cells to study birefringent solutions were constructed as follows. A thin plastic film was sandwiched between two slide glass plates somewhat wider than the film. The longer edges of the plates were sealed with a quick adhesive. About one hour later, the film was pulled out, leaving a thin cavity to be used as the solution compartment. The cell thickness d was adjusted by changing the film thickness. Thicker cells were constructed by binding two plates with strips of Scotch tape; d was adjusted by the number of strips placed. The cells constructed in these ways, empty or filled with water, showed negligible optical rotation, and the thickness of each cell was determined to within an accuracy of

± 2 μm. The cells were filled with solutions under reduced pressure and sealed at their ends with an adhesive.

2-5 Refractive Index and Density

Refractive indices n for light of wavelengths 436 and 546 nm were measured on aqueous schizophyllan at polymer concentrations up to 15 wt% at 25°C. A Bausch & Lomb precision sugar refractometer was used.

The values of n obtained are plotted against w in Figure 2.2, where the solid curves fit the data points for the respective wavelengths. Because of the difficulty in handling highly viscous solutions and a limited amount of the sample available, no sufficient data were obtained to determine the n vs. w relationship accurately. Therefore, an equation for n was determined in such a way that it gives an initial slope consistent with the literature specific refractive index increment at infinite dilution[84] and a reasonable n value at w = 1, i.e., for the pure polymer.[87] The resulting equations are

$$n = 1.3339 + 0.1416w + 0.123w^2 - 0.03124w^3 \quad (546\ nm) \quad (2.6)$$

$$n = 1.3397 + 0.1446w + 0.115w^2 - 0.02430w^3 \quad (436\ nm) \quad (2.7)$$

Densities of aqueous schizophyllan at different

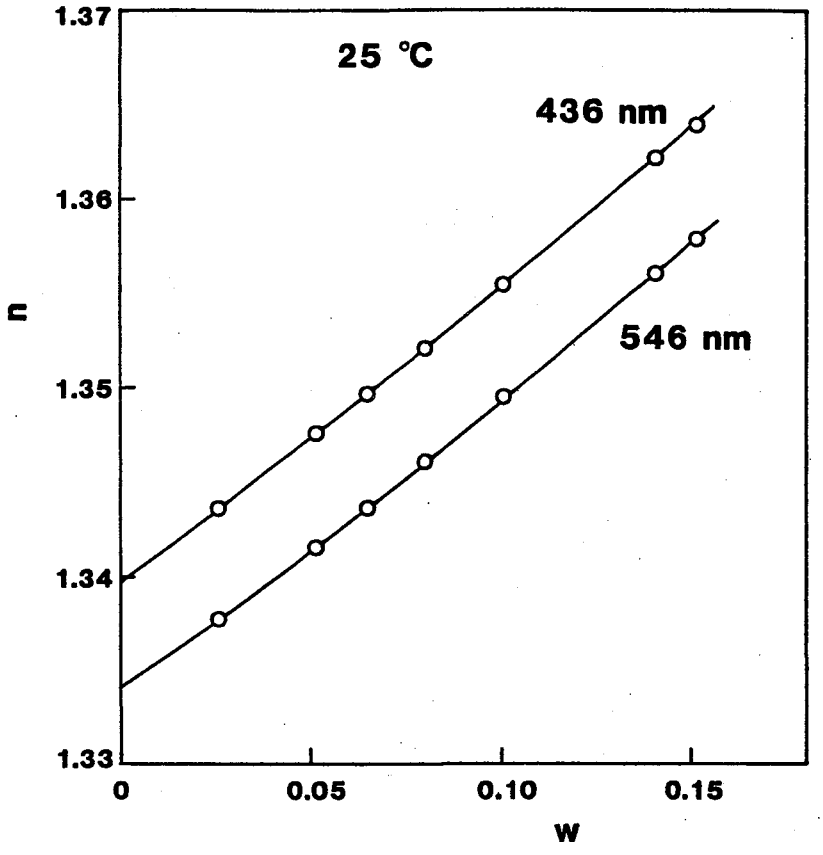

Figure 2.2 Concentration dependence of refractuve indices n of schizophyllan solutions for 436 and 546 nm at 25°C; solid lines, calculated from Eq. (2.6) and (2.7); w, the weight fraction of the polymer.

polymer concentrations at 25°C were measured on a Lipkin-Davison type pycnometer of 5 cm^3 capacity up to 9.5 wt% of the polymer. The data for the specific volume v of the isotropic solutions were fitted by the equation (Figure 2.3)

$$v = 1.003 - 0.384w + 0.03w^2 \qquad (2.8)$$

This was determined by the same method as used in

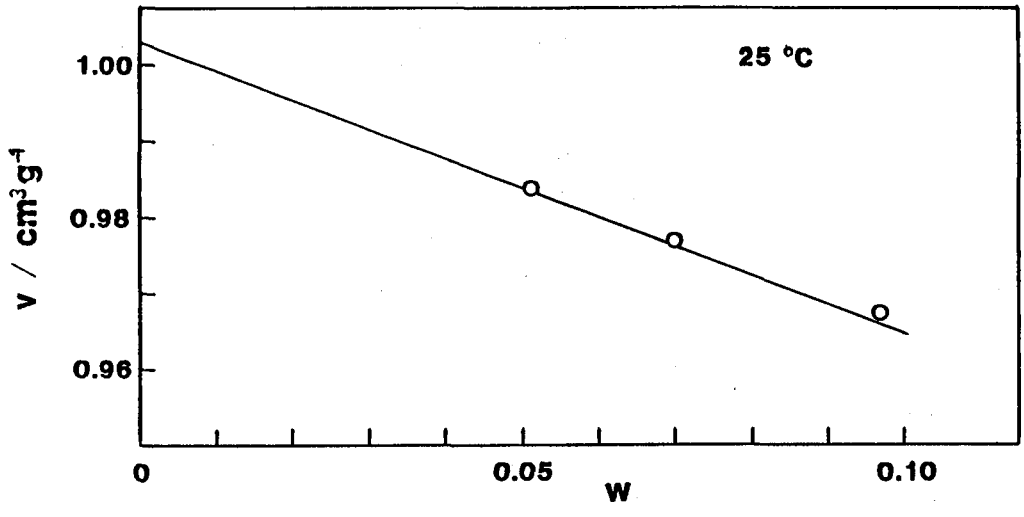

Figure 2.3 Concentration dependence of the specific volume v of schizophyllan solutions at 25°C; solid line, calculated from Eq. (2.8).

deriving Eq. (2.6) and (2.7).

2.6 Light Scattering

2-6-1 Measurement

A Fica 50 automatic photogoniometer was used with cylindrical cells of 1.8 cm in diameter. Intensities of scattered light were measured for vertically polarized incident light of 546 and 436 nm wavelengths at scattering angles θ between 30 and 150°. An appropriate neutral density filter was used to attenuate strong 436 nm intensities. The transmittance of the filter was determined from the ratio of the 90° scattering intensities measured with and without it on schizophyllan solutions or a polystyrene-xylene solution.

In most cases, the intensity $I_{\theta,Uv}$ of scattered light for vertically polarized incident light was measured with no analyzer. The reduced scattering intensity R_θ (= $R_{\theta,Uv}$) was calculated from $I_{\theta,Uv}$ by

$$R_\theta = \psi I_{\theta,Uv} n^2 \qquad (2.9)$$

The calibration constant Ψ for the photogoniometer was determined with benzene at 25°C, with the Rayleigh ratio[88] assumed to be 46.5×10^{-6} cm^{-1} at 436 nm and 16.1×10^{-6} cm^{-1} at 546 nm, and the depolarization determined by Yu's method.[89]

2-6-2 Optical Purification

Optical purification included in order purification of a given sample, preparation of a concentrated solution, and filteration followed by centrifugation. Conventional procedures for dilute solutions would have had a large loss of the solution because of its high viscosity. Hence, light scattering cells were directly subjected to centrifugation. The cells used were about 1.8 cm in diameter, and the minimum volume of the filling solution was about 3 cm^3.

Satisfactory optical purification of the solutions of sample R23 could be made as follows. A necessary amount of the sample was dissolved in water at a concentration of about 1 wt%, filtered through a millipore filter GSWPO 2500 of pore size 0.22 μm, and freeze-dried. Its concentrated solution was passed

through the same filter into a light scattering cell, and centrifuged at about 3000 times the gravity for 15 - 20 min, using Sorvall RC2-B centrifuge.

2-6-3 Optical Anisotropy

Optical anisotropy was estimated from the ratio of $I_{90,Hv}$ to $I_{90,Vv}$, where $I_{90,Hv}$ is the scattering intensity for vertically polarized light measured with an analyzer set in the horizontal direction and $I_{90,Vv}$, that measured with an analyzer set in the vertical direction.

The optical anisotropy of aqueous schizophyllan increased with increasing concentration, reaching 0.015 at w = 0.1316. When estimated by the method applied to dilute solutions, errors in the determination of R_0 due to optical anisotropy were less than 4 %. However, the data for R_0 were not corrected for this effect.

2-6-4 Concentration Determination

The concentrated solution used for light scattering measurements was diluted with water and subjected to a refractive index increment measurement

at 25°C by using a modified Schulz-Cantow differential refractometer. The polymer mass concentration was determined from the excess refractive indices for 546 and 436 nm using the specific refractive index increments: 0.1416 $cm^3\ g^{-1}$ for 546 nm and 0.1446 $cm^3\ g^{-1}$ for 436 nm.[84] The polymer weight fraction of the original solution was calculated from the average of the determinations at the two wavelengths.

2-7 Centrifugation

2-7-1 Sedimentation Equilibrium Measurement on Isotropic Solutions

Sedimentation equilibrium measurements on isotropic schizophyllan solutions were made at 25°C, using a Beckmann-Spinco Model E ultracentrifuge equipped with a schlieren optical system and a Kel-F 12 mm or an Epon 30 mm double-sector cell. The solution column was adjusted to a length between 0.7 and 1.5 mm. The rotor speeds ranged 3000 - 4000 rpm.

2-7-2 Sedimentation Equilibrium Measurement on Biphasic Solutions

Sedimentation equilibrium measurements on schizophyllan solutions in the biphasic region were made as follows. An appropriate volume of a schizophyllan solution was placed in a Kel-F cell, and the cell assembly was kept at 30°C at least for two days to effect phase separation. The cell assembly was then loaded onto a J-rotor heated at 30°C and centrifuged at a rotor speed between 2000 and 5600 rpm. The phase separation was monitored by a schlieren optical system. The length of the solution column was adjusted to 1.5 - 4.3 mm.

2-7-3 Phase Separation

A biphasic solution was prepared in a calibrated glass tube by mixing appropriate amounts of a sample and water. The mixture was stirred for several days by a magnetic bar in an air bath thermostated at 25°C. Then, the tube was left standing for several days in the air bath without stirring at the same temperature. Finally, the tube was centrifuged at a rotor speed of 2500 or 3000 rpm at 25°C for 35 - 45 h, with occasional intermissions, by using a Hitachi 65P-7 automatic preparative ultracentrifuge with a RPS 27-2 rotor.

The volume of each separated phase was determined from the length of the phase, and then each phase was diluted with water to determine its w and M_v. The method described in the previous section was used for the determination of w.

Appendix

Light traveling through a solution is diffracted when the Bragg condition Eq. (2.2) is satisfied.[13] Since both the incident and diffracted beams are refracted at interfaces between layers with different refractive indices, the direction of the diffracted beam in the solution is not always the same as that in air. This refraction effect must be considered to deduce correct θ from experimentally obtainable data. Stein and Keane[90] developed a method for correcting light scattering from thin films for a similar refraction effect. Their method was applied to our system by noticing that our system is not a single layer like a film but consists of three layers, i.e., two glass walls and a cholesteric solution.

Correction for Refraction

Consider a cell consisting of two parallel glass walls, each with a thickness ε and a refractive index n' (Figure 2.4). Let a light beam be incident into the cell perpendicularly to its walls. The incident beam is diffracted at point M in the solution to the

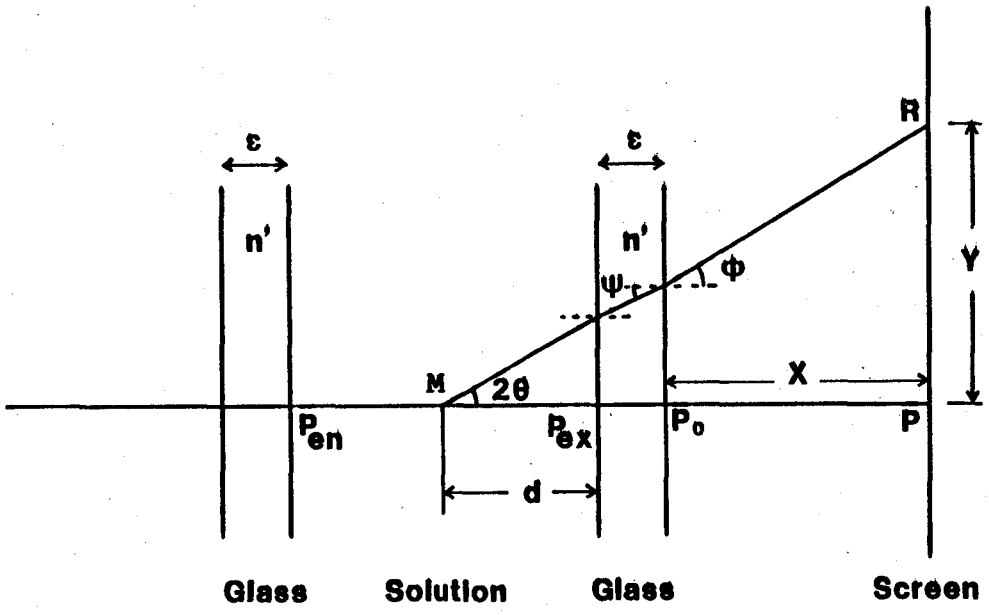

Figure 2.4 Propagation of light in a solution sandwiched between glass walls, each having thickness ε and refractive index n'.

direction making an angle 2θ with its direction. It is then refracted at the solution-glass and glass-air interfaces and reaches point R on the screen, which is placed normal to the incident beam at point P. The distance between P and the outer cell wall P_0 is denoted by x. Denoting the incidence and refraction angles at the glass-air interface by ψ and φ, respectively, we find

$$\sin 2\theta = n^{-1}\sin \phi \qquad (A.1)$$

Substitution of this equation into Eq. (2.2) gives Eq. (2.3).

The angle ϕ is expressed in terms of x and the distance y between points R and P (i.e., the radius of the diffraction ring) as

$$\tan \phi = (1/x)(y - \delta) \qquad (A.2)$$

with

$$\delta = d\tan 2\theta + \varepsilon\tan \psi \qquad (A.3)$$

where d is the distance between point M and the inner cell wall P_{ex} at the exit end. Thus, ϕ can be evaluated if y, δ, and x are determined, though accurate determination of these values is not always easy.

If the cell is moved in the direction of the incident beam to two different positions $x = x_i$ and $y = y_i$ (i = 1,2), tan ϕ for either of these cell

positions is given by Eq. (A.2), in which x and y are replaced by x_i and y_i, respectively. Eliminating from the resulting two equations under the assumption that d is the same for both cell positions (see below for this assumption), we obtain Eq. (2.5). This equation may be preferred to Eq. (A.2), because the distances $(y_2 - y_1)$ and $(x_2 - x_1)$ may be determined more accurately than the absolute values of y, x, and δ.

Uncertainty due to the Finite Cell Thickness

Since the cell has a finite thickness d_0, the position R varies with the point in the solution at which the incident beam is diffracted. This effect gives rise to a finite breadth in the diffraction ring, making the estimation of y inaccurate. Let y_{en} and y_{ex} be the y values for the beams diffracted from the two extreme positions, i.e., the entrance P_{en} and exit P_{ex} of the cell (Figure 2.4), respectively. Then, we have

$$\begin{aligned} \tan \phi &= (y_{en} - d_0 \tan 2\theta - \varepsilon \tan \psi)/x \\ &= (y_{ex} - \varepsilon \tan \psi)/x \end{aligned} \qquad \text{(A.4)}$$

which gives

$$y_{en} - y_{ex} = d_0 \tan 2\theta \qquad (A.5)$$

If y_{en} is used instead of the "correct" value y_{ex} in the second of Eq. (A.4), an apparent ϕ value, ϕ', is obtained, which is related to ϕ by

$$\tan \phi' = [1 + (d_0/x)\tan 2\theta/\tan \phi]\tan \phi \qquad (A.6)$$

The correction term $d_0 \tan 2\theta/(x \tan \psi)$ increases as either x or ϕ or both decrease; note that $\tan 2\theta/\tan \phi$ increases from zero to $1/n$ as ϕ decreases from $\pi/2$ to zero. However, even for a set of parameters such as $x = 40$ mm, $\phi \sim 0$, $d_0 = 2$ mm, and $n = 1.4$, this correction term is only 0.036, and hence $\tan \phi'$ can be equated to $\tan \phi$ with an error less than 3.7 %.

Oblique Incidence

Stein and Keane[90] derived an equation describing the refraction effect on light scattering from thin films. It can be shown that their equation is applicable to our system as well, although our system

is not a single layer but a solution sandwiched between two glass plates. For an oblique incidence angle α, it can be written in our notation as

$$\sin(\phi + \alpha) = n\sin[2\theta + \sin^{-1}(n^{-1}\sin\alpha)] \quad (A.7)$$

where 2θ and ϕ are measured anticlockwise from the direction of the undiffracted beam. This equation reduces to Eq. (A.1) for normal incidence, i.e., $\alpha = 0$.

According to Eq. (A.7), ϕ is an increasing function of α for a given value of θ, indicating that the apparent S value estimated by using Eq. (A.1) should decrease with increasing α. In usual cases where α is as small as 5^{o}, the estimated S is substantially equal to the correct value. It should be noted that the finite thickness of the cell walls has no consequence in any of the final expressions Eq. (2.3), (2.5), and (A.7).

Chapter 3

LIQUID CRYSTAL FORMATION IN AQUEOUS SOLUTION

3-1 Introduction

Schizophyllan in aqueous media exists as a rodlike triple helix.[84-86] Therefore, it may be expected that aqueous solutions of schizophyllan form a mesophase above a certain critical concentration. Since schizophyllan is optically active in water, its triple helix should have a definite sense. Thus, it follows that the mesophase, if formed, may be cholesteric.

Those typical optical properties exhibited by cholesterics are as follows: Cholesterics (1) are birefringent, (2) exhibit fingerprint patterns with characteristic textures, and (3) have a very strong optical rotatory power. (2) and (3) distinguish cholesterics from nematics and smectics, and arise from a multi-layer structure in which molecules in each of the layers are parallel and the directors in

successive layers differ by a constant angle.[93,94]

In the present study, concentrated aqueous solutions of schizophyllan were investigated by microscopy, laser light diffraction, and optical rotatory dispersion to comfirm whether the above expectation was true. In this chapter, the results obtained are described in detail and discussed.

3-2 Results

3-2-1 Microscopic Observation

Aqueous solutions of schizophyllan in drum-shaped cells were observed between crossed polars. At low concentrations, the solutions looked dark and were found to be isotropic. Above a certain concentration, however, they became birefringent and showed complicated patterns, being bright, dark, and various color. After the cell was kept at 30°C for several weeks, alternate bright and dark lines spread over the entire area of the cell.

Typical photographs of the birefringent solutions are shown in Figure 3.1. In panel (a) of Figure 3.1, fine parallel lines run along the cell wall in its neighbor, but in various directions in the central

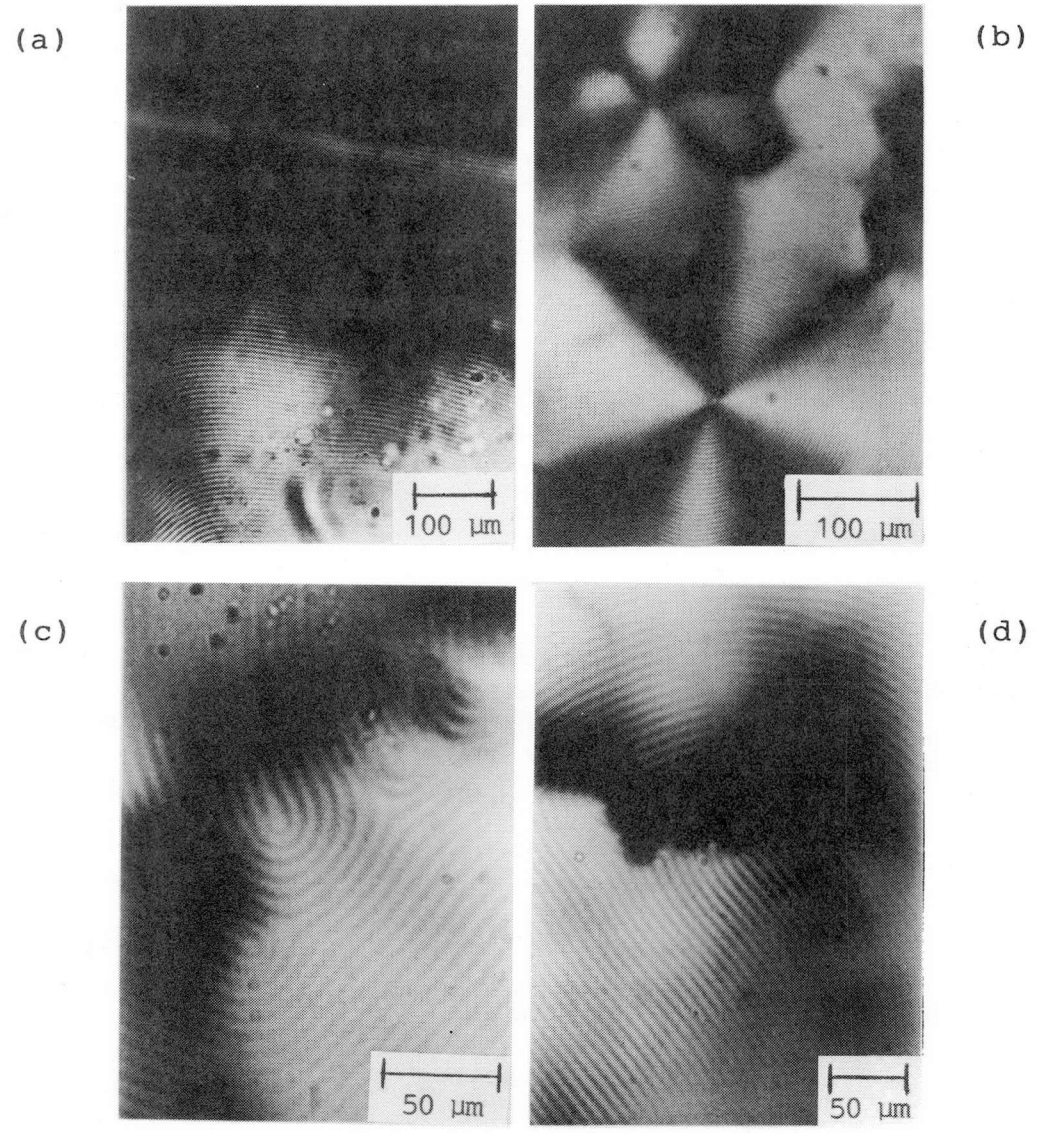

Figure 3.1 Aqueous solutions of schizophyllan viewed between crossed polars. (a), (c), and (d), sample D40, w = 0.127; (b), sample D-4, w = 0.183.

area. In some cases, focal conic patterns as shown in panel (b) of Figure 3.1 were observed. Different microscopic patterns were observed when the microscope was focused at different depths of the solution. These observations are summarized as follows.

(1) There are wide areas where parallel lines are seen.

(2) When the objective is focused at a fixed depth, the parallel lines curve and disappear at some points.

(3) Patterns with characteristic disclinations are observed. For example, panels (c) and (d) of Figure 3.1 contain patterns resembling closely λ^+ or λ^- disclinations frequently observed in cholesterics (see Appendix for disclination).[93-96]

In a cell thinner than 100 μm, a liquid crystal solution showed no birefringence and was almost dark between crossed polars; as exemplified by Figure 3.2, where white streaks (or threads) can be seen in the dark background. In most cases, these streaks consisted of bundles of alternating bright and dark parallel lines, i.e., fingerprint patterns. As seen in Figure 3.2, in each streak, the parallel

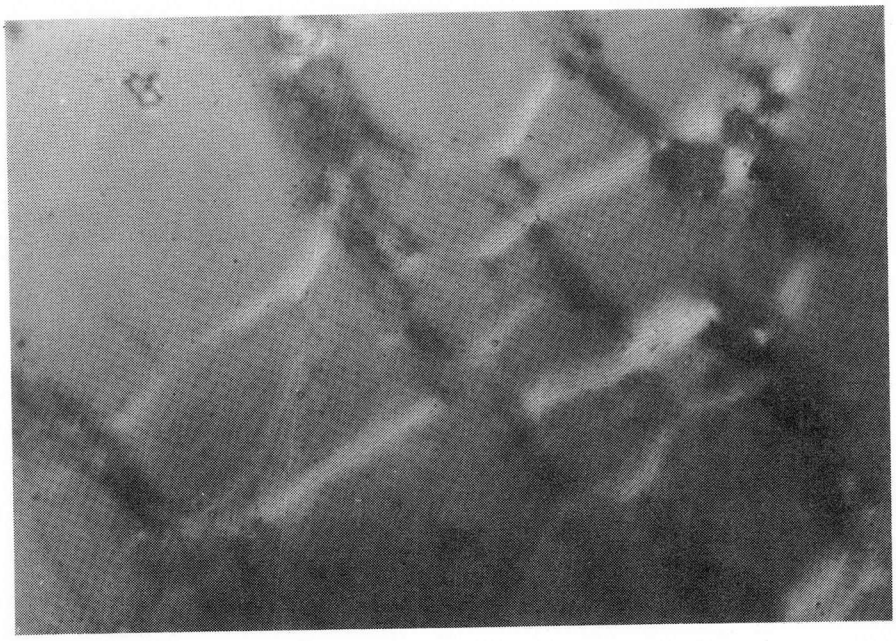

Figure 3.2 Planar texture in a parallel quartz cell viewed between crossed polars. Sample V-1, w = 0.183; cell thickness = 81 μm.

lines run in the longitudinal direction. The streaks parallel to one polar were almost invisible, but those inclined by 45° from that polar were brightest. Those normal to the brightest were darker than the background. This dark background resembles the uniform area, i.e., a planar texture, reported for polypeptide liquid crystals.[13,15] Indeed, this dark area was found to have a planar texture, because this

preparation showed a very large optical rotation, as will be mentioned below.

At relatively low concentration, the birefringent phase first appeared as spherulites. A typical photograph of such a spherulite is shown in Figure 3.3, where the directions of the polars are indicated by arrows. A Maltase cross is seen in the directions of the polars. The spherulite has one radial disclination line and shows a spiral pattern of bright and dark lines.

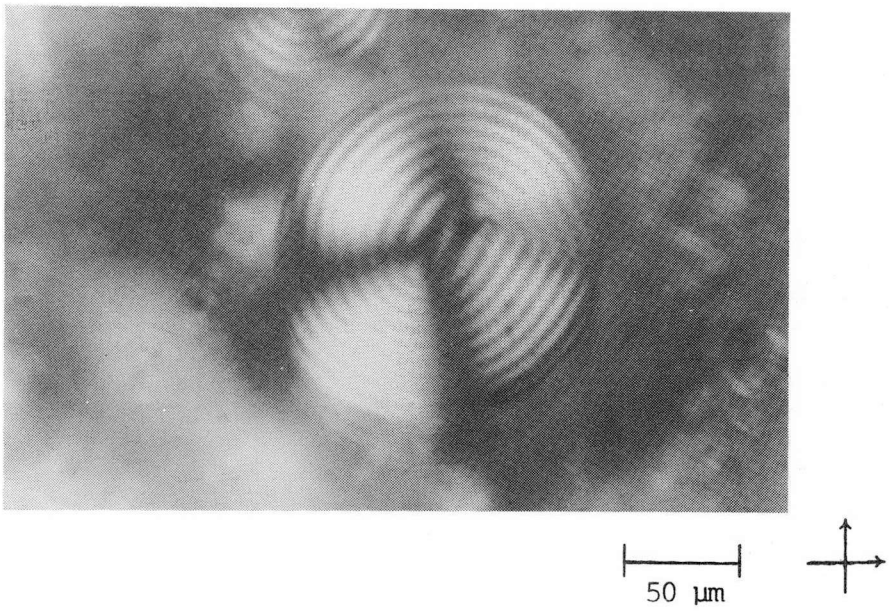

Figure 3.3 Large spherulite viewed between crossed polars; sample D40, w = 0.101.

3-2-2 Spacing

The spacing S between adjacent bright (or dark) lines was determined from photographs of various areas and for different birefringent solutions. Soon after the parallel lines began visible, it appeared that their spacings would change with one place to another and also with time. But within a week, they became practically constant over the entire area except for narrow peripheral ones. The equilibrium S values for solutions of sample D40 are summarized in Table 3.1.

When a birefringent solution of schizophyllan was illuminated by laser light without polars, it projected a diffraction ring (sometimes two rings) on the screen; such a diffraction pattern is shown in Figure 3.4. This indicates the formation of a multi-layer structure, which must be associated with the parallel lines observed by microscopy. The spacing S was determined from such diffraction patterns by the method described in Chapter 2. The results are also shown in Table 3.1.

Two S values at a given w from polarizing microscopy and diffraction were in close agreement,

Table 3.1

Spacing S for Birefringent Solutions of a Schizophyllan Sample D40 at 30 °C

w	S / 10^{-4} cm	
	microscope	diffraction
0.139	5.2_6	5.1_6
0.152	4.2_8	4.3_1
0.165	3.7_4	3.6_4
0.181	2.9_1	2.8_6
0.215	2.2_5	2.2_1
0.274	1.3_4	1.4_1
0.302	-	1.1_7
0.388	-	0.7_9

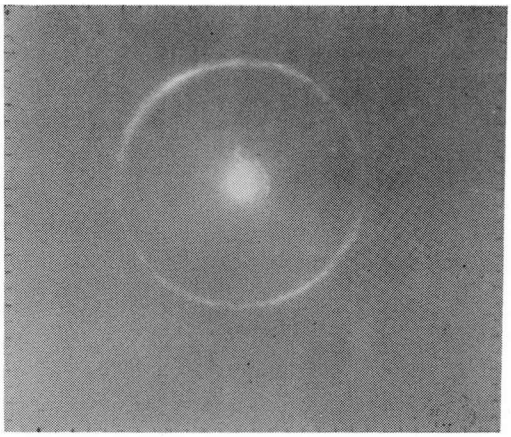

Figure 3.4 Diffraction pattern obtained for an aqueous solution of D40 with w = 0.183. S = 3.7 μm.

as can be seen from Table 3.1, substantiating the formation of a multi-layer structure. Therefore, the two values were averaged to obtain S as a function of w. Figure 3.5 shows a double-logarithmic plot of S vs. w, where the straight line indicated has a slope -1.9. This concentration dependence of S is similar to that reported for poly(γ-benzyl L-glutamate) (PBLG) and poly(γ-methyl L-glutamate) by Robinson et al.[14] However, polypeptide-solvent systems exhibiting

a different concentration dependence have also been reported.[31,39]

3-2-3 Optical Rotatory Dispersion

Optical rotatory dispersion (ORD) measurement was made on the birefringent solution used for the

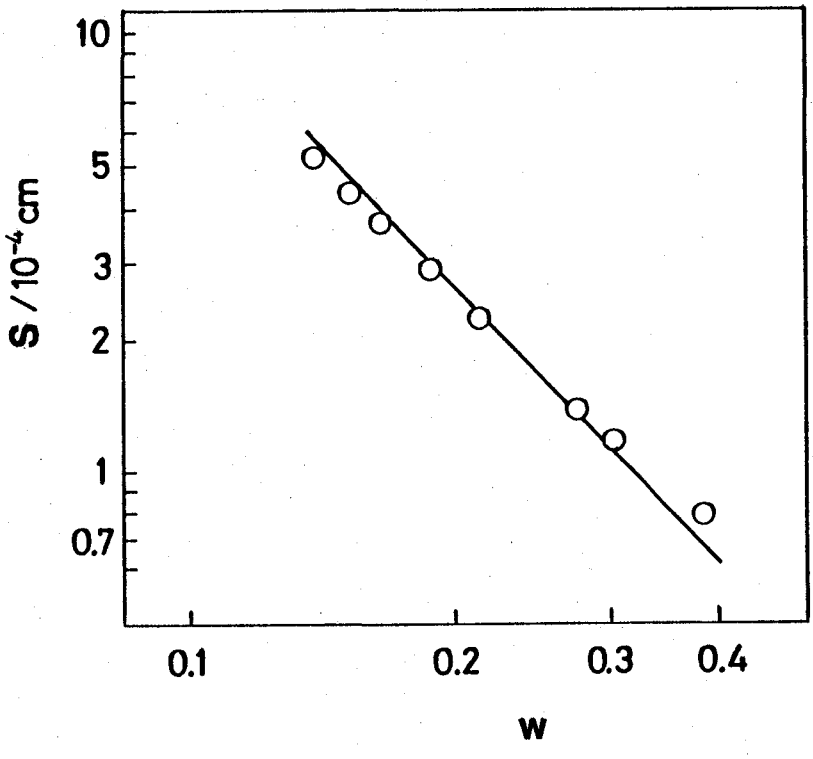

Figure 3.5 Concentration dependence of S for birefringent solutions of D40 at 30°C. The straight line, drawn to have a slope of -1.9.

microscopic observation; the cell thickness was 81 μm. When the solution was illuminated by light normal to the cell wall, it showed a very large optical rotation. Figure 3.6 compares the ORD data for this solution (unfilled circles) with those for an isotropic solution (filled circles). It can be seen that the two curves are distinctly different. The specific rotation for the birefringent solution is nearly two orders of magnitude larger than that for the isotropic solution at fixed wavelength.

3-3 Discussion

3-3-1 Formation of a Cholesteric Mesophase

That an aqueous solution of a triple-helical schizophyllan forms a cholesteric mesophase above some critical concentration was demonstrated by the following observations.

(1) Between crossed polars, colored patterns with alternate bright and dark lines were observed. The spacing between the adjacent bright (or dark) lines was of the order of a few microns and constant throughout the solution. The patterns exhibited some disclinations

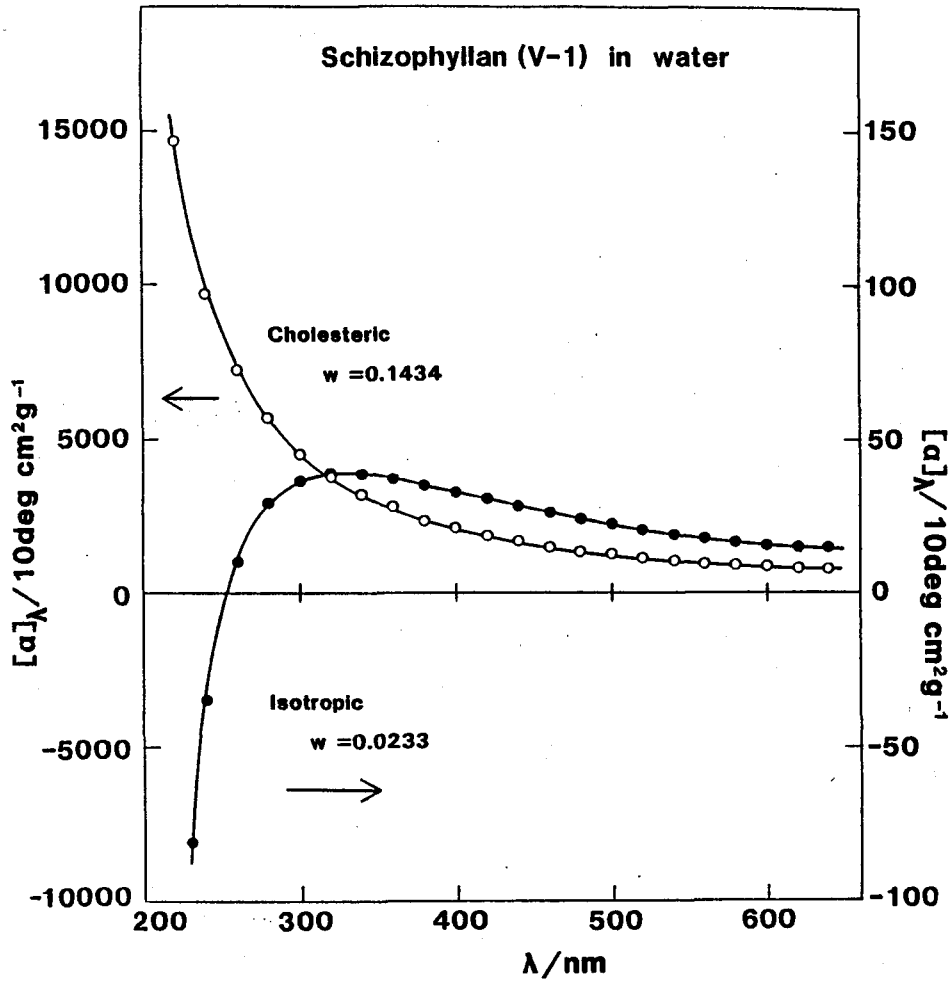

Figure 3.6 Comparison of ORD curves at 25°C for an isotropic solution (sample V-1, w = 0.0233) and a birefringent solution (sample V-1, w = 0.1434).

resembling closely those characteristic of cholesteric mesophases.

(2) When illuminated by laser light without polars, a birefringent solution gave a diffraction ring, which was associated exactly with the spacing S observed by microscopy. The concentration dependence of S for our system was essentially the same as that found by Robinson et al.[14] for polypeptide liquid crystals, which are cholesteric.

(3) A birefringent solution showed a very strong optical rotatory power. The ORD curve of the solution differed from that of an isotropic solution.

Some cellulose derivatives become cholesteric either in bulk or in solution.[55-66] However, they are not rodlike polymers. Thus, schizophyllan is the first rodlike polysaccharide which has been found to form a cholesteric mesophase. Recently, Maret et al.[67] found a cholesteric mesophase to be formed in aqueous solutions of xanthan, another rodlike polysaccharide.[97]

3-3-2 Structure of the Schizophyllan Liquid Crystal

As shown in Figure 3.2, a schizophyllan liquid crystal solution confined in a thin cell exhibits a

planar texture of a cholesteric mesophase. This indicates that a pile of cholesteric layers is viewed in the direction normal to the layers. Streaks appear in the area where the cholesteric layers are oriented normal to the cell wall. The planar texture appears as a result of the restraint due to the cell walls which forces the layers of the cholesteric mesophase to align parallel to the cell walls. This restraint explains why, near the wall of a drum-shaped cell, lines running parallel to the wall were observed, as shown in Figure 3.1 (a). The area distant from the cell walls should be free from such restraint, thus exhibiting complicated textures as shown in Figure 3.1 (b)-(d).

A schizophyllan birefringent solution contained in a thin capillary showed parallel lines running in the direction of the capillary axis. Microscopic observation with a λ plate revealed that the higher refractive index was in the direction of these parallel lines. Assuming that the higher refractive index of the schizophyllan triple helix is along its axis, we can conclude that the helix axis is tangential to the parallel lines, i.e., it is in a layer.

A structural model for cholesteric liquid crystals was first proposed by Robinson to explain the experimental results on polypeptide liquid crystals. We use a similar structure model for the schizophyllan liquid crystal, schematically shown in Figure 3.7, where the schizophyllan triple helices are indicated by dashes tangential to any of the parallel planes. In each plane, all the helices are oriented to a preferred direction, the director, indicated by an arrow. A straight line normal to the planes is referred to as the cholesteric axis. The arrowheads form a spiral with its axis parallel to the cholesteric axis. Since the angle between the directors in the planes A and B is 180^{o}, the distance between the two planes is one half a pitch of the spiral and equal to S obtainable by microscopy and laser light diffraction. As will be shown in Chapter 4, the sense of the spiral is right-handed. The values of the pitch are about several μm (Table 3.1).

For the above structure model, the interplane distance p and the twist angle β per molecule in the direction of the cholesteric axis may be estimated as follows. Since, in most cholesteric liquid crystals,

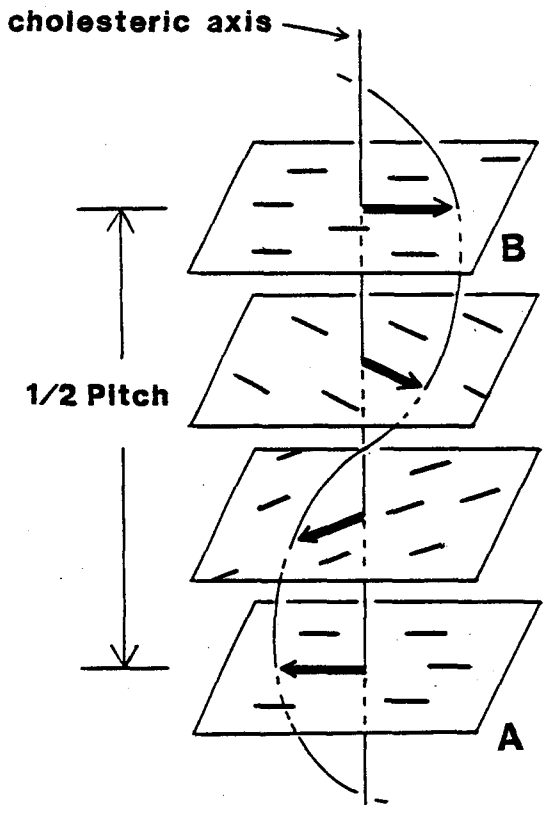

Figure 3.7 Schematic representation of a schizophyllan liquid crystal. Dashes, schizophyllan triple helices; an arrow, a director.

β is of the order of ten minutes, the directors in a local region of the size much smaller than the cholesteric pitch may be almost parallel with each other. Therefore, we here assume that, locally,

schizophyllan helices are oriented parallel and packed in a two-dimensional hexagonal array without dilution in the direction of the helix axis, as suggested by Robinson et al.[14] for polypeptide liquid crystals. On this assumption, p can be related to ϕ by the equation

$$p^2 = \frac{\sqrt{3}M_L v_p}{2N_A \phi} = 1.9 \times 10^{-14} / \phi \qquad (3.1)$$

where N_A is the Avogadro constant. Since β is equal to 180° x (p/S), it can be calculated by using the p value from Eq. (3.1) and the experimental S value (Table 3.1). The calculated p and β were in the ranges 4.5 - 2.6 nm and 0.16 - 0.59°, respectively. These β values indicate that, locally, the average direction of schizophyllan helices, i.e., the director, should be almost parallel to its neareat neighbors.

When illuminated by a laser beam, a schizophyllan liquid crystal solution exhibited a diffraction pattern which usually contained a strong first-order ring but seldom higher-order ones. This is at variance with the results reported for polypeptide liquid crystals which exhibited even the eighth-order

ring.[13] Small-angle X-ray scattering measurements on schizophyllan liquid crystal solutions revealed no indication of definite interchain distance. These observations show that our liquid crystal is less completely ordered than the polypeptide liquid crystals; even the latter do not form a perfect two-dimensional hexagonal array.[14,15] The small β values estimated do not necessarily mean that all the schizophyllan helices are parallel each other. Rather it is suggested that their directions fluctuate considerably about the director, giving rise to the less ordered structure.

3-3-3 Birefringence of the Cholesteric Layer

The birefringence Δn of a cholesteric layer is defined by $\Delta n = n_{//} - n_{\perp}$, with $n_{//}$ and $n_{\perp}$ being the refractive indices of the layer parallel and normal to the director, respectively (Figure 3.7).
We estimated Δn of the schizophyllan liquid crystal by the method described below. When observed between crossed polars with a quartz wedge inserted along a streak, the streak exhibited a retardation relative to the background showing no birefringence. The

retardation was judged to be negative from the colors of the two areas. When the wedge was displaced slightly in the direction of increasing retardation, the streak restored the original color of the background. The streak normal to the wedge made a positive contribution to the retardation. From the known geometry and birefringence of the wedge, we estimated the change in retardation ΔR due to this displacement.

If the streak represents the cross-sectional view of a layer structure developing normal to the cell walls all the way from the upper cell wall to the bottom, ΔR may be related to the birefringence $n_{//}' - n_{\perp}'$ of the streak and the cell thickness d by

$$\Delta R = (n_{//}' - n_{\perp}')d \qquad (3.2)$$

where $n_{//}'$ and $n_{\perp}'$ are the average refractive indices parallel and normal to the streak, respectively. Since the cholesteric layers are aligned parallel to the streak, $n_{\perp}'$ can be equated to $n_{\perp}$. The refractive index parallel to the streak is expected to vary periodically between $n_{//}$ and $n_{\perp}$ in the direction normal

to the streak, and hence $n_{//}'$ can be taken as the arithmetic mean of $n_{//}$ and $n_{\perp}$, i.e., $n_{//}' = (1/2)(n_{//} + n_{\perp})$. Therefore, we have

$$\Delta R = d\Delta n/2 \qquad (3.3)$$

Relatively thin preparations which might develop a layer structure over the entire cell thickness were examined to find appropriate streaks. A number of measurements on such streaks at different places and for different preparations were averaged to give $\Delta n = 0.0012$ and 0.0018 for $w = 0.1434$ and 0.1993, respectively. The accuracy was only moderate. In the following chapter, these values of Δn will be compared with the values obtained from ORD measurement.

Appendix[93,94]

A disclination represents a singularity in a liquid crystal, where the director orientation changes discontinuously. The discontinuity may be located at a point (a point disclination) or on a line (a line disclination). In most cholesterics, certain singular lines (disclination lines) are found. Two disclinations in cholesterics are schematically shown in Figure 3.8, where dots, dashes, and nails signify that the director

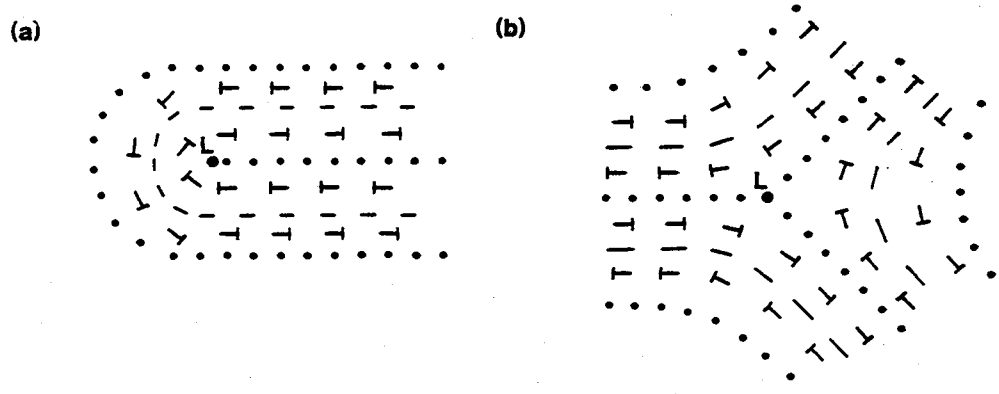

Figure 3.8 Schematic representation of typical disclination lines. (a) line λ^{+}. (b) line λ^{-}. Dots, director axis normal to the paper; dashes, axis parallel to the paper; nails, axis tilted.

axis is normal, parallel, and tilted to the plane of paper, respectively. The disclination lines L indicated in Figures 3.8 (a) and (b) are referred to as λ^+ and λ^-, respectively.

Chapter 4

OPTICAL ROTATORY DISPERSION OF SCHIZOPHYLLAN LIQUID CRYSTALS

4-1 Introduction

A striking optical property of a cholesteric mesophase is a very large optical rotation for light propagating along its optical axis. Such optical rotation arises from the helical structure of the cholesteric schematically shown in Figure 3.7. Actually, it can be observed for a thin film of a cholesteric with a planar texture.

Robinson[13,15] first observed a large optical rotation with polypeptide liquid crystals. He showed that his ORD data were consistent with the theoretical prediction of de Vries[98] for cholesterics, which is based on a layer model essentially the same as that shown in Figure 3.7. Existing data for polymer liquid crystals[32,57,64,66,67] appear in favor of the de Vries theory at least in a limited range of wavelength, although there is some argument against it.[34]

It was shown in Chapter 3 that aqueous solutions of schizophyllan form a cholesteric mesophase above a certain critical concentration. Therefore, we expected that the optical rotation behavior characteristic of cholesterics should be observed for schizophyllan liquid crystals. A prerequisite for the observation of this behavior was to obtain a liquid crystal film with a planar texture. This was achieved by using thin cells constructed as described in Chapter 2, and allowed ORD measurement to be made on a number of liquid crystal samples.

4-2 Results

4-2-1 Cholesteric Pitch

The cholesteric pitch P (2S) was measured for liquid crystal solutions of samples V-1 and U-1 confined in drum-shaped cells and/or thick parallel glass cells. The results are shown in Figure 4.1, where P is plotted against polymer weight fraction w. The data points for V-1 (unfilled circles) and U-1 (filled circles) are scattered around the solid line indicated. It should be noted that P varied from 2 to 11 μm in

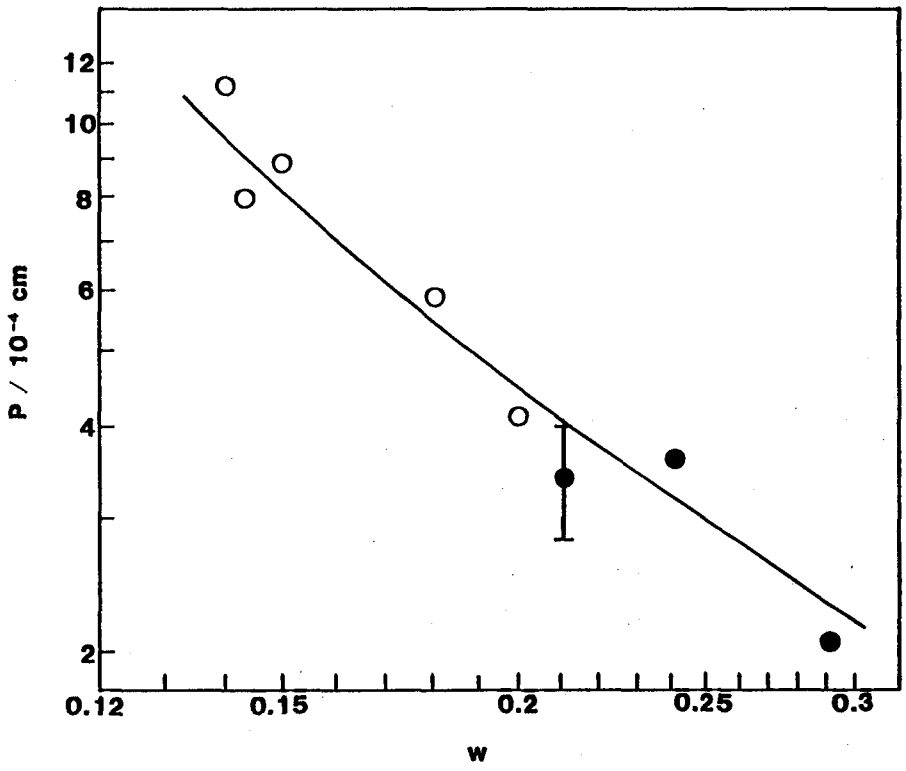

Figure 4.1 Plots of S vs. w for aqueous solutions of V-1 (unfilled circles) and U-1 (filled circles).

the w range examined. These P values are used for analyzing the ORD data given below.

4-2-2 ORD Measurement

Thin films of liquid crystal solutions were measured for optical rotatory dispersion. It was

found that their ORD behavior varied greatly with the film thickness d. For films thinner than 100 μm, the optical rotation increased gradually during about one month after the cells were filled with solutions and then approached an equilibrium value. On the other hand, for thicker films, the change in optical rotation was irregular and less reproducible.

Figure 4.2 shows the d dependence of specific rotation $[\alpha]_\lambda$ for an 18.03 wt% solution at fixed wavelengths. Most data were taken more than one month after the cell filling and thus pertained to the equilibrium state. It can be seen that $[\alpha]_\lambda$ stays almost constant at smaller d. The reproducibility of data was fairly good in this d range. However, for d greater than 130 μm, it was very poor; for one thick film, the sign as well as magnitude of $[\alpha]_\lambda$ were different depending on whether one side of the film faced toward the light beam or the other. Optical rotations of some thick films were much larger than those shown in Figure 4.2.

As mentioned in Chapter 3, a liquid crystal film thinner than 100 μm gave a planar texture similar to that shown in Figure 3.2. On the other hand, for films

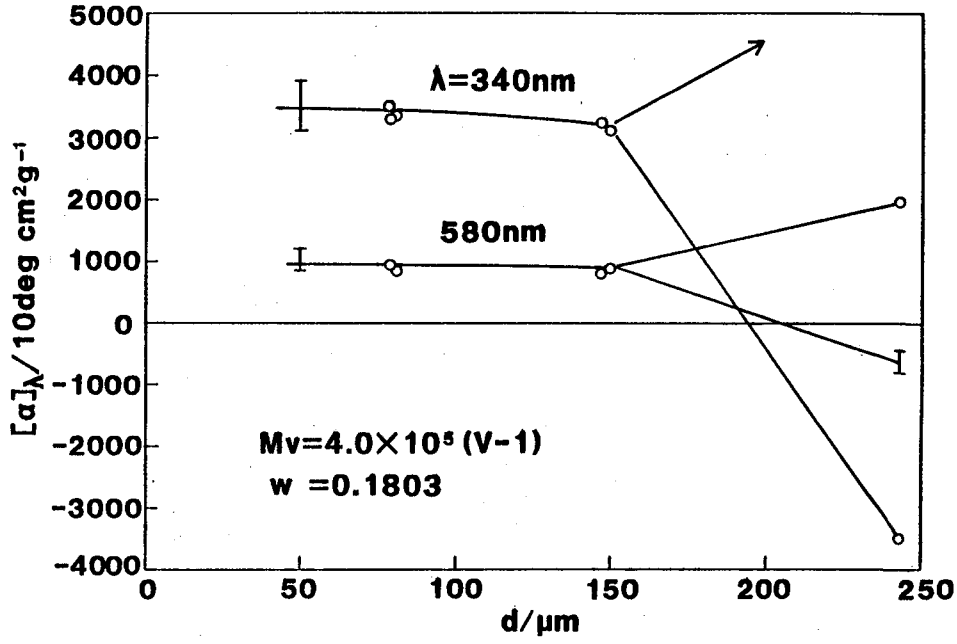

Figure 4.2 Dependence of optical rotation $[\alpha]_\lambda$ on cell thickness d at the indicated wavelenths λ, w = 0.1803.

thicker than 100 μm, they showed no planar texture but were occupied by the multi-domain structure which may be an assembly of microscopic cholesteric domains aligned in various directions. At present, we suspect that this multi-domain structure is responsible for the anomaly found in the thick films. The scattering of data,

for either thinner or thicker films, may be due partly to the experimental difficulty in handling viscous solutions. In the discussion to follow, attention will be focused on the normal ORD behavior of thinner films which exhibited a planar texture.

Figure 4.3 shows the ORD curves of cholesteric solutions of V-1 with different concentrations, where Θ is the optical rotation per unit length of the solution. Any curve exhibits the feature of cholesteric mentioned in the previous chapter (see Figure 3.6). It should be noted that neither Θ nor $[\alpha]_\lambda$ varies systematically with polymer concentration. This is in contrast to the behavior of isotropic solutions, in which $[\alpha]_\lambda$ at 580 nm decreases monotonously from 2.0 deg cm^2g^{-1} at infinite dilution to 1.3 deg cm^2g^{-1}at w = 0.10.

4-3 Discussion

4-3-1 Analysis by the de Vries Theory

According to the theory of de Vries,[98] the optical rotation for light of wavelength λ (in vacuo) propagating normal to a cholesteric layer, that is, parallel to the cholesteric axis, is given by

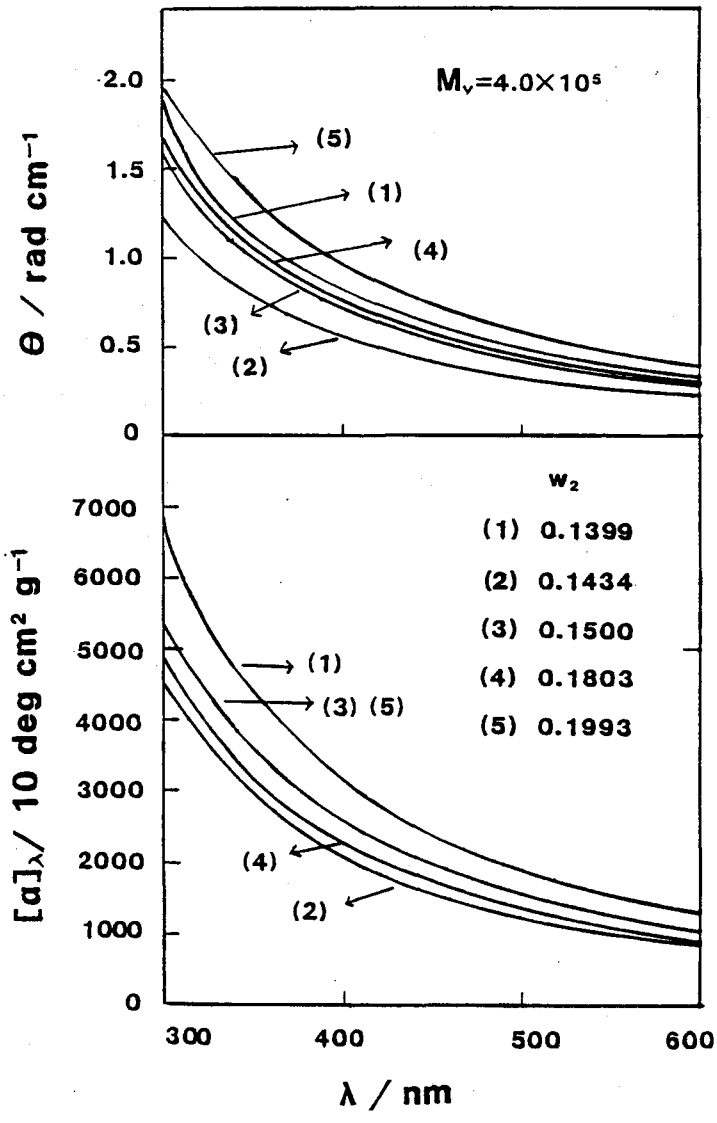

Figure 4.3 ORD curves for cholesteric solutions of V-1 with different concentrations.

$$\Theta = \frac{\pi(\Delta n)^2 P}{4\lambda^2(1 - \lambda^2/\lambda_0{}^2)} \qquad (4.1)$$

provided that $\lambda >> \Delta nP$. Here, $\lambda_0 = nP$, with P the cholesteric pitch and n the average refractive index of the cholesteric, and Δn the layer birefringence defined in Chapter 3 3-3. We follow the convention that Θ is positive for right-handed cholesterics. For most cholesterics, $\lambda << \lambda_0$, and hence Eq. (4.1) is simplified to

$$\Theta = \frac{\pi(\Delta n)^2 P}{4\lambda^2} \qquad (4.2)$$

In sum, we may use this equation under the condition

$$\Delta nP << \lambda << \lambda_0 \qquad (4.3)$$

To test the validity of the de Vries theory, we check two points: (1) whether the λ dependence of Θ obeys Eq. (4.2) under the condition (4.3), and (2) whether the value of Θ can be predicted by Eq. (4.2) from experimentally available data. This is actually

what was done by Robinson with his polypeptide liquid crystals.[13,15]

For the schizophyllan liquid crystals in the concentration range for ORD measurements, the layer birefringence Δn was of the order of 10^{-3} (Chapter 3) and the cholesteric pitch was in the range 2 - 11 μm (see Figure 4.1). Thus, our system meets the condition (4.3).

Figure 4.4 shows plots of Θ vs. λ^{-2} for different preparations. It can be seen that, at smaller wavelengths, the plot for any preparation follows a straight line passing through the origin, conforming to Eq. (4.2). Similar plots were obtained with the data for other preparations. Therefore, Δn was estimated by Eq. (4.2) from the slope values of the straight lines together with the P values presented above. The results are summarized in Table 4.1; Δn is positive as shown in Chapter 3.

Figure 4.5 shows a plot of Δn vs. polymer volume fraction ϕ, where half-filled circles and unfilled circles are for U-1 and V-1, respectively; filled circles represent the data from the retardation measurement described in Chapter 3. It can be seen

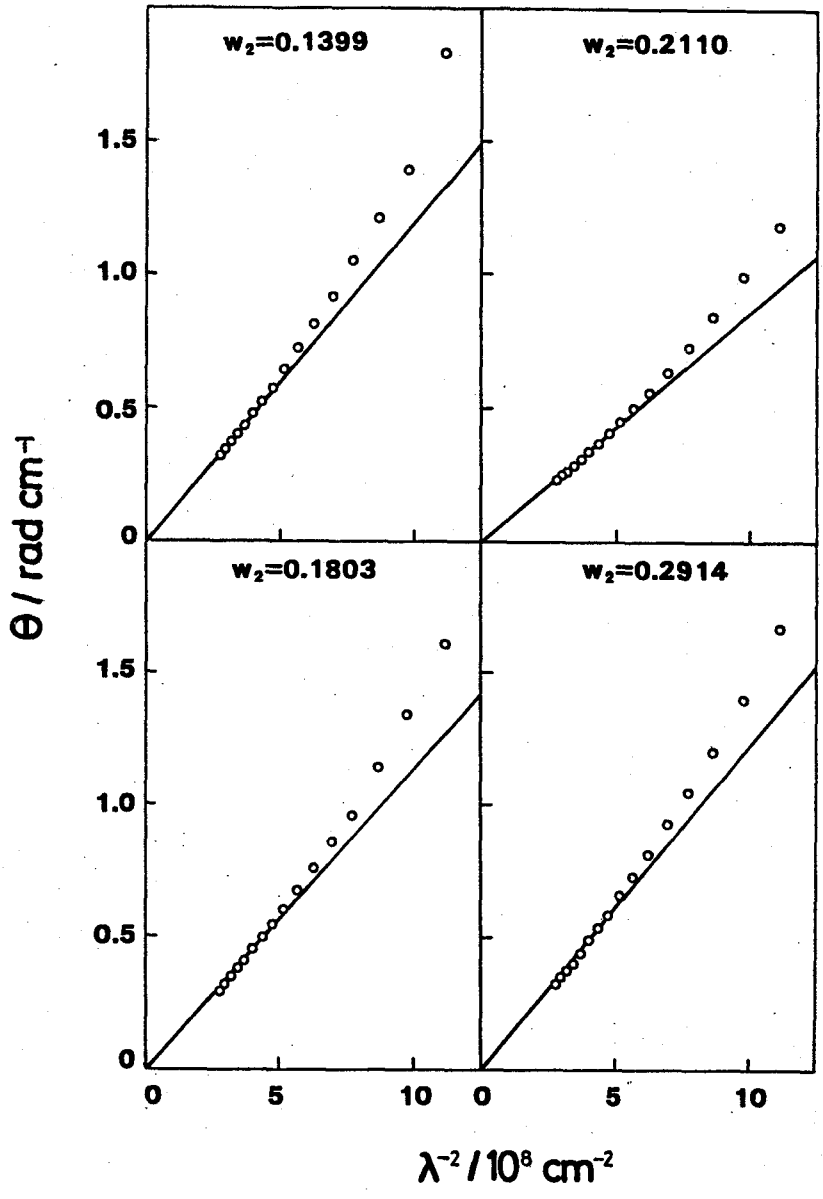

Figure 4.4 Plots of Θ vs. λ^{-2} for aqueous solutions of V-1 (w = 0.1399, 0.1803) and U-1 (w = 0.2110,0.2914).

Table 4.1

Birefringence of the Schizophyllan Liquid Crystal Determined from ORD and Retardation Data

Samples	w	P/μm	ORD Δn x 10^3	Retardation Δn x 10^3
V-1	0.1399	11.2 ± 0.2	1.1_6 ± 0.04	-
	0.1434	8.0 ± 0.2	1.1_5 ± 0.04	1.2 ± 0.2
	0.1500	8.9	1.2_2 ± 0.03	-
	0.1803	5.9	1.5_6 ± 0.03	-
	0.1993	4.1 ± 0.1	2.1_0 ± 0.05	1.8 ± 0.3
U-1	0.2110	3.4 ± 0.6	1.7 ± 0.1	-
	0.2490	3.0_3*	2.1_9 ± 0.05	-
	0.2914	2.0_6	2.7_6 ± 0.03	-

* Determined from the solid curve indicated in Figure 4.1.

that the values of Δn obtained by the two independent methods are in good agreement. In sum, the validity of Eq. (4.2) has been confirmed by our data at least in the specified range of wavelength.

It must be noted that, according to Eq. (4.2), the positive optical rotation for $\lambda << \lambda_0$ indicates

the schizophyllan liquid crystal to be right-handed.

4-3-2 Birefringence of the Cholesteric Layer

Figure 4.5 shows that Δn increases approximately linearly with ϕ, yielding an average of 0.014 for $\Delta n/\phi$. This $\Delta n/\phi$ value is smaller than 0.029 and 0.024-0.038 for polypeptide liquid crystals reported by Robinson[15] and DuPré and Lin,[99] respectively, and

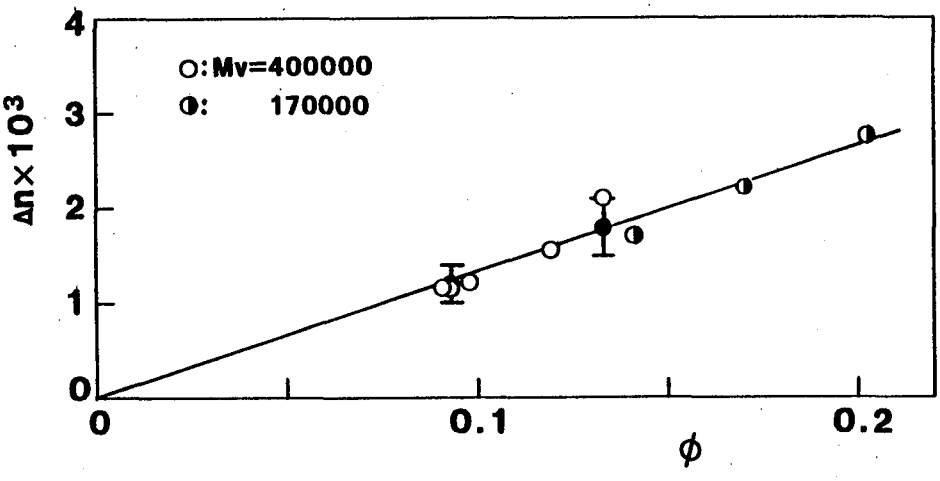

Figure 4.5 Dependence of the layer birefringence Δn on polymer volume fraction ϕ. Unfilled circles, from ORD data for sample V-1; filled circles, from retardation data for V-1; half-filled circles, from ORD data for U-1.

0.04 (0.025 cm^3g^{-1}) by Maret et al.[67] for xanthan liquid crystals, deduced from either a similar analysis or direct measurement; Δn was negative for the xanthan liquid crystal.[100] All these values are smaller than 0.07 reported for crystalline cellulose[101] which consists of β-1,4-linked D-glucose residues in an almost fully extended conformation.[102]

The birefringence of a lyotropic liquid crystal arises from uniaxially oriented rodlike molecules which are intrinsically anisotropic in polarizability. Therefore, it is reasonable to assume that Δn is expressed by the product of the intrinsic birefringence $n_\alpha - n_\gamma$ of the molecule, the number of molecules in unit volume, and the degree of their orientation. The last factor may be taken into account by the order parameter S defined by

$$S = (1/2)\langle 3\cos^2\theta - 1\rangle \qquad (4.3)$$

where θ is the angle between the long axis of a molecule and the director, and $\langle\cdots\rangle$ means the average over all molecules. It follows from the above assumption that Δn may be expressed as[103]

$$\Delta n = (n_\alpha - n_\gamma)\phi S \qquad (4.4)$$

At present, no experimental information on either $n_\alpha - n_\gamma$ or S is available for schizophyllan liquid crystals. A theoretical consideration on nematic liquid crystals[104] suggested that S increases from about 0.5 to unity as ϕ tends to unity. Thus, the value of $n_\alpha - n_\gamma$ for the system schizophyllan + water may be larger than 0.014 by a factor not greater than 2, yielding 0.028 as the upper limit; the most probable value may be around 0.02.

Therefore, even when correction is made for the molecular orientation, there still remains a large difference in intrinsic birefringence among cellulose, xanthan, and schizophyllan. This difference may be due to the difference in chain conformation among these glucans; the reason is as follows. Schizophyllan in water exists as a triple helix consisting of loosely wound β-1,3-D-glucan chains,[84] while xanthan consists of β-1,4-D-glucan chains as cellulose and has a more extended helical conformation than the schizophyllan helix.[97,105,106] In the crystalline

state, the virtual bond connecting the oxygen atoms attached to the 1 and 4 carbon atoms is in the direction of the maximum polarizability of the glucose residue and inclined from the crystalline c axis by 66^{o}, 30.9^{o}, and 18.4^{o}, for schizophyllan,[107] xanthan,[108] and cellulose,[102] respectively.

Thus, the main chain glucose residues in schizophyllan should make a small negative contribution to $n_{\alpha} - n_{\gamma}$. The side chain glucose residue of this polymer, about 1/3 as heavy as the main repeating unit, cannot make a contribution larger than 0.082/4. The sum of the two contributions is expected to yield the small $n_{\alpha} - n_{\gamma}$ value observed.

For xanthan, the contribution per main chain glucose residue is estimated to be about 0.05. The contribution from ionizable pendent groups, about twice the main chain weight, may be large enough to offset this main chain contribution, yielding a negative $n_{\alpha} - n_{\gamma}$ as observed. Thus, we see in these two polysaccharides that the movable pendent groups play the same important role as the main chain in determining $n_{\alpha} - n_{\gamma}$.

4-3-3 Optical Rotatory Dispersion

As remarked in connection with Figure 4.4, Eq. (4.2) does not hold accurately over an extended range in wavelength. Indeed, for any case examined, the plot of Θ vs. λ^{-2} was curved upward at shorter wavelength, as exemplified in Figure 4.4. A similar deviation from the de Vries equation can be noted in polypeptide data,[13,15,32] although the deviation is not very apparent because of the data being limited to relatively large wavelength.

It is usual to express ORD data for helical polymers by an equation of the Moffitt-Yang type, which reads

$$[\alpha]_\lambda = \frac{a_0 \lambda_0^{\,2}}{\lambda^2 - \lambda_0^{\,2}} + \frac{b_0 \lambda_0^{\,4}}{(\lambda^2 - \lambda_0^{\,2})^2} \qquad (4.4)$$

where a_0, b_0, and λ_0 are numerical constants. This equation reduces to a simple Drude equation for $b_0 = 0$. Here the dispersion factor and residue molecular weight are omitted for simplicity.

It can be shown that our data for schizophyllan solutions obey Eq. (4.4), irrespective of concentration.

Figure 4.6 shows typical data for an isotropic solution and a cholesteric film. The former data obey the Moffitt-Yang equation, whereas the latter obey the Drude equation ($b_0 = 0$). Patel and DuPré[34] have remarked the same kind of difference between isotropic and cholesteric solutions. Thus, the fact that ORD curves of liquid crystal solutions are of the type

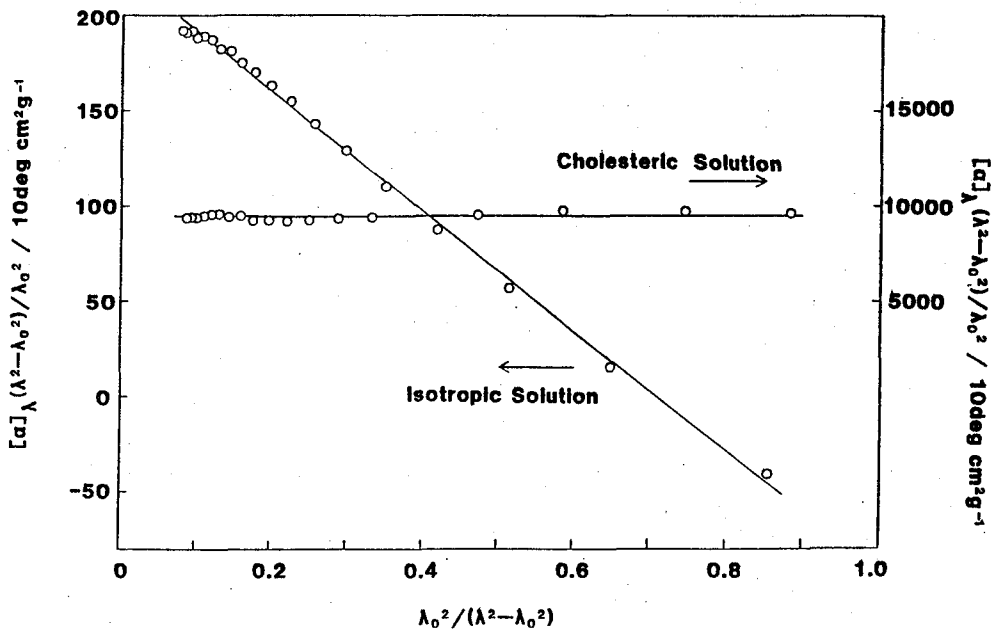

Figure 4.6 Moffitt-Yang plots for an isotropic solution (w = 0.0233, λ_0 = 163 nm) and a cholesteric solution (w = 0.1434, λ_0 = 170 nm).

expressed by a simple Drude equation cannot be due to the chiral nature of individual macromolecules but the characteristic of liquid crystals. No theoretical interpretation of this fact has as yet been given.

For a thin film of V-1 with w = 0.1434, the optical rotation remained substantially constant

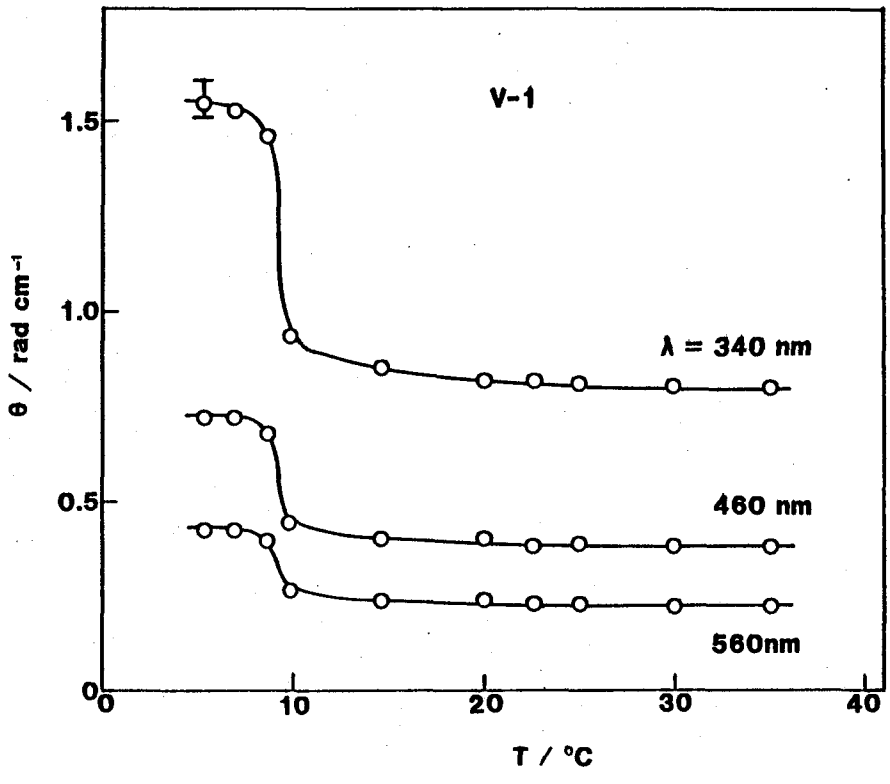

Figure 4.7 Dependence of Θ on temperature T at the indicated wavelengths λ. Sample, V-1; w = 0.1434.

between 15 and 35°C, but increased adruptly at about 9°C, as illustrated in Figure 4.7. It was found that the change in Θ was accompanied by a change in S. DSC measurement on another preparation revealed an anomalous change in the same temperature region. No exact correlation of these changes has been established.

chapter 5

THERMODYNAMIC PROPERTIES OF CONCENTRATED SCHIZOPHYLLAN SOLUTIONS

5-1 Introduction

A solution of a rodlike polymer forms an anisotropic phase at high concentration, and separates into equilibrium isotropic and anisotropic phases at a certain intermediate concentration. Such phase behavior as well as the thermodynamic properties of these phases can in principle be predicted if relevant expressions are available for the chemical potentials of the components involved. The theories so far developed along this line of thought indicated that an asymmetric shape of the polymer is of primary importance for the formation of an anisotropic phase.[72-78] However, it has been predicted[78] that intermolecular interactions also play an important role in the phase behavior. Thus, knowledge of the chemical potentials is essential for testing theoretically predicted phase relationships. As far as

we are aware, attempts to approach such knowledge have been made only by Kubo and Ogino,[26,27] who studied the system poly(γ-benzyl L-glutamate) + dimethylformamide. They obtained thermodynamic data that could be compared favorably with the prediction of Cotter's theory.[76] Applicability of this theory to other systems is yet to be seen.

For the reason given below, aqueous schizophyllan, in which this rodlike polysaccaride[84,85] forms a cholesteric mesophase at high concentrations, cannot be regarded as an athermal solution of hard rods in a non-interacting medium. The average value of the second virial coefficient for aqueous schizophyllan at 25°C is 1.25×10^{-4} mol cm^3 g^{-2}.[84,85] Analysis of this value by Zimm's theory of rodlike polymers[109] gives 1.2 nm for the diameter of the schizophyllan triple helix. This is smaller than 1.67 nm calculated from the partial specific volume of schizophyllan in water at infinite dilution (0.619 cm^3 g^{-1}) and the molecular weight per unit length M_L of 2140 nm^{-1}, and also smaller than the hydrodynamic diameter 2.2 - 2.6 nm reported by Norisuye and coworkers.[84,85]

These disparities suggest that concentrated

aqueous schizophyllan is non-athermal and its thermodynamic properties cannot be described only in terms of the geometry of the schizophyllan helix. Therefore, we attempted a direct evaluation of the thermodynamic properties of aqueous schizophyllan. Thus, light scattering and sedimentation equilibrium measurements were made on isotropic solutions and sedimentation measurement was made on biphasic mixtures, and the data were analyzed by the methods of Scholte.[110,111] This chapter describes the experimental results and their comparison with theoretical predictions.

5-2 Treatment of Light Scattering and Sedimentation Equilibrium Data

Consider a solution consisting of a polymer and a single solvent; the polymer may or may not be monodisperse in molecular weight. In a light scattering measurement, vertically polarized light is incident on the solution, and the intensity of scattered light is measured as a function of the scattering angle θ to obtain the reduced excess scattering intensity R_θ. The quantity Z_{LS} defined by

$$Z_{LS} = - \frac{RTKM_0 wv}{R_0} \qquad (5.1)$$

can be related to the thermodynamic properties of the solution. Here, R_0 is the value of R_θ extrapolated to the zero scattering angle, M_0 the molecular weight of the solvent,[112] v the specific volume of the solution, and K the optical constant defined by

$$K = \frac{4\pi^2(\partial n/\partial w)^2 n^2}{N_A \lambda_0^4} \qquad (5.2)$$

with N_A the Avogadro constant, $\partial n/\partial w$ the specific refractive index increment on the weight fraction basis, and λ_0 the wavelength of incident light in vacuo. For a monodisperse solute, Z_{LS} is equal to the partial derivative $[\partial \Delta\mu_0/\partial w]$ of the solvent chemical potential $\Delta\mu_0$ with respect to w at fixed temperature and pressure.[110,111]

For aqueous schizophyllan, the values of $\partial n/\partial w$ and v as functions of w can be obtained using the established relations (Eq. (2.6) - (2.8)). Thus, with the known values of N_A and λ_0, light scattering

measurement allows Z_{LS} to be evaluated for isotropic solutions of schizophyllan. In so doing, M_0 was taken to be 2210 for the reason given in the following section.

Next, consider the same polymer solution at sedimentation equilibrium in an ultracentrifuge cell. A sedimentation equilibrium measurement gives the refractive index gradient dn/dr in the solution as a function of the distance r from the center of rotation. A quantity Z_{SED} (essentially the same as Z_{LS}) is obtained from dn/dr by

$$Z_{SED} = \frac{M_0 w(r) r\omega^2 (\partial v/\partial w)(\partial n/\partial w)}{v(dn/dr)} \qquad (5.3)$$

where ω is the angular velocity, w(r) the polymer weight fraction at r, and $\partial v/\partial w$ the partial derivative of v with respect to w. When the rotor speed is low and the solution column is short, the concentration gradient developed in the cell is almost constant throughout the entire solution, and w(r) at the midpoint of the solution is very close to the weight fraction in the original solution, which is hereafter denoted by w. Thus, the sedimentation equilibrium

method allows Z_{SED} to be determined for a known w. A similar analysis may be made for phase-separated solutions as well if w(r) at the phase boundary can be determined.

Actually, sedimentation equilibrium measurements on isotropic solutions of schizophyllan were carried out under the conditions specified above, and the data were analyzed by Eq. (5.3) along with the data for $\partial n/\partial w$, v, and $\partial v/\partial w$ presented in Chapter 2. Similar measurements were also made on biphasic mixtures, using solution columns somewhat longer than those for the isotropic solutions.

In what follows, we express Z_x (x = LS, SED) in terms of the polymer volume fraction ϕ defined by

$$\phi = wv_p/[wv_p + (1 - w)v_0] \qquad (5.4)$$

where v_p is the partial specific volume of the polymer at infinite dilution and v_0 the specific volume of the pure solvent; $v_p = 0.619$ cm^3 g^{-1},[84] and $v_0 = 1.0029$ cm^3 g^{-1}. Thus, we use $[\partial\Delta\mu_0/\partial\phi]_x$ defined by

$$[\partial\Delta\mu_0/\partial\phi]_x = Z_x(\partial w/\partial\phi) \quad (x = LS, SED) \qquad (5.5)$$

5-3 Results

5-3-1 Light Scattering Data

Figure 5.1 shows the scattering angle θ dependence of n^2/R_θ for light of wavelength 546 nm at different polymer concentrations, where n is the refractive index of the solution. It can be seen that the data points at each concentration are fitted closely by a straight line, allowing an accurate estimation of the ordinate intercept n^2/R_0 to be made. The resulting values of R_0 were used to calculate $[\partial\Delta\mu_0/\partial\phi]_{LS}$ by the procedure described in the previous section. The data at 436 nm showed substantially the same trend as those at 546 nm and analyzed in the same way. The numerical data of $[\partial\Delta\mu_0/\partial\phi]_{LS}$ for sample R23 are summarized in Table 5.1. The values of $[\partial\Delta\mu_0/\partial\phi]_{LS}$ at 546 and 436 nm agree with each other, except for w = 0.1281.

From the slope S_0 of the straight line in Figure 5.1 we calculated the quantity $\langle S^2\rangle_{app}$ defined by

$$\langle S^2\rangle_{app} = 3c\lambda_0{}^2 M_w K_c S_0/(16\pi^2 n^2) \qquad (5.6)$$

where c is the mass concentration of the polymer and

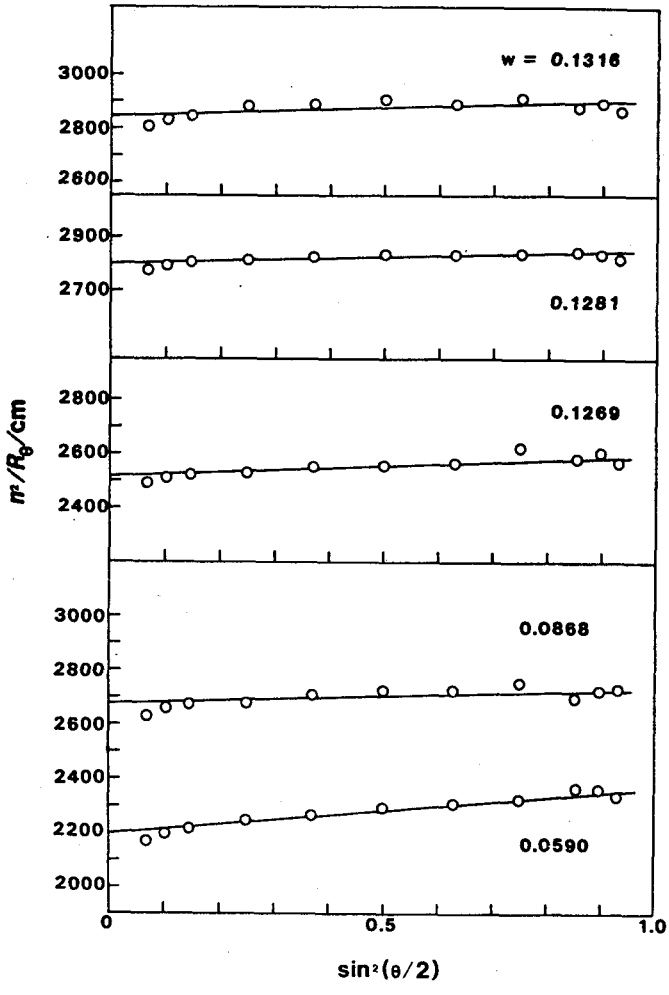

Figure 5.1 Plots of n^2/R_θ for light of wavelength 546 nm vs. $\sin^2(\theta/2)$ for isotropic solutions of sample R23 at 25°C.

Table 5.1

Light Scattering Data for Aqueous Solutions of Sample R23 at 25 °C

w	ϕ	546 nm				436 nm			
		n^2/R_0	$\langle S^2\rangle_{app}^{1/2}$	$-[\partial\Delta\mu_0/\partial\phi]_{LS}$	$-[\partial\Delta\mu_0/\partial\phi]_{Mn}$	n^2/R_0	$\langle S^2\rangle_{app}^{1/2}$	$-[\partial\Delta\mu_0/\partial\phi]_{LS}$	$-[\partial\Delta\mu_0/\partial\phi]_{Mn}$
			nm	J mol^{-1}	J mol^{-1}		nm	J mol^{-1}	J mol^{-1}
0.0590	0.0373	2190	34	193	207	900	36	200	209
0.0868	0.0554	2670	25	362	370	1075	26	365	373
0.1269	0.0823	2510	34	531	539	1010	38	532	540
0.1281	0.0831	2800	29	597	605	1080	32	575	583
0.1316	0.0855	2840	33	627	635	1120	26	616	624

K_c is equal to K with $\partial n/\partial w$ replaced by $\partial n/\partial c$. $\langle S^2\rangle_{app}$ reduces to the mean-square radius of gyration of the polymer, $\langle S^2\rangle_z$ at infinite dilution. It can be seen in Table 5.1 that the values of $\langle S^2\rangle_{app}^{1/2}$ are close to 33 nm, which is the $\langle S^2\rangle_z^{1/2}$ value interpolated at the sample's M_w from the $\langle S^2\rangle_z^{1/2}$ - M_w relationship of Kashiwagi et al.[86] This agreement guarantees the accuracy of measured R_0. Indeed, our experience showed that larger $\langle S^2\rangle_{app}$ were obtained for larger R_0, suggesting that optical purification was incomplete in such cases.

5-3-2 Sedimentation Equilibrium Data for Isotropic Solutions

Sedimentation equilibrium measurements on isotropic solutions of sample R23, D40, and SPG-3' were performed using relatively short solution columns and low rotor speeds, so that centrifugal fractionation might be minimized. The results obtained at different rotor speeds agreed with each other within experimental error. The results are given in Table 5.2 through 5.4.

Table 5.2

Sedimentation Equilibrium Data for Concentrated Isotropic Solutions of Sample R23 at 25 °C

w	ϕ	Rotor Speed / rpm	dn/dr / 10^{-3} cm^{-1}	$-[\partial\Delta\mu_0/\partial\phi]_{SED}$ / J mol^{-1}	$-[\partial\Delta\mu_0/\partial\phi]_{Mn}$ / J mol^{-1}
0.0590	0.0373	4400	8.69	210	219
0.0868	0.0554		8.44	331	339
0.1281	0.0831		8.09	527	535

Table 5.3

Sedimentation Equilibrium Data for

Concentrated Isotropic Solutions of Sample D40 at 25 °C

w	ϕ	Rotor Speed / rpm	dn/dr / 10^{-3} cm^{-1}	$-[\partial\Delta\mu_0/\partial\phi]_{SED}$ / J mol^{-1}	$-[\partial\Delta\mu_0/\partial\phi]_{Mn}$ / J mol^{-1}
0.0196	0.0122	2980	3.88	69.8	74.4
0.0321	0.0200		4.13	108	113
0.0494	0.0311	2980	4.28	165	169
		3370	5.42	163	167
0.0618	0.0391	2980	4.11	216	220
0.0712	0.0452		4.14	251	255
0.0794	0.0505		4.07	286	290
0.0905	0.0579		4.10	327	331

Table 5.4

Sedimentation Equilibrium Data for

Concentrated Isotropic Solutions of Sample SPG-3' at 25 °C

w	ϕ	Rotor Speed / rpm	dn/dr / 10^{-3} cm^{-1}	$-[\partial\Delta\mu_0/\partial\phi]_{SED}$ / J mol^{-1}	$-[\partial\Delta\mu_0/\partial\phi]_{Mn}$ / J mol^{-1}
0.0246	0.0153	3370	3.43	129	143
0.0249	0.0155		3.65	122	136
0.0503	0.0316		4.21	218	231
0.0700	0.0444		4.29	303	316
0.0745	0.0473		4.36	318	331
0.0981	0.0629		4.19	445	458
0.1082	0.0697		4.07	509	522
0.1285	0.0834		3.82	654	667
0.01539	0.1009		3.80	801	813

5-3-3 Chemical Potential of the Solvent

According to Flory and Abe,[80] the chemical potential of the solvent in an isotropic solution of polydisperse rods is expressed as

$$\Delta\mu_0 = RT[\ln (1 - \phi) + (1 - 1/x_n)\phi + \chi\phi^2] \quad (5.7)$$

where x_n is the number-average axial ratio and χ is the interaction parameter which may depend on ϕ; $\chi = 0$ for an athermal solution. Except for some trivial terms, this expression and those for the solute chemical potentials are the same as their counterparts for isotropic solutions of flexible polymers. Therefore, we use Scholte's methods[110,111] for flexible polymers to obtain the solvent chemical potential from light scattering and sedimentation equilibrium data.

His method utilizes the relation:

$$[\partial\Delta\mu_0/\partial\phi]_{Mn} = [\partial\Delta\mu_0/\partial\phi]_x - RTM_0(1/M_n - 1/M_w)(d\phi/dw) \quad (x = LS, SED) \quad (5.8)$$

where the subscript Mn indicates differentiation to be

performed at fixed Mn. This relation shows that both light scattering and sedimentation equilibrium measurements should give the same information, i.e., $Z_{LS} = Z_{SED}$.

In our analysis, M_w/M_n was assumed to be 1.25 for all the samples.[113] The schizophyllan triple helix was approximated by a uniform cylinder of diameter d, and the axial ratio x_n was calculated from M_n by

$$x_n = M_n v_p/(N_A \pi d^3/4) \qquad (5.9)$$

Here, as mentioned in the Introduction, d was taken to be 1.67 nm to be consistent with the helix geometry.[84,85] The molecular weight M_0 of the solvent was calculated from the relation $M_0 = (N_A \pi d^3/4)/v_0$ to be 2210. The values obtained for $[\partial \Delta\mu_0/\partial\phi]_{Mn}$ are summarized in Table 5.2 through 5.4. As seen in these tables, the polydispersity correction expressed by the second term on the right-hand side of Eq. (5.8) is not very appreciable even at small ϕ and becomes rapidly negligible with increasing ϕ.

Figure 5.2 shows the values of $[\partial \Delta\mu_0/\partial\phi]_{Mn}$ for sample R23 as a function of ϕ. The light scattering

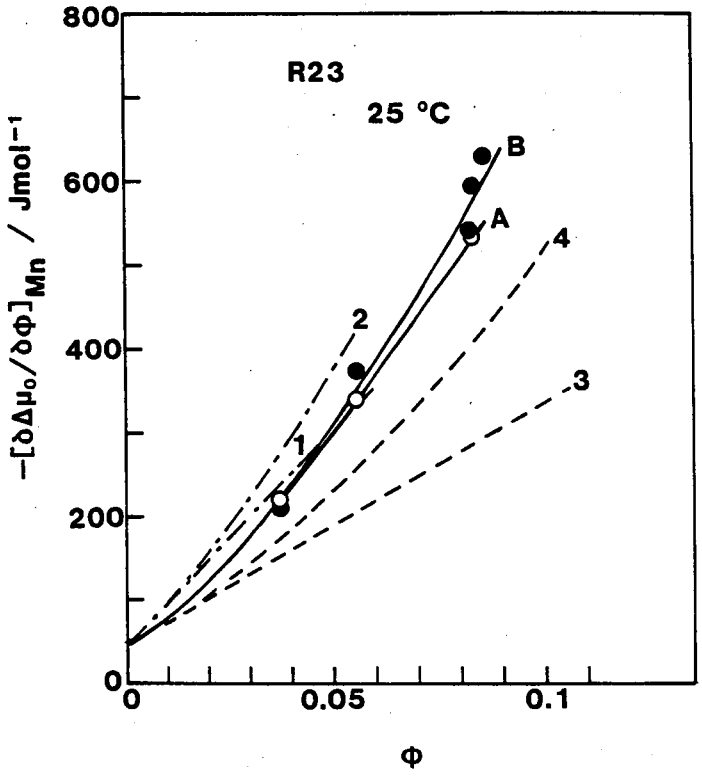

Figure 5.2 Plot of $-[\partial\Delta\mu_0/\partial\phi]_{Mn}$ vs. ϕ for isotropic solutions of sample R23 at 25°C. Unfilled circles, sedimentation equilibrium data; filled circles, light scattering data. Solid curve B, calculated from the Flory-Abe theory (Eq. (5.7)) with Eq. (5.15) and x_n = 54.7; solid curve A, with Eq. (5.14) and x_n = 54.7. Dot-dash curves 1 and 2, calculated for x = 54.7 from the Onsager and Cotter theories, respectively; dashed curves 3 and 4, for x = 29.3 (see the text)

(filled circles) and sedimentation equilibrium (unfilled circles) data are consistent with each other though not exactly. The discrepancy is somewhat more conspicuous at higher concentrations, but the reason is not clear. Figure 5.3 and 5.4 show plots of $[\partial\Delta\mu_0/\partial\phi]_{Mn}$ vs. ϕ for samples D40 and SPG-3'.

5-4 Discussion

5-4-1 Interaction Parameter

As mentioned in the Introduction, aqueous schizophyllan may be characterized by a non-vanishing interaction parameter $\chi(\phi)$ in the framework of the Flory theory. For simplicity, we assume that $\chi(\phi)$ is expressed by a polynomial in ϕ as

$$\chi(\phi) = \chi_0 + \chi_1\phi + \chi_2\phi^2 + \chi_3\phi^3 \qquad (5.10)$$

where the χ_i (i = 0-3) depend on temperature. As is well known, χ_0 is related to the sedimentation second virial coefficient A_2 of the solution by

$$A_2 = (v_p^2/M_0v_0)(1/2 - \chi_0) \qquad (5.11)$$

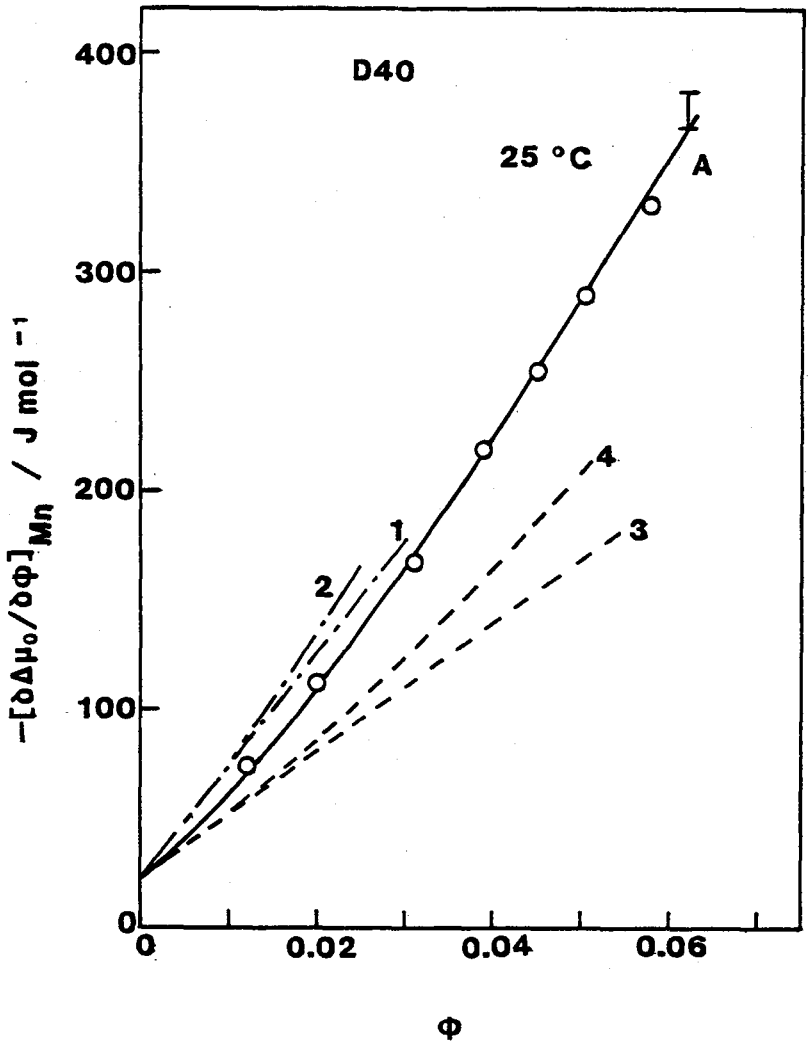

Figure 5.3 Dependence of $-[\partial\Delta\mu_0/\partial\phi]_{Mn}$ on ϕ for sample D40 at 25°C. Solid curve A, calculated by Eq. (5.7) with Eq. (5.12) and x_n = 107; dot-dash curves 1 and 2, calculated for x = 107 from the Onsager and Cotter theories; dashed curves 3 and 4, for x = 59.4 (see the text).

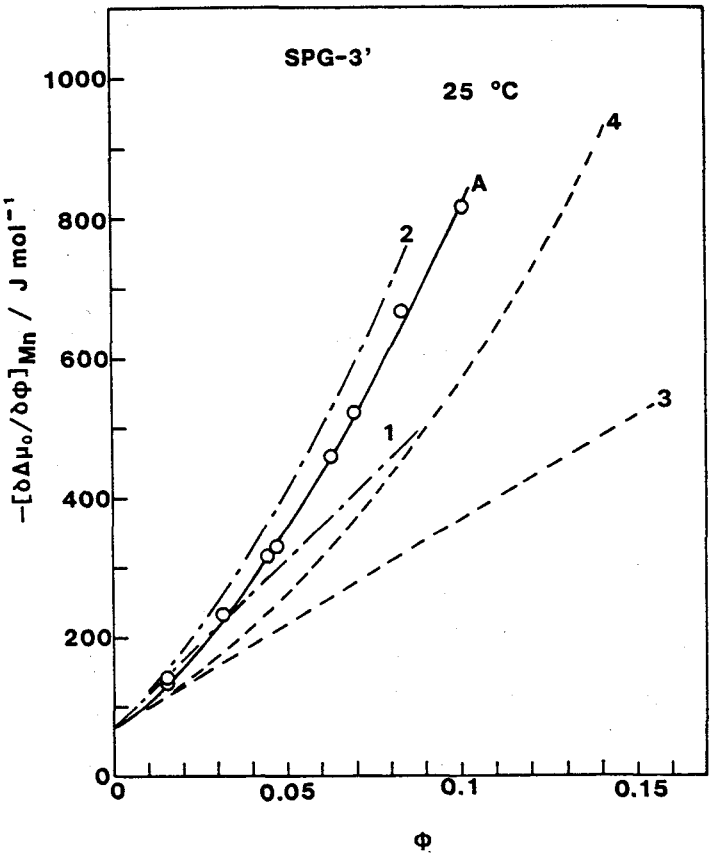

Figure 5.4 Dependence of $-[\partial\Delta\mu_0/\partial\phi]_{Mn}$ on ϕ for sample SPG-3' at 25°C. Solid curve A, calculated by Eq. (5.7) with Eq. (5.13) and x_n = 35.5; dot-dash curves 1 and 2, calculated for x = 35.5 from the Onsager and Cotter theories; dashed curves 3 and 4, for x = 19.2 (see the text).

Substitution of Eq. (5.10) into Eq. (5.7) followed by differentiation with respect to ϕ gives an explicit expression in ϕ for $[\partial\Delta\mu_0/\partial\phi]_{Mn}$. Fitting experimental data for $[\partial\Delta\mu_0/\partial\phi]_{Mn}$ to this expression allows the χ_i coefficients to be evaluated. This was done for three sets of sedimentation equilibrium data, and the following results were obtained:

$$\chi(\phi) = -0.101 - 9.45\phi + 73.4\phi^2 - 374\phi^3 \quad \text{(D40)} \quad (5.12)$$

$$\chi(\phi) = -0.055 - 11.41\phi + 66.9\phi^2 - 228\phi^3 \quad \text{(SPG-3')} \quad (5.13)$$

$$\chi(\phi) = -0.021 - 9.03\phi + 42.7\phi^2 - 55\phi^3 \quad \text{(R23)} \quad (5.14)$$

where χ_0 in each equation has been determined from available experimental data for A_2 by Eq. (5.11). A similar analysis was performed on the light scattering data for R23, yielding

$$\chi(\phi) = -0.021 - 9.16\phi + 38\phi^2 - 75.9\phi^3 \quad \text{(R23)} \quad (5.15)$$

Figure 5.5 shows $\chi(\phi)$ plotted against ϕ. For any sample, $\chi(\phi)$ is negative and decreases monotonously

with increasing ϕ. For sample R23, the values of $\chi(\phi)$ obtained from the two different methods are in good agreement. Differences in $\chi(\phi)$ among the three samples are not appreciable, wherever comparison can be made. The thick curves A in Figure 5.2 through 5.4 represent $[\partial\Delta\mu_0/\partial\phi]_{Mn}$ calculated with the $\chi(\phi)$

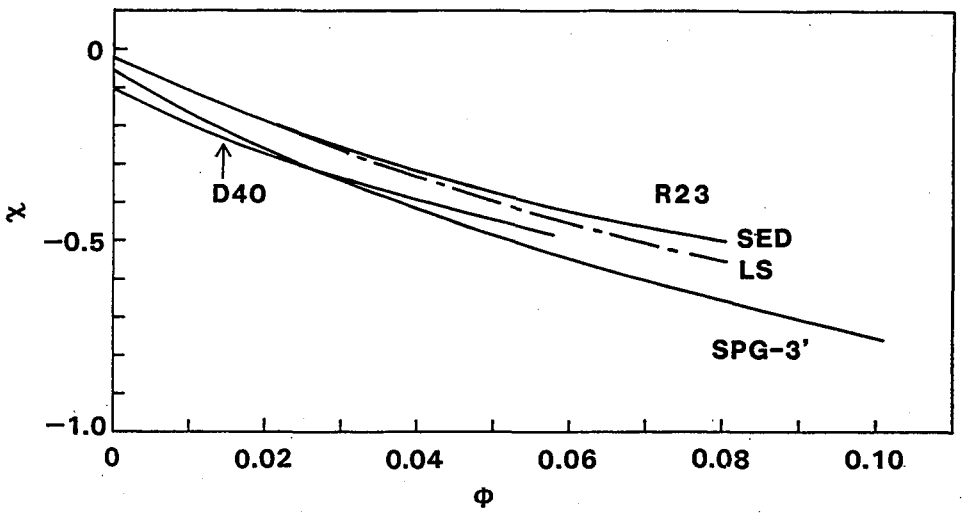

Figure 5.5 Plots of χ vs. ϕ for aqueous schizophyllan at 25°C. Solid curves, determined from sedimentation equilibrium data; dot-dash curve, from light scattering data.

given by Eq. (5.12) - (5.14). They fit the experimental data closely. It can be concluded from these findings that the system schizophyllan + water is not athermal in the framework of the Flory-Abe theory.

5-4-2 Comparison with Other Theories

The theory of Onsager[72] is concerned with an imperfect gas of cylindrical particles, and should be valid for long cylinders in dilute solution. Its validity at higher concentration is skeptical, because of the use of a free energy expression linear in ϕ. Note that no such limitation exists in the Flory theory.[78,80] Various attempts have been made to extend the Onsager theory to higher concentration.[74-77,114] Recently, Cotter[77] has modified the Onsager theory using the scaled particle theory[115] and Lasher's calculation for the phase boundary concentrations.[75] We here confine ourselves to the Onsager theory with no intermolecular interaction and the Cotter theory[77] in analyzing experimental data.

According to these theories, the excess chemical potential $\Delta\mu_0$ of the solvent is expressed in terms of the axial ratio x, the volume fraction ϕ, and the

molar volume V_p of the polymer as follows:

$$\Delta\mu_0 = - \frac{RTM_0v_0}{V_p} f(x, \phi) \qquad (5.16)$$

Different $f(x, \phi)$ are used by different authors. The theories of Onsager and Cotter give the same expression for the second virial coefficient:

$$A_2 = \left(\frac{3x^2 + 6x - 1}{3x - 1}\right)(v_p^2/V_p) \qquad (5.17)$$

It can be shown on the basis of the Onsager theory that for a polydisperse solute, the light scattering and sedimentation equilibrium second virial coefficients are related to M_w, whereas the osmotic one to M_n. However, there is no significant polydispersity effect on A_2 for moderately narrow distribution samples of high molecular weight, because A_2 is essentially independent of molecular weight except for low molecular weight. In addition, there is no method for evaluating the polydispersity effect on $\Delta\mu_0$ at higher concentration. Thus, it appears to be a reasonable first approximation to use the same type of average for V_p and x in Eq. (5.16) to compute theoretical values of $\Delta\mu_0$.

First, we used $M_n v_p$ for V_p and x_n given by Eq. (5.9) for x. In Figure 5.2 through 5.4 our schizophyllan data are compared with the predictions of the two theories under consideration; the theoretical curves indicated by the dot-dash lines (curves 1 and 2) are terminated at the respective A-points. The linear dependence predicted by the Onsager theory is not in agreement with the experimental data. On the other hand, the values calculated by the Cotter theory are rather close to the experimental data for sample SPG-3'. The theoretical values tend to deviate progressively upward from the data as the molecular weight is increased.

Secondly, we used $M_w v_p$ for V_p and x_w calculated by Eq. (5.9) with M_w instead of M_n for x. We found deviations of the theoretical values from the experimental data for $[\partial \Delta\mu_0 / \partial \phi]_x$ (x = LS, SED) similar to those noted above.

Kubo and Ogino[26,27] showed their osmotic pressure data for the system poly(γ-benzyl L-glutamate) + dimethylformamide to agree with the prediction of the Cotter theory, when x was calculated from A_2 by Eq. (5.17) with $V_p = M_n v_p$. The dashed curves (3 and 4) in Figure 5.2 - 5.4 represent the theoretical values calculated with x obtained in the same way. In contrast with the Kubo and Ogino case, no satisfactory agreement between theory and experiment is seen.

We compared $[\partial\Delta\mu_0/\partial\phi]_x$ (x = LS, SED) data with the theoretical values calculated with x obtained from A_2 by Eq. (5.17) with $V_p = M_n v_p$ to find no satisfactory agreement between theory and experiment.

Finally, we used $M_n v_p$ for V_p and x_w for x in $f(x, \phi)$, which was calculated by $x_w = M_w/(M_L d)$ with d = 2.6 nm, hydrodynamic diameter of the schizophyllan triple helix.[84,85] The values of $[\partial\Delta\mu_0/\partial\phi]_{Mn}$ computed by the Cotter theory[77] with x thus obtained are shown in Figure 5.6. The agreement between theory and experiment is excellent. However, it must be noted that the experimental ϕ_A for D40 is 1.7 times as large as the theoretical ϕ_A. This discrepancy cannot be attributed to chain flexibility, against the argument of Kubo and Ogino,[26,27] since the triple helix in this range of molecular weight is completely rigid.[84,85] Thus, the above agreement between calculated and experimental values of $[\partial\Delta\mu_0/\partial\phi]_{Mn}$ does not necessarily support the validity of the Cotter theory. A similar

discrepancy in the phase boundary concentration is also seen in the analysis of Kubo and Ogino. In conclusion, neither Onsager theory nor Cotter theory can explain our data quantitatively.

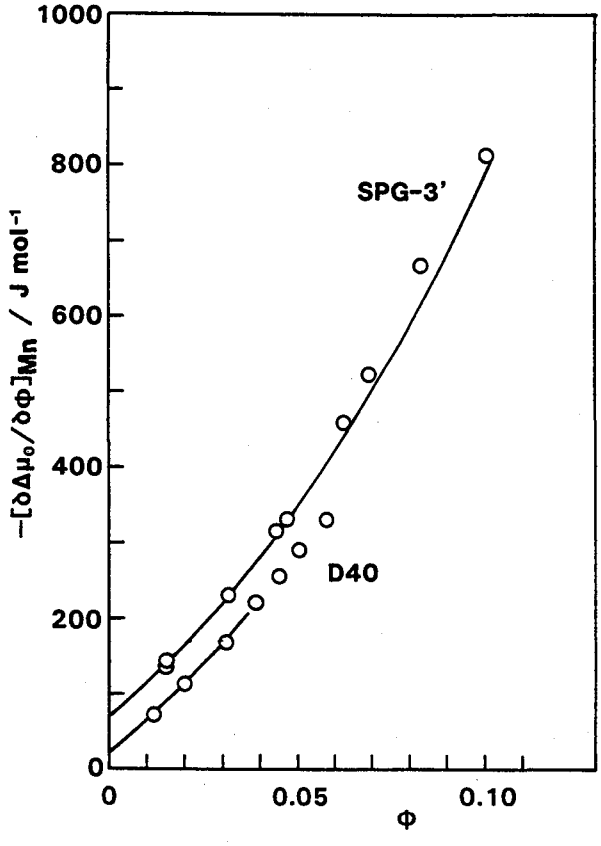

Figure 5.6 Dependence of $-[\partial\Delta\mu_0/\partial\phi]_{Mn}$ on ϕ for isotropic solutions of samples D40 and SPG-3' at 25°C. Solid curves, calculated from the modified Cotter theory with x = 85.4 for D40 and x = 28.5 for SPG-3'.

5-4-3 Chemical Potential in the Biphasic Region

When centrifuged at a rotor speed above 2000 rpm, an aqueous solution of sample D40 in the biphasic region separated into two layers, isotropic and cholesteric phases. Observation by a schlieren optical system revealed that the isotropic phase appeared on top of the cholesteric phase with a wide meniscus between the two phases. The volume ratio of the two phases changed very gradually with time, suggesting that it would take quite long to attain the true equilibrium state. It was always possible to observe a schlieren pattern in the isotropic phase, and dn/dr was extrapolated to the meniscus between the two phases, r_m.

Figure 5.7 shows $r\omega^2/(dn/dr)$ at r_m plotted against $\omega^2 t$ at different overall concentrations ϕ^o, where t is the time from the start of a centrifugation. It can be seen that within a relatively short period of time $r\omega^2/(dn/dr)$ reaches an equilibrium value which does not depend appreciably on ϕ^o. From these equilibrium values of $r\omega^2/(dn/dr)$, $[\partial\Delta\mu_0/\partial\phi]_{SED}$ at r_m were calculated on the assumption that $w(r_m)$ equals the A-point concentration at 30°C, i.e., $w(r_m) = 0.097$. The numerical results obtained are summarized in

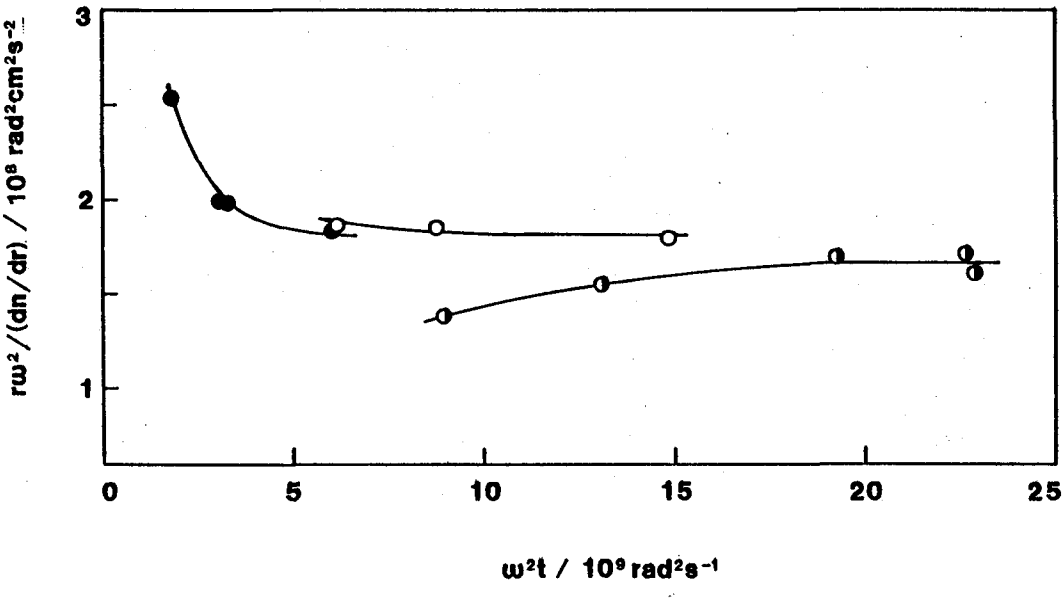

Figure 5.7 Plots of $r\omega^2/(dn/dr)$ vs. $\omega^2 t$ for the isotropic phase in biphasic mixture with different overall concentration ϕ^o. Unfilled circles, ϕ^o = 0.0678, the rotor speed = 2980 rpm; filled circles, ϕ^o = 0.0719, 1980 rpm; half-filled circles, ϕ^o = 0.0805, 2200rpm.

Table 5.5. Note that they satisfy the requirement that $[\partial\Delta\mu_0/\partial\phi]_{SED}$ should be independent of the rotor speed.

It was possible to observe schlieren patterns of the cholesteric phase for two solutions of higher concentrations. Values of $[\partial\Delta\mu_0/\partial\phi]_{SED}$ at the meniscus

Table 5.5

Sedimentation Equilibrium Data for

Biphasic Solutions of Sample D40 at 30 °C

w	ϕ^o	Rotor Speed / rpm	Isotropic phase: $\omega^2 r_m/(dn/dr)$ / 10^8 rad^2 cm^2 sec^{-2}	Isotropic phase: $-[\partial\Delta\mu_0/\partial\phi]_{SED}$ / J mol^{-1}	Cholesteric phase: $\omega^2 r_m/(dn/dr)$ / 10^8 rad^2 cm^2 sec^{-2}	Cholesteric phase: $-[\partial\Delta\mu_0/\partial\phi]_{SED}$ / J mol^{-1}
0.1001	0.0644	2200	1.79_1	372	-	-
0.1055	0.0678	2980	1.78_9	371	-	-
		5560	1.81_2	376	-	-
0.1115	0.0719	1980	1.81_0	376	-	-
		2980	1.84_3	382	-	-
		5560	1.79_0	371	-	-
0.1192	0.0771	2200	-	-	0.92_0	262
0.1242	0.0805	2200	1.68_0	349	0.86_0	245

in the cholesteric phase were determined by assuming that $w(r_m)$ in the cholesteric phase was equal to the B-point concentration, 0.129 (Chapter 6). The numerical results are also given in Table 5.5.

Figure 5.8 shows $[\partial\Delta\mu_0/\partial\phi]_{SED}$ at the meniscus plotted against ϕ^o, where the arrows A and B indicate the A- and B-points, respectively. It can be seen that, in either phase, $[\partial\Delta\mu_0/\partial\phi]_{SED}$ is almost constant;

$[\partial\Delta\mu_0/\partial\phi]_{SED}$ = -375 J mol^{-1} in the isotropic phase and -250 J mol^{-1} in the cholesteric phase. If it is assumed that the chemical potential of the solvent does not depend appreciably on temperature, these data may be compared with those for isotropic solutions at 25°C. Figure 5.3 shows that the latter can be smoothly extrapolated to the meniscus value (vertical segment).

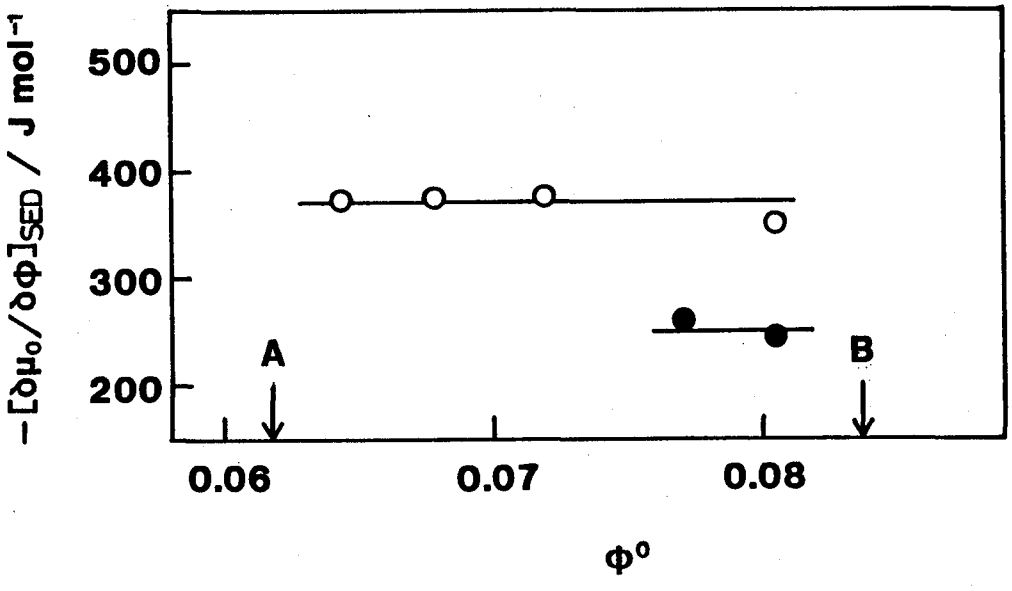

Figure 5.8 Plots of $-[\partial\Delta\mu_0/\partial\phi]_{SED}$ vs. ϕ^o for biphasic mixtures at 30°C. Unfilled circles, isotropic phase; filled circles, cholesteric phase.

Integration of $[\partial\Delta\mu_0/\partial\phi]_{Mn}$ by ϕ along with the meniscus value and Eq. (5.12) provides $\Delta\mu_0$ as a function of ϕ; the result is shown in Figure 5.9. The thin curve represents the Flory theory with the non-vanishing χ given by Eq. (5.12). The agreement between theory and experiment is only qualitative for both $\Delta\mu_0$ and the phase boundary concentrations.

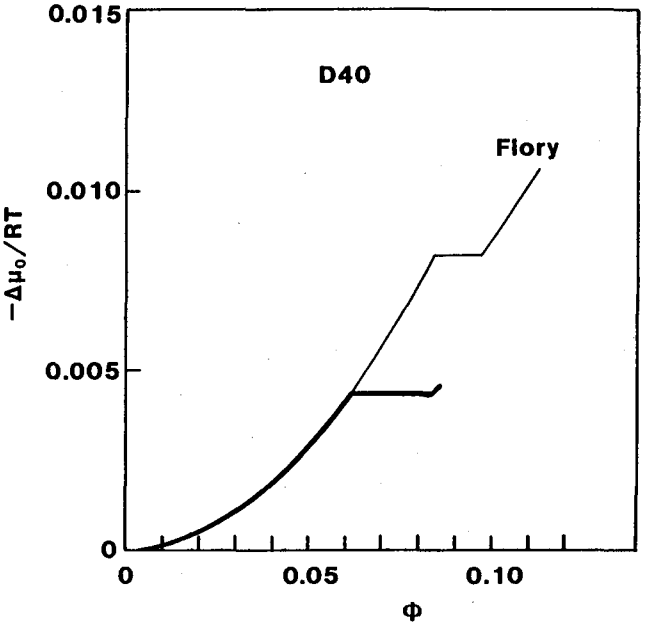

Figure 5.9 Excess chemical potential $\Delta\mu_0$ of the solvent as a function of ϕ for sample D40. Thick solid curve, experiment; thin curve, the Flory theory.[78]

Chapter 6

ISOTROPIC-LIQUID CRYSTAL PHASE EQUILIBRIUM

6-1 Introduction

As described in Chapter 3, an aqueous solution of schizophyllan forms a cholesteric mesophase above a certain concentration. There is an intermediate range of concentration, where isotropic and cholesteric phases coexist at equilibrium. In this chapter, we take up this phase equilibrium in detail. In order to obtain the temperature-concentration phase diagram, two new methods were applied to the present system: one using the concentration dependence of the cholesteric pitch as a function of temperature and polymer concentration, and the other, a sedimentation analysis of solutions consisting of the isotropic and cholesteric phases at equilibrium. The former method was effective for determining the B-point, which otherwise, was not easy to be determined accurately.[14,21]

Recently, Itou[116] obtained similar phase

equilibrium data for samples with different molecular weights by using these same methods. All the results, combined with the thermodynamic data described in chapter 5, are used to test theoretical predictions for rodlike polymers.

6-2 Results

6-2-1 Cholesteric Pitch

Aqueous solutions of schizophyllan sample D40 filled in drum-shaped cells were kept at 30°C for several weeks and examined by polarizing microscopy and laser light diffraction, first at 30°C. Rough estimate on the basis of microscopic observation showed that the solutions were isotropic below w = 0.0975, biphasic between 0.0975 and 0.127, and liquid crystalline above 0.127.

The biphasic solutions looked considerably turbid. When one of such solutions with w not too close to the boundary values was left standing at a fixed temperature, e.g., 30°C, it separated into two layers. Figure 6.1 shows a photomicrograph of the boundary between the two layers in such a biphasic mixture. The lower layer is filled with fingerprint

Figure 6.1 Photomicrograph of a two-phase solution of sample D40 with w = 0.101 at 30°C. Unless specified, w denotes the overall concentration of a solution.

patterns and the upper one contains many spherulites or small domains of fingerprint patterns buried in a dark area of the isotropic phase. It should be remarked that complete separation into the two phases never occurred on standing but was possible only by centrifugation as will be illustrated below.

When illuminated by laser light without polars,

the lower layer showed a diffraction ring. The S value for this layer was determined from the diffraction pattern according to the procedure described in Chapter 2. For both layers, S was also obtained directly from their photomicrographs. It was found that S was substantially the same in both layers. Therefore, for the biphasic solutions, S was determined mainly from the photographs. For liquid crystal solutions, both the microscopic and diffraction measurements were made to determine S.

Figure 6.2 shows a plot of S vs. w for D40 at $30^{o}C$, where half-filled and unfilled circles represent the data for the biphasic and cholesteric solutions, respectively; the latter data are reproduced from Figure 3.5. It can be seen that in either of the two concentration regions, the data points follow a smooth line but that the entire S vs. w relationship is represented by a smooth curve with a break point.

Solutions containing a liquid crystal phase had viscosities higher than 5 kg $m^{-1}s^{-1}$ at $30^{o}C$. Thus it seemed that, when the temperature was changed suddenly, it would take some time before the liquid crystal phase adjusted itself to a new equilibrium state.

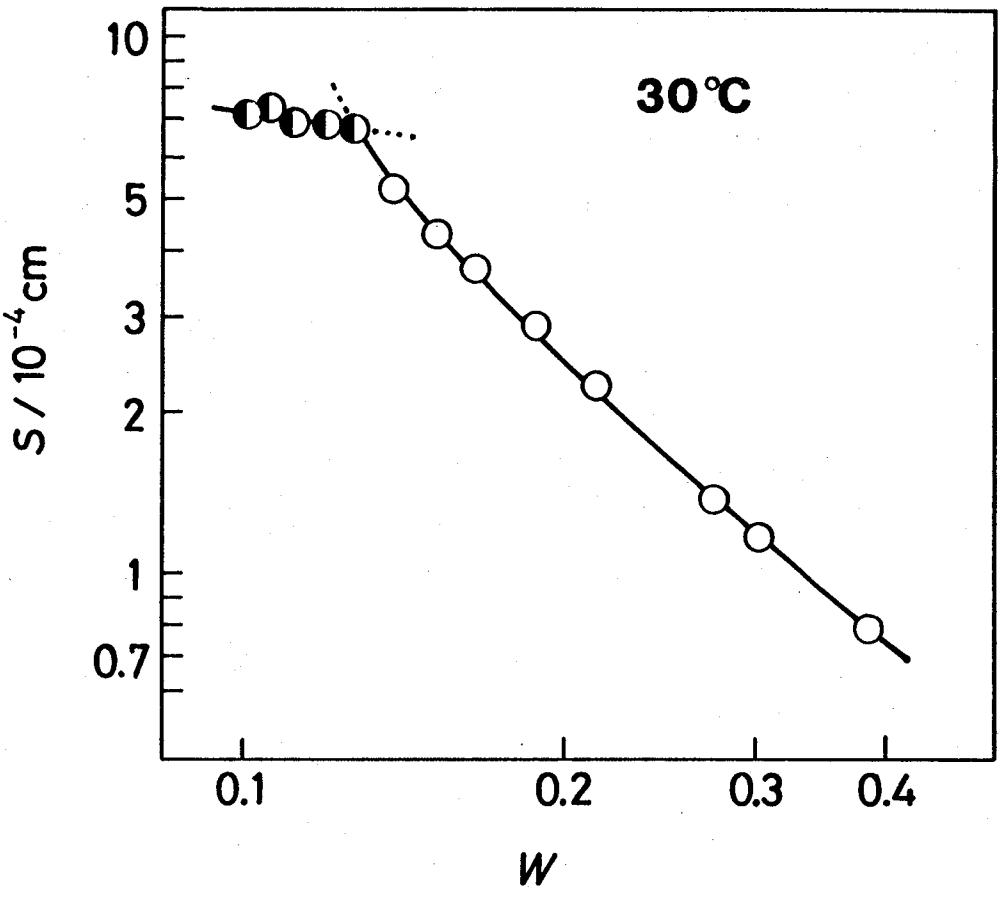

Figure 6.2 Plot of S vs. w for sample D40 in water at 30°C. Unfilled circles, the cholesteric region; half-filled circles, the biphasic region.

This time effect was examined by measuring S as a function of the time elapsed after the temperature change. Figure 6.3 illustrates typical results with

w = 0.165, where the arrows indicate the changes in temperature. From these and similar results at other concentrations, we conclude that the values of S after three days may be regarded as the equilibrium values.

Similar measurement of S was made at different

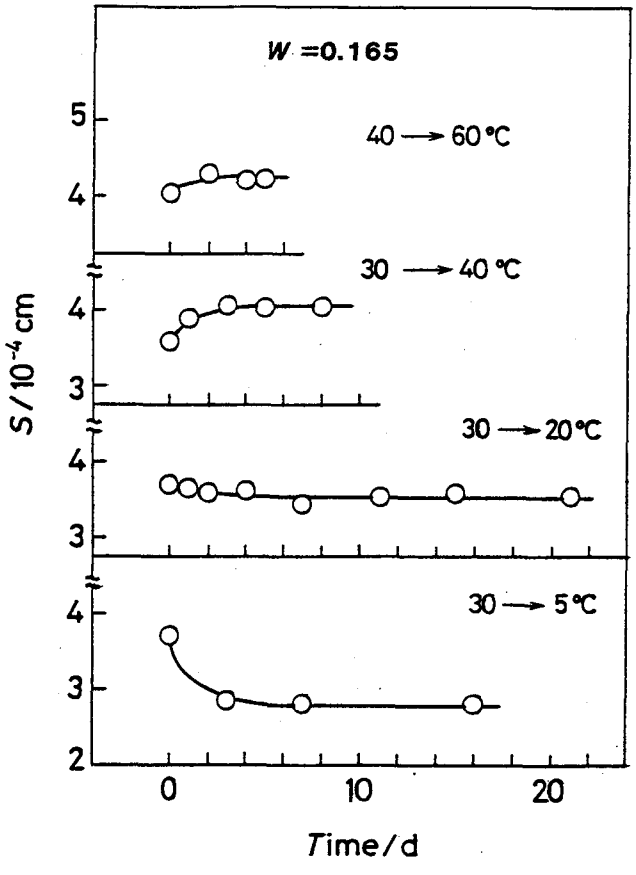

Figure 6.3 Variation in S with the time elapsed after the temperature jump for sample D40, w = 0.165.

concentrations and temperatures. The results are summarized in Table 6.1, where the data above dashed lines are for biphasic solutions and those below the lines are for cholesteric solutions.

In some cases at higher temperature, S appeared to be too small for the condition examined, suggesting that the solution was concentrated probably due to evapolation of water from the inlet tube sealed. Then the inlet tube of the cell containing such a solution was sealed off again and S was redetermined at 30°C. The S values thus redetermined are given in parentheses in Table 6.1. The concentrations of the solutions were recalculated from these S values by using the S vs. w relationship established with other data at 30°C and the solutions were subjected to further measurement.

After being examined at a series of different temperatures, each solution was examined again at 30°C, and it was found that S was the same within $\pm$3 % before and after the heating cycle. Thus, we conclude that S is a unique function of temperature T and w for a given schizophyllan sample. Figure 6.4 shows plots of S vs. w with the data at 5 and 60°C. It can be

Table 6.1

Spacing S as a Function of

Polymer Weight Fraction w and Temperature T

w	T / °C 5	20	30	40	60	80
0.098	7.1_6	$7.7_5 \pm 0.2$	-	-	-	-
0.100	6.5_8	$7.8_2 \pm 0.2$	-	-	-	-
0.101	-	-	$7.1_1 \pm 0.7$	-	-	-
0.106	6.4_0	$7.2_4 \pm 0.2$	7.4_4	7.2_4	-	-
0.112	6.2_2	6.8_0	$6.9_4 \pm 0.3$	7.0_4	$6.8_8 \pm 0.3$	-
0.120	5.7_2	$6.0_9 \pm 0.4$	$6.9_4 \pm 0.3$	6.9_1	$6.9_4 \pm 0.3$	$6.7_3 \pm 0.3$
0.127	$4.8_0 \pm 0.2$	6.4_4	$6.7_5 \pm 0.1$	6.8_0	$6.6_2 \pm 0.2$	-
0.134*	$4.6_1 \pm 0.2$	-	$(5.8_3 \pm 0.1)$	$6.0_5 \pm 0.1$	$6.5_9 \pm 0.1$	6.4_3
0.137*	-	-	(5.4_2)	-	-	6.0_1
0.139	-	5.2_5	5.2_1	-	-	-
0.140*	-	-	(5.2_3)	-	-	$6.4_3 \pm 0.6$
0.152	-	-	4.3_0	-	4.9_2	$5.7_0 \pm 0.1$
0.165	2.8_2	3.6_2	3.6_9	$3.9_9 \pm 0.1$	4.2_4	-
0.181	$2.5_2 \pm 0.1$	$2.8_8 \pm 0.1$	2.8_9	3.1_0	-	-
0.182*	-	-	(2.9_9)	-	-	$4.0_4 \pm 0.2$
0.215	1.8_0	$2.1_7 \pm 0.1$	2.2_3	$2.3_4 \pm 0.1$	2.5_7	-
0.224*	-	-	(2.0_0)	-	-	2.6_4
0.243*	-	-	(1.7_1)	-	2.0_1	-
0.251*	-	-	(1.6_3)	1.7_1	-	2.3_3
0.274*	1.2_2	1.5_0	(1.3_6)	-	-	-
0.302	-	-	1.1_7	-	1.3_3	1.5_4
0.388	-	0.7_9	0.7_9	0.9_1	0.9_9	1.0_9

* Concentrations determined from the S values at 30 °C as described in the text.

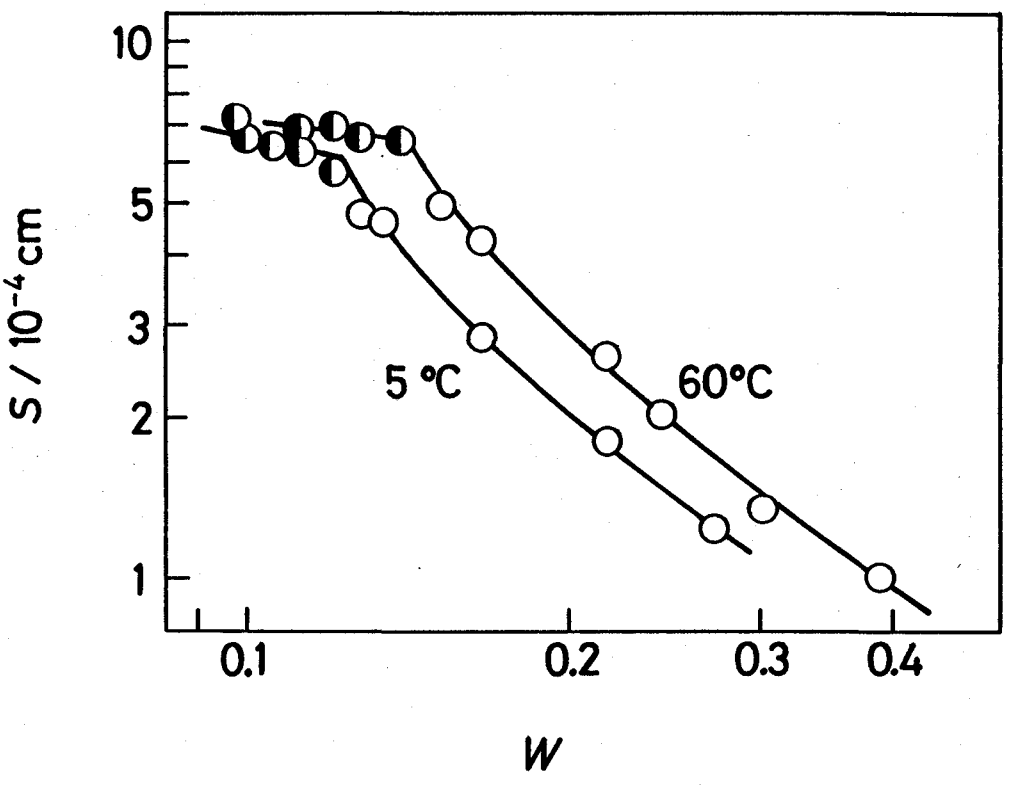

Figure 6.4 Plots of S vs. w for sample D40 at 5 and 60°C.

shown that the data at other temperatures as well as at these temperatures have essentially the same feature as that at 30°C illustrated in Figure 6.2.

Figure 6.5 shows the temperature dependence of S at the indicated concentrations. It can be seen that S is almost constant except 5°C for the biphasic

solutions, but, for the liquid crystal solutions, it increases almost linearly with raising temperature. Thus, irrespective of concentration, the schizophyllan liquid crystal has a positive temperature coefficient, i.e., $dS/dT > 0$.

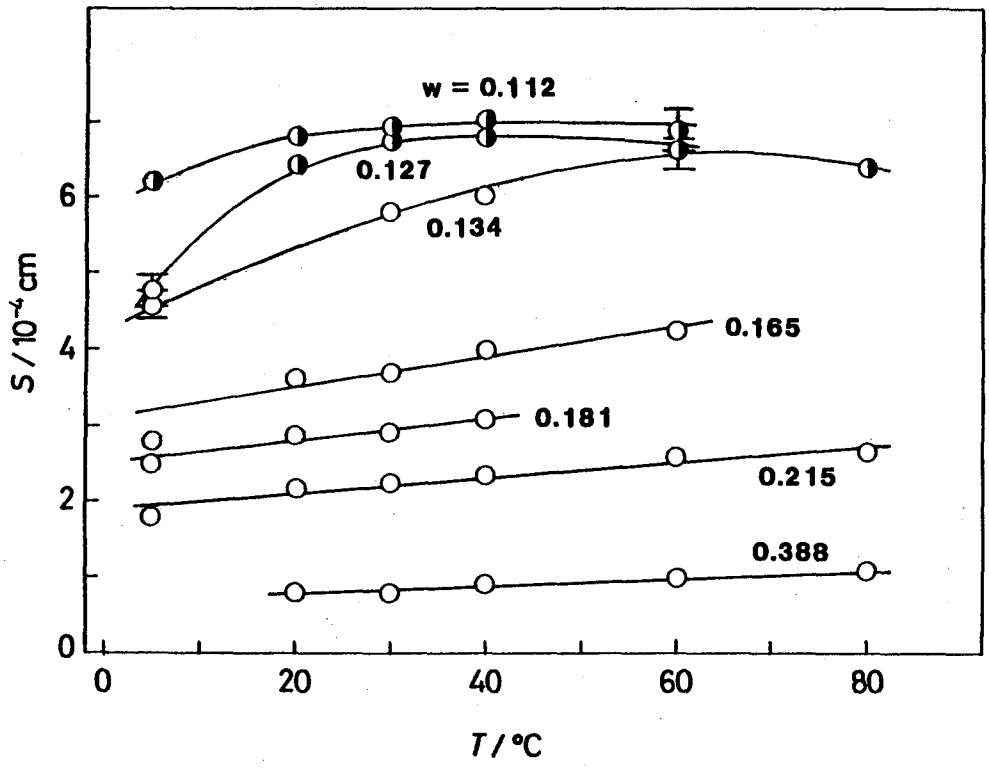

Figure 6.5 Temperature dependence of S for aqueous solutions of sample D40 with indicated concentrations. Unfilled circles, the cholesteric region; half-filled circles, the biphasic region.

Effects of temperature on cholesteric pitch have been studied extensively for polypeptide liquid crystals.[28,31-33] The results from such studies show that the sign of dS/dT is related to the handedness of the liquid crystal. That is, it is positive for a cholesteric structure of the positive sense, and vice versa. As shown in Chapter 4, the schizophyllan liquid crystal is right-handed, i.e., its sense is positive. Therefore, the positive dS/dT found above may be related to this right-handed structure.

6-2-2 Phase Diagram

The data for the concentration dependence of S presented above show the following features.

(1) S is substantially constant in the biphasic region.

(2) S decreases monotonously with increasing concentration in the cholesteric region.

(3) The entire S vs. w curve has a clearly defined break point.

The feature (1) may be anticipated if a biphasic solution is to separate into two phases of fixed concentrations irrespective of the total concentration.

On the other hand, the feature (2) results from the fact that S is essentially determined by the concentration in the cholesteric phase. Thus, the feature (3) naturally follows from the features (1) and (2), and hence the break point of the S vs. w curve can be identified as the boundary between the biphasic and cholesteric regions, i.e., the B-point, w_B.

Table 6.2

B-point Concentrations w_B Determined from the S-w Relationship at Various Temperatures

$\frac{T}{^oC}$	w_B
5	0.123 ± 0.001
20	0.127 ± 0.001
30	0.129 ± 0.001
40	0.132 ± 0.001
60	0.141 ± 0.001
80	0.150 ± 0.001

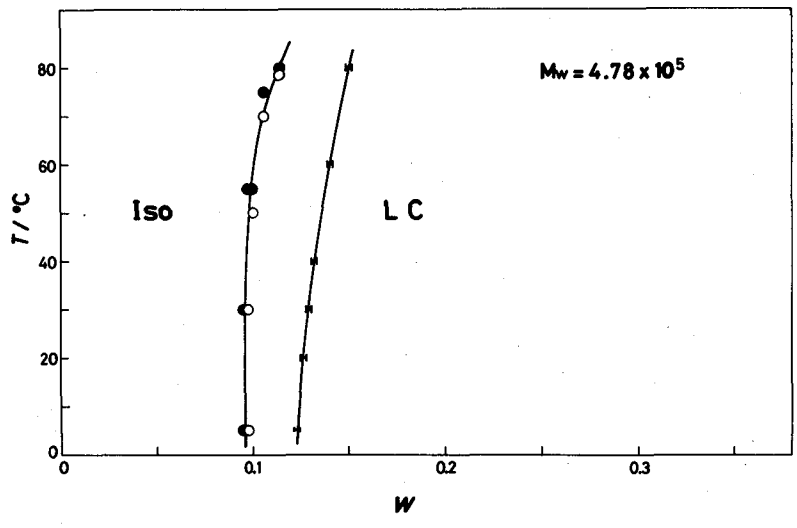

Figure 6.6 Temperature-concentration phase diagram for the system sample D40 + water. Horizontal segments, uncertainties associated with the graphical determination; filled circles, the isotropic region; unfilled circles, the biphasic region.

The values of w_B determined in this way at different temperatures are summarized in Table 6.2. The phase boundary curve extending from 5 and 80°C obtained from these results is shown in Figure 6.6, where horizontal segments indicate the uncertainty associated with the graphical determination. It was

found that the cholesteric liquid crystal region extends at least up to 38.8 wt%.

The boundary between the isotropic and biphasic regions, i.e., the A-point, was determined as follows. First, a solution with an overall concentration w as prepared or stored for a long time period at a specified temperature T was examined by a polarizing microscope so as to prove it to be isotropic. This set of w and T gives one data point in the isotropic region and is indicated by a filled circles in Figure 6.6. Next, a slightly more concentrated solution was examined at the same temperature to prove it to be birefringent. This set gives another data point for the same temperature in the biphasic region and is represented by an unfilled circle. The phase boundary at T can thus be located between these two data points. The numerical results are summarized in Table 6.3.

The existence of a temperature-induced isotropic-cholesteric phase transition was found as follows. The solution with w = 0.0975 was biphasic at 30^{o}C. When the temperature was raised, it became progressively isotropic. It was observed that some regions of the

Table 6.3

A-point Concentrations w_A and Temperatures T_A Determined from Microscopic Observations

w	$\frac{T_A}{^oC}$	$\frac{T}{^oC}$	w_A
0.097_5	30 - 55	5	0.095_0 - 0.097_5
0.100	50 - 55	20	0.095_0 - 0.097_5
0.106	71 - 75	30	0.095_0 - 0.097_5
0.114	78 - 80	60	0.100 - 0.106

solution resisted more strongly higher temperature than others, and the final traces of the cholesteric phase remained up to a temperature as high as 55°C. When cooled, the solution still remained isotropic at 40°C but was found distinctly biphasic again at 30°C. Thus the phase boundary temperature should be around 40°C but no precise determination could be made.

Similar experiments were conducted with other solutions. These results are also summarized in Table 6.3 and included in Figure 6.6. It can be seen that

the higher the overall concentration, the smaller the gap between the unfilled and filled circles for the same w. In spite of the large temperature gaps at the lower concentrations, the A-point curve can be determined with reasonable accuracy, since it is almost vertical.

6-2-3 Centrifugal Analysis of Phase Separation

As remarked in the subsection 6-2-1, no biphasic mixture separated completely into the two phases on standing. However, when centrifuged on a Beckman-Spinco Model E Ultracentrifuge, such a mixture separated into two distinct layers. The isotropic phase appeared on top of the cholesteric phase with a relatively wide meniscus between them. The volume Φ of the isotropic phase relative to the total solution volume was estimated from the height of this phase relative to the total solution height.

To examine the effect of centrifugal field on the phase separation, experiments were made at different rotor speeds and duration t of centrifugation. Figure 6.7 shows plots of Φ vs. $\omega^2 t$ for four solutions, where ω is the angular velocity. It can be seen that

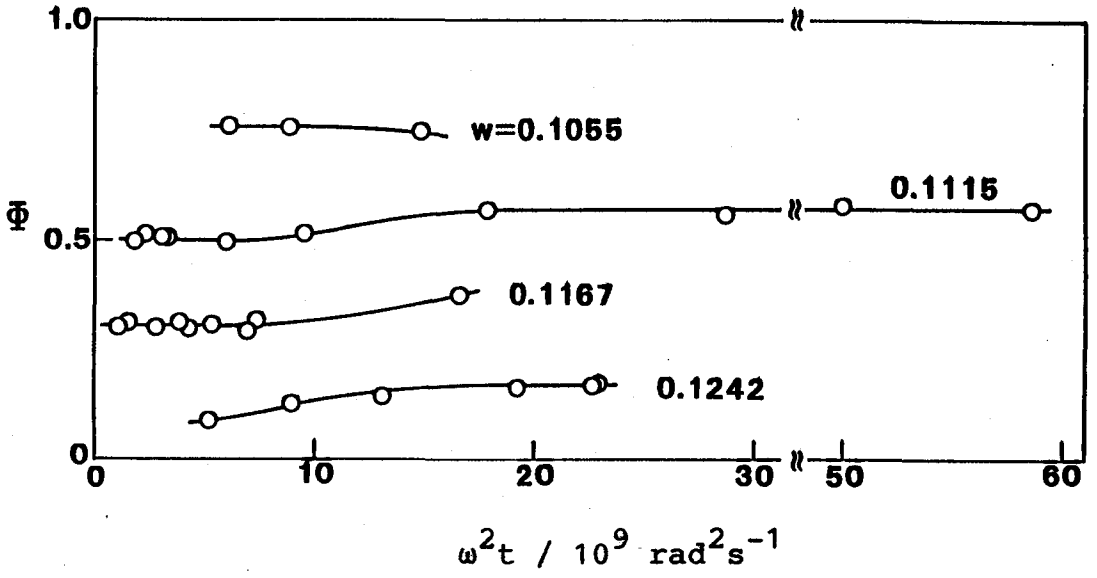

Figure 6.7 Dependence of the volume Φ of the isotropic phase relative to the total solution volume on $\omega^2 t$ for biphasic solutions with indicated concentrations at 30°C. Sample, D40.

Φ stays almost constant for $\omega^2 t$ lower than 9×10^9 $rad^2 s^{-1}$, changes gradually above that, and finally approaches another constant value.

This change in Φ may be explained as follows. Before the centrifugation, the mixture was kept at 30°C to attain a microscopic phase separation. Therefore, the system separated into the respective

phases at the initial stage of centrifugation. However, prolonged centrifugation tended to transform the system into another equilibrium state. This transformation may be a very slow process, because it should be accompanied by a redistribution of the components between the two phases. Therefore, we regard the ϕ values at $\omega^2 t$ smaller than 9×10^9 $rad^2 s^{-1}$ as not being disturbed by the centrifugal field. At this low centrifugal field, the redistribution of the polymer species in either phase was negligible. The undisturbed Φ values thus obtained are given in Table 6.4.

If it is assumed that the phase separation takes place according to the lever rule as in a binary solution, Φ should be linearly related to the overall concentration c of the polymer by

$$\Phi = (c_B - c)/(c_B - c_A) \qquad (6.1)$$

where c_A and c_B stand for the mass concentrations corresponding to the A-point and B-point, respectively. Recently, Flory and Frost[81,82] investigated theoretically biphasic equilibria in athermal solutions of polydisperse rodlike polymers. It can be shown

Table 6.4

Data of Sedimentation Equilibrium Measurements for D40 Solutions at 30 °C

w	$\frac{c^{a}}{g\ cm^{-3}}$	Φ	$\frac{c_A\ \&\ c_B{}^{b}}{g\ cm^{-3}}$
-	-	1	$0.101_2 \pm 0.001$
0.1001	0.103_7	$0.937 \pm 0.03_7$	-
0.1055	0.109_6	0.75_5	-
0.1115	0.116_1	0.50_0	-
0.1167	0.121_7	0.30_0	-
0.1192	0.124_5	0.20_0	-
0.1242	0.129_9	0.08_5	-
-	-	0	$0.130_5 \pm 0.001$

[a] Concentrations calculated from w by the equation $c = w/v$; $v = 1.003 - 0.384w + 0.03w^2$

[b] c_A and c_B were obtained by extrapolating the line in Figure 6.8 to $\Phi = 0$ and 1, respectively.

that their numerical results, when recast in the form of Eq. (6.1), predict Φ decreasing approximately linearly with c for a polymer solute with the Poisson distribution in size. Polymers having the most probable distribution do not obey Eq. (6.1). In the case of the Gaussian distribution, Eq. (6.1) holds provided that the breadth of the distribution is not large.[83,118] Thus, we may use this equation to analyze experimental phase separation data provided that the samples are not too broad in molecular weight distribution. Indeed, Conio et al. applied Eq. (6.1) to their phase separation data for poly (benzamide) solution.[119]

Figure 6.8 shows the above Φ data for D40 at 30°C. plotted against c, according to Eq. (6.1). The data points indicated by unfilled circles are scattered around the solid line, which may be extrapolated to $\Phi = 0$ and 1 to give $c_B = 0.131$ g cm^{-3} and $c_A = 0.101$ g cm^{-3}, respectively. These values are compared favorably with the phase boundary concentrations found on the phase diagram in Figure 6.6 (indicated by arrows A and B). Thus, the lever rule holds at least approximately for the schizophyllan - water system,

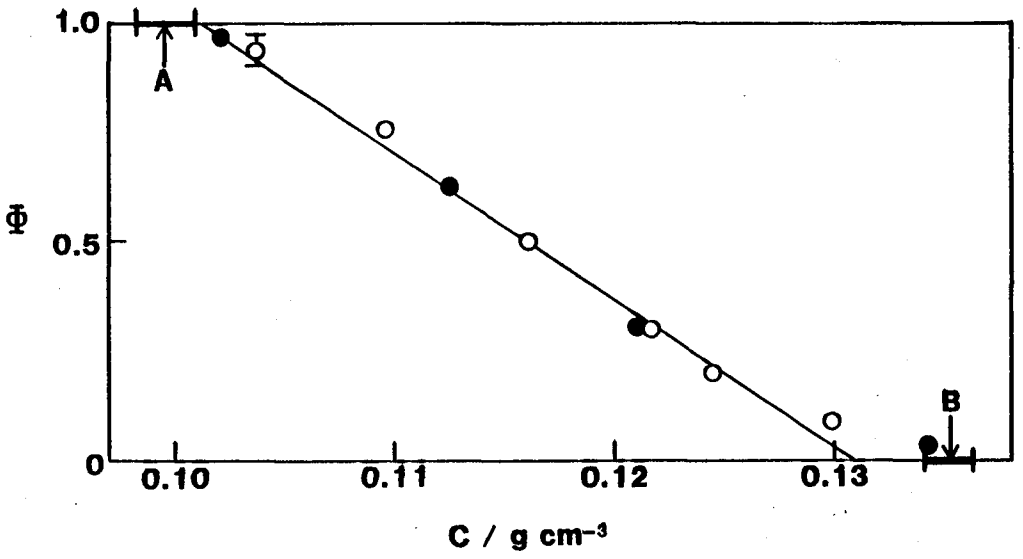

Figure 6.8 Φ plotted against the overall mass concentration c for sample D40. Unfilled circles, data at 30°C; filled circles, at 25°C.

although the sample is not monodisperse.

According to the procedure described in Chapter 2, phase separation was studied alternatively by centrifuging a biphasic mixture in a calibrated tube at 25°C and analyzing each of the separated phases for the volume and the average concentration and molecular weight of the polymer contained. The results obtained are summarized in Table 6.5. Here

and in what follows, the quantities with a prime and a double prime refer to the isotropic and cholesteric phases, respectively, and those without prime to the original mixture.

Figure 6.9 illustrates how the quantities examined vary with ϕ. For either phase, the viscosity-average molecular weight differs from that of the original sample, increasing almost linearly with ϕ. This

Table 6.5

Data of Phase Separation Measurements for Biphasic Solutions of D40 at 25 °C

w	ϕ	Isotropic phase			Cholesteric phase			$\dot{M}_v''/M_v'$
		w'	$[\eta]'$ / 10^2 cm^3 g^{-1}	M_v' / 10^4 g mol^{-1}	w''	$[\eta]''$ / 10^4 cm^3 g^{-1}	M_v'' / 10^4 g mol^{-1}	
-	-	0.097*	$4.6_0 \pm 0.04$*	$4.1_4 \pm 0.04$*	-	-	-	-
0.098_7	$0.096_8 \pm 0.03$	0.097_3	4.58	4.13	-	-	-	-
0.108_4	0.62_1	0.099_4	4.23	3.9_2	0.121	5.22	4.5_2	1.1_5
0.116_3	0.30_0	0.102	3.83	3.7_0	0.121	4.84	4.2_8	1.1_6
0.128_5	0.03_0	-	-	-	0.128_5	4.67	4.1_7	-
-	0	-	-	-	0.128*	4.68*	4.1_9*	-

* Values extrapolated to $\phi = 0$ or $\phi = 1$

indicates that molecular weight fractionation takes place on the phase separation. All these findings

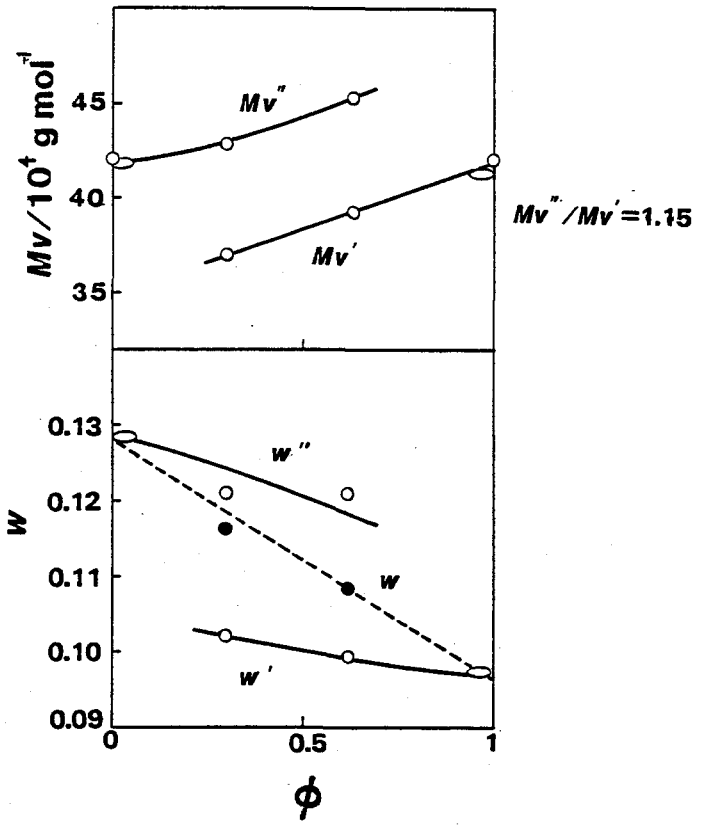

Figure 6.9 Phase separation data for sample D40 at 25°C. Quantities with a prime, the isotropic phase; quantities with a double prime, the cholesteric phase; quantities without prime, the whole mixture.

are consistent with the theoretical predictions for athermal solutions of polydisperse rodlike polymers.[81-83,118] Similar fractionation effects have been reported for other polymer-solvent systems.[47,52,119]

The filled circles in Figure 6.8 represent the data for w at 25°C converted to c. Excellent agreement between the two sets of data is consistent with the almost vertical phase boundary curve shown in Figure 6.6.

6-3 Discussion

6-3-1 Phase Diagram

The phase diagram in Figure 6.6 is characterized by a narrow almost vertical biphasic region separating the isotropic region from the cholesteric region. The phase boundary curves tend to bend toward higher concentration at higher temperature. This phase diagram resembles those reported by Miller and coworkers[21,24,28] for poly(γ-benzyl L-glutamate) (PBLG) in dimethylformamide (DMF), except that it has no broad biphasic region at the bottom. A similar bent in the phase boundary curves has also been found

for the polypeptide solutions, and is explained in terms of the fact that the polypeptide helix becomes more flexible as the temperature is raised.[21,24] Figure 6.10 shows the temperature dependence of intrinsic viscosity of schizophyllan D40 in water, which suggests that the molecular dimension of schizophyllan decreases with increasing temperature. Therefore, we ascribe the bent phase boundary curves in Figure 6.6 to this increasing flexibility at higher temperature, as in the case of the polypeptide solutions.

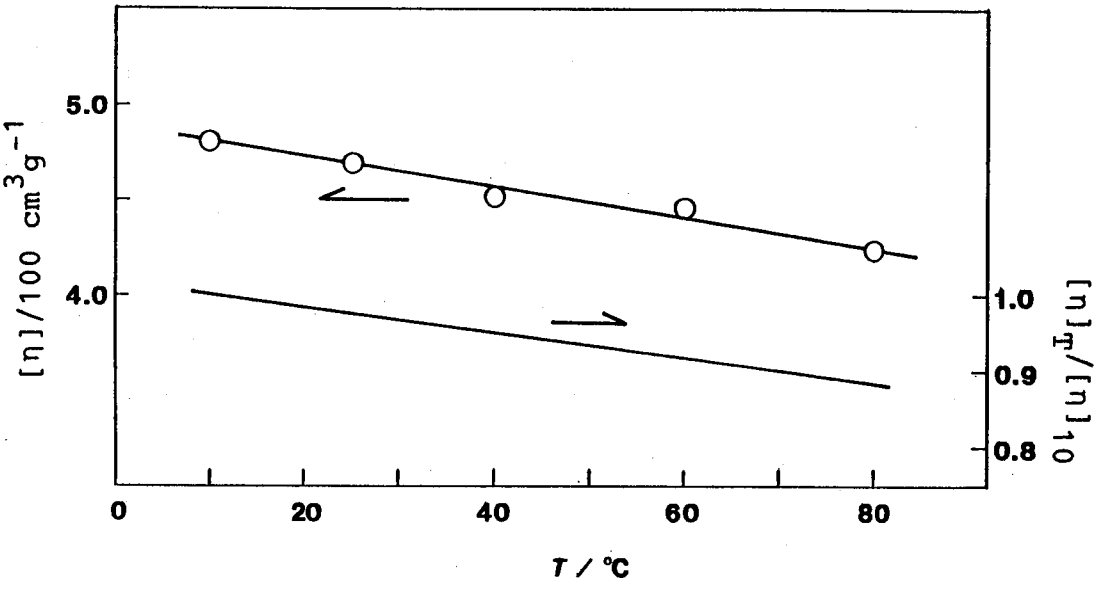

Figure 6.10 Temperature dependence of intrinsic viscosity for sample D40 in water.

Recently, Yanaki et al.[120] reported the formation of a cholesteric liquid crystal in aqueous solutions of scleroglucan, a triple-helical polysaccharide consisting of the same repeating unit as that of schizophyllan. Irrespective of concentration, an aqueous solution of scleroglucan became turbid when it was cooled below about 5°C.[121] Taking literally, this indicates that the phase diagram of aqueous scleroglucan has a broad immiscible region at lower temperature, probably biphasic one. According to the Flory theory,[78] such a biphasic region appears when the solubility of the polymer diminishes so that the interaction parameter becomes definitely positive (see Figure 1.2). Therefore, we consider at present that the difference in phase behavior between the two glucans is explained by the fact that scleroglucan is somewhat less soluble in aqueous media than schizophyllan.[122]

6-3-2 Theories of Rodlike Polymers by Flory and Onsager

Various theories[71-78,123] have been proposed to describe the isotropic-anisotropic phase equilibrium

for a solution of rodlike polymers. Here we consider the theory of Onsager[72] for straight cylinders and the lattice theory of Flory.[78]

Onsager was the first to show that molecular asymmetry alone is sufficient to produce a phase transition from isotropic to anisotropic. He treated a solution of rodlike polymers as an imperfect gas and predicted that the phase boundary concentrations should vary with the axial ratio x of the polymer as

$$\phi_A = 3.3/x, \qquad \phi_B = 4.5/x \tag{6.2}$$

where ϕ_A and ϕ_B are the A- and B-point concentrations, respectively, expressed in terms of the volume fraction of the polymer.

Flory developed a statistical thermodynamic theory of a solution of impenetrable rods by using a lattice model. According to his theory, the excess chemical potential $\Delta\mu_0$ of the solvent and that of the solute $\Delta\mu_1$ are described by the volume fraction ϕ, x, and the polymer-solvent interaction parameter χ. For the isotropic phase

$$\Delta\mu_0'/RT = \ln (1 - \phi') + (1 - 1/x)\phi' + \chi\phi'^2 \quad (6.3)$$

$$\Delta\mu_1'/RT = \ln (\phi'/x) + (x - 1)\phi' - \ln x^2 + \chi x(1 - \phi')^2 \quad (6.4)$$

and for the anisotropic phase

$$\Delta\mu_0''/RT = \ln (1 - \phi'') + \phi''(y - 1)/x + 2/y + \chi\phi''^2 \quad (6.5)$$

$$\Delta\mu_1''/RT = \ln (\phi''/x) = (y - 1)\phi'' + 2 - \ln y^2 + \chi x(1 - \phi'')^2 \quad (6.6)$$

where y is the disorientation index related to ϕ'' and x as

$$\phi'' = [x/(x - y)][1 - \exp (-2/y)] \quad (6.7)$$

As mentioned in Chapter 1, y varies from x (random order) to unity (perfect order).

The phase boundary concentrations ϕ_A and ϕ_B for the solution of hard rods with x can be calculated by

solving the simultaneous equations

$$\Delta\mu_0'(\phi') = \Delta\mu_0''(\phi''), \qquad \Delta\mu_1'(\phi') = \Delta\mu_1''(\phi'') \tag{6.8}$$

Flory and Ronca[123] and Cotter[77] have modified the Flory and Onsager theories, respectively. In either of the modified theories, the phase diagram is essentially the same as that of the original one but has a slightly narrower biphasic gap, i.e., smaller ϕ_B/ϕ_A, than that of the original one.

6-3-3 Comparison between Theory and Experiment

All the above-mentioned theories[71-78,123] for a solution of rodlike polymers predict that the anisotropy in shape of the polymer molecule is primarily responsible for the formation of a liquid crystal phase. Therefore, first we assume that our schizophyllan + water system is athermal and consider the Onsager theory[72] for straight cylinders and the Flory theory[78] for an athermal system, i.e., $\chi = 0$, neglecting possible difference between nematics and cholesterics.

The experimental phase boundary concentrations given in terms of the weight fraction were converted to the volume fraction by using Eq. (2.1). The schizophyllan triple helix was approximated by a straight cylinder with a diameter d = 1.67 nm and x was calculated from

$$x = M_w v_p / (N_A \pi d^3/4) \qquad (6.9)$$

Figure 6.11 shows a comparison between the theories and experiments using the data for aqueous schizophyllan at 25°C. Here, the filled circles represent the boundary concentrations ϕ_A between the isotropic and biphasic regions, i.e., A-point concentrations and unfilled circles represent those ϕ_B between the biphasic and cholesteric regions, B-point concentrations. The data points at x = 133 were obtained in this study and other data points were obtained by Itou[116] using the methods described in the previous section. The two pairs of solid curves represent the theoretical predictions for ϕ_A and ϕ_B. The curves for the Onsager theory were calculated from Eq. (6.2) and those for the Flory theory were

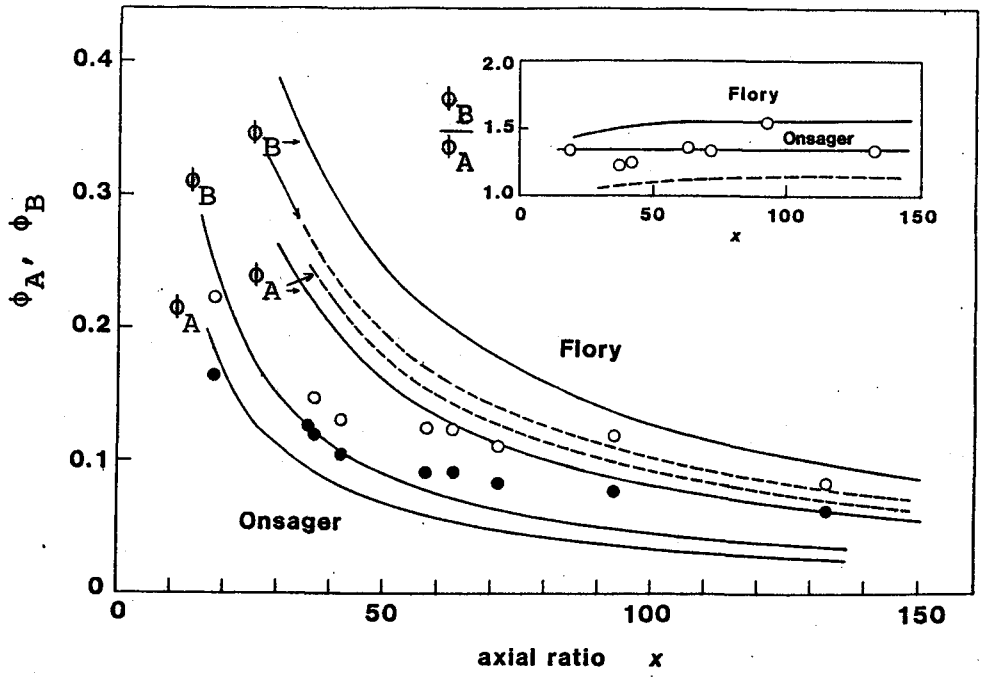

Figure 6.11 Plots of phase boundary concentrations vs. axial ratio x. Unfilled circles, the boundary between the biphasic and cholesteric regions; filled circles, the boundary between the isotropic and biphasic regions; data at x = 133, present study; other data, from Itou.[116] Theoretical predictions: solid curves, the Flory theory[78] and Onsager theory;[72] dashed curves, the Flory with non-vanishing χ (see the text).

calculated from Eq. (6.8) with Eq. (6.3)-(6.7) and $\chi = 0$.

It can be seen in Figure 6.11 that the data points for the two highest molecular weight samples are close to the Flory curves. However those for the other samples are significantly below these curves. On the other hand, when compared with the Onsager theory, the data points for the lowest molecular weight sample are close to the theoretical curves but those for other samples deviate upwards. As mentioned in Chapter 1, the phase diagram data for PBLG in DMF show a similar downward deviation from the Flory prediction at low molecular weight.

The insert in Figure 6.11 shows that the observed ratio ϕ_B/ϕ_A is smaller than the Flory value except that of the sample with x = 93. Itou showed that this sample was the broadest in molecular weight distribution. Thus, the larger value of ϕ_B/ϕ_A for this sample may be attributed to the broad distribution.

In the following we shall discuss possible causes of the discrepancy between theory and experiment mainly from an experimental point of view.

(1) Polydispersity. The theories cited above are concerned with monodisperse polymers, but the schizophyllan samples studied are polydisperse. The recent theories for polydisperse polymers predict a remarkable polydispersity effect on the phase diagram.[80-83,118] As shown in Figure 6.9 and Table 6.5, this prediction is qualitatively materialized in the experimental data. However, it has been shown[116,117] that most of the samples studied are reasonably well-fractionated as judged from the observed M_z/M_w and M_v''/M_v' close to unity except for the sample with x = 93. Therefore we conclude that the discrepancy is too large to be attributed only to samples' polydispersity.

(2) Flexibility. According to Norisuye's analysis of dilute solution data, the schizophyllan triple helix is represented by a wormlike cylinder with a persistence length as large as 200 nm.[84-86] The average number of Kuhn statistical segments per molecule, L/2q is about one half for the highest molecular weight sample, where L is the contour length of the triple helix. Thus, the triple helix is almost completely rigid and straight in the molecular

weight range studied here.

(3) Axial ratio and volume fraction. In the present analysis, the schizophyllan helix is approximated by a smooth hard-core cylinder with the volume equal to that calculated with $v_p = 0.619$ cm^3 g^{-1} and $M_L = 2140$ nm^{-1}; x, ϕ_A, and ϕ_B have been calculated on this assumption. It is also possible to take the hydrodynamic diameter[23,24] for d in Eq. (6.9) to evaluate x. However it was impossible to adjust the values of M_L and v_p within allowable ranges which would give rise to good agreement between theory and experiment over the entire molecular weight range.

(4) Athermal approximation. In the above discussion, we assumed that the schizophyllan solutions are athermal. As remarked in Chapter 5, aqueous schizophyllan is not strictly athermal. It is non-athermal in that the interaction parameter χ is finite and depends on ϕ. Therefore, we modify the Flory theory by replacing χ in Eq. (6.3) and (6.5) with $\chi(\phi')$ and $\chi(\phi'')$, respectively, and χ in Eq. (6.4) and (6.6) with $\chi_p(\phi')$ and $\chi_p(\phi'')$, respectively.

In Figure 5.5, we can see that $\chi(\phi)$ for sample SPG-3' at large ϕ is approximated by

$$\chi(\phi') = -0.26 - 4.7\phi' \qquad (6.10)$$

Therefore, $\chi_p(\phi')$ for this sample is obtained from Eq. (6.10) as

$$\chi_p(\phi') = -2.61 - 4.7\phi' \qquad (6.11)$$

For simplicity, we assume that these equations are valid irrespective of axial ratio and in the cholesteric region as well.

The dashed curves in Figure 6.11 represent the values of ϕ_A and ϕ_B calculated on this assumption; the difference in $\chi(\phi')$ and $\chi_p(\phi')$ among SPG-3', D40, and R23 was found to have negligible influence on the calculated phase diagram. It is indicated that the biphasic gap is narrower than that for the athermal case but the x dependence is essentially unchanged. Thus, consideration of non-vanishing interaction parameter does not solve the discrepancy.

In sum, the qualitative features of the theoretical predictions are substantiated in the present

experimental data. However, the schizophyllan data cannot be described quantitatively by the existing theories.

Chapter 7

OPTICAL PROPERTIES OF ISOTROPIC SOLUTION NEAR THE A-POINT

7-1 Introduction

As mentioned in Chapter 5, when a schizophyllan solution of the concentration just below the isotropic-biphasic boundary concentration, i.e., the A-point concentration w_A was cooled below the phase boundary temperature T_A, it became birefringent and separated a cholesteric phase. It is interesting to ask how does the cholesteric phase evolve from the isotropic solution.

Recently, Patel and DuPré[34] performed optical rotatory dispersion measurements on poly(γ-benzyl glutamate) solutions of concentrations just below w_A and observed a remarkable enhancement of optical rotatory power when the temperature was made close to T_A. They attributed this enhancement to the short-range ordering of the polypeptide helices, and called it a "pretransitional phenomenon." We therefore

thought it worthwhile to clarify whether the cholesteric phase evolved directly from the isotropic phase or there was an intermediate stage where some embryonic anisotropic domains appeared before phase separation; the latter may be identified with the "pretransitional phenomenon" of Patel and DuPré. As an experimental approach to this problem, we performed light scattering and ORD measurements on aqueous solutions of sample R23 near the A-point. These techniques were chosen because ORD is sensitive to chiral ordering as demonstrated by Patel and DuPré and light scattering may be sensitive to the presence of large objects.

7-2 Experimental

An aqueous solution of R23 of w slightly lower than 0.13 was prepared. This concentration was chosen because w_A for R23 at 25°C was estimated to be 0.130 from the phase diagram shown in Figure 6.11. The solution was stirred by a magnetic bar in an air bath thermostatted at 25°C for three days and purified by filtration followed by centrifugation. The filtration was performed under warm air by using the filtration device heated above 25°C. The filtered solution was

centrifuged in a light scattering cell at 25°C. It became clear except for the bottom part which appeared white and glittering.

An aliquot of the clear solution was transferred into an ORD cell 1 mm thick. A few drops of liquid paraffin was placed over the solution to prevent the evaporation of water. The cell was sealed by a ground stopper and kept at 25°C for later ORD measurement and microscopic observation. This solution is designated as solution ORD.

The solution remaining in the light scattering cell, referred to as solution LS, was used for light scattering measurement. Only a small bottom portion of the solution was glittering and well away from the light path. After completion of a series of measurements, a small volume of the clear solution, referred to as solution MIC, was taken up in a drum-shaped cell for microscopic observation, and the rest was used for concentration determination after dilution, yielding w = 0.1316. Figure 7.1 illustrates the actual experimental steps, where each arrow indicates how the temperature was changed at each step.

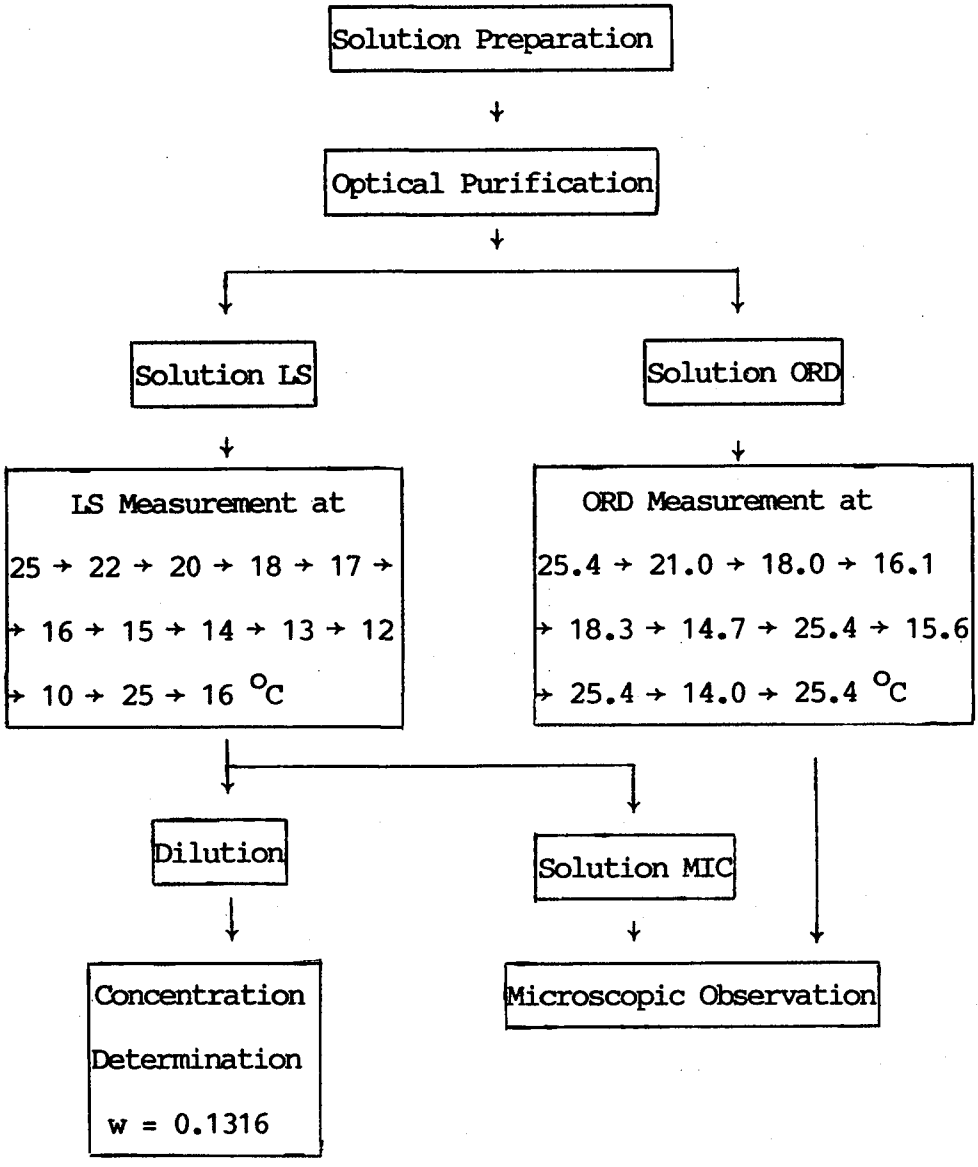

Figure 7.1 Experimental Steps

7-3 Results and Discussion

7-3-1 Microscopic Observation

After being confirmed to be completely isotropic, solutions ORD and MIC were kept at 18°C for 18 h and observed under a polarizing microscope. Spherulites were found to evolve gradually in both solutions. The solutions became clear again after being kept at 25°C for about two days. Then, solution MIC was cooled down to 18°C and after one h started evolving a trace amount of spherulites. The spherulites grew both in number and in size as time went on, but no macroscopic phase separation took place at this stage. We conclude from these observations that the A-point temperature for this solution can be located between 18 and 25°C.

7-3-2 Light Scattering Measurement

Solution LS was first kept at 28°C for about 10 min and the scattered intensity for incident light of the wavelengths 546 and 436 nm was measured. After this measurement, the solution was left standing in the xylene bath at the same temperature for one h to repeat the measurement again at 546 nm. Then, the

solution was transferred to an air bath thermostatted at 25°C, while the temperature of the xylene bath was adjusted to the next measuring temperature, e.g., 25°C. Similar series of measurements were repeated at different temperatures down to 12°C following the steps illustrated in Figure 7.1. For adjusting the bath temperature below 17°C, the solution was left at room temperature. Scattering intensity data are represented in terms of n^2/R_θ, where R_θ is the reduced excess scattering intensity at the scattering angle θ and n the refractive index of the solution.

It was found that R_θ remained almost unchanged within one h after the jump to any temperature between 12 and 28°C. Figure 7.2 shows the temperature dependence of the steady-state n^2/R_θ at 546 nm as a function of θ. No significant change in n^2/R_θ is seen at θ higher than 60°. The values below 60° are constant at temperatures higher than a certain critical temperature T_o but decrease gradually with decreasing temperature below T_o. It can be shown that T_o increases with lowering scattering angle, approaching about 20°C at 30°.

The T_o of 20°C at 30° is within the A-point range

detected by microscopic observation. Thus, the decrease in n^2/R_θ with decreasing temperature at low scattering angles may be attributed to the appearance of large scattering objects, probably to the growth of the spherulites first evolved at about 20°C. It must be noted, however, that the solution appeared

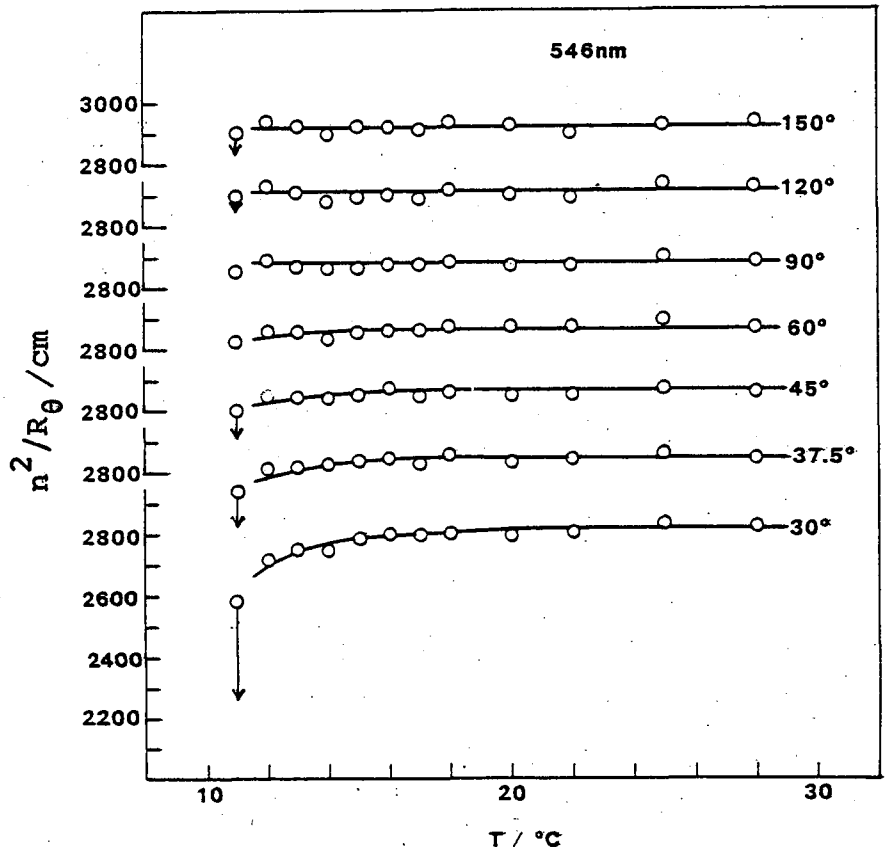

Figure 7.2 Temperature dependence of n^2/R_θ at 546 nm as a function of the indicated scattering angle θ.

clear even at 12°C at least for one h. This, along with the fact that the light scattering intensity at larger scattering angles remained almost unchanged, indicates that the amount of spherulites evolved was probably small.

R_θ was measured as a function of the time t elapsed after the temperature jump to 16°C. There was no significant change in the 30° intensity and optical anisotropy R_{Hv}/R_{Vv} (= $R_{90,Hv}/R_{90,Vv}$) untill t of 200 min. However, the solution became whitely glittering by 1150 min, with significant increases in R_{30} and R_{Hv}/R_{Vv}. A similar experiment was performed at 10°C, with the result shown in Figure 7.3. It can be seen that n^2/R_{30} decreases linearly with t, while the decrease is very gradual at other angles. The optical anisotropy increases steadily with time. This differs from the behavior observed between 12 and 28°C where the optical anisotropy was almost constant. At t > 500 min, the entire solution looked whitely glittering. The arrowheads in Figure 7.2 indicate that at 10°C, the n^2/R_θ values at 500 min are significantly lower than the 1 h values for lower scattering angles.

After the measurements at 10°C, the solution was

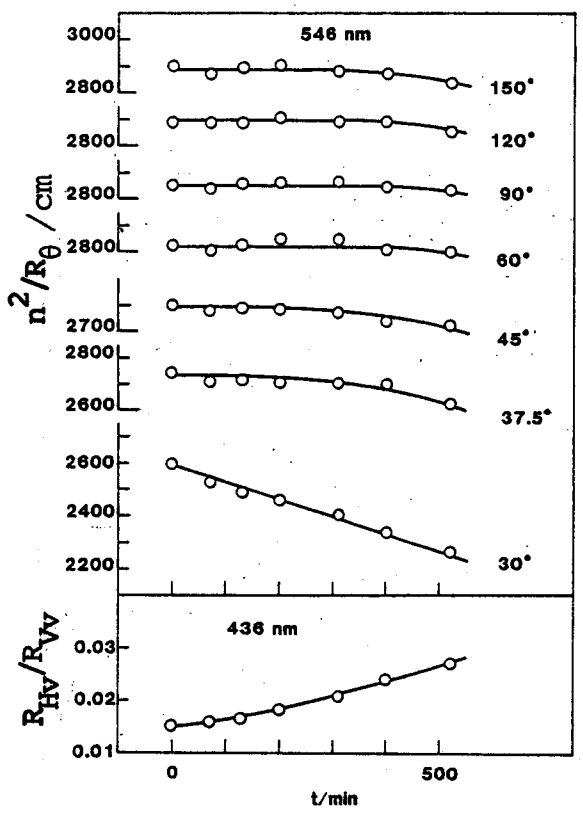

Figure 7.3 Variation in n^2/R_θ at 546 nm and R_{Hv}/R_{Vv} at 436 nm with the time t elapsed after the temperature jump to 10°C.

kept at 25°C for 11 days untill it became clear again. Light scattering measurement was made on this solution at 25°C. The scattering intensity agreed with those at the same temperature obtained before the temperature change. This indicates that the formation and

collapse of the liquid crystal phase are slow but reversible.

7-3-3 Optical Rotatory Dispersion

The optical rotation per unit length of the solution, $\theta(t)$ (deg cm^{-1}), was obtained as a function of the wavelength λ of light in vacuo at the temperatures indicated in Figure 7.1. It was found that $\theta(t)$ at 25.6, 21.0, and 18.0°C stayed almost constant within one h, although a small number of spherulites were found at 18°C.

At temperatures below 16.1°C, however, $\theta(t)$ changed rapidly with time. Figure 7.4 shows the change in $\theta(t)$ with t, where the arrows indicate the respective temperature jumps. On the jump from 18.3 to 14.7°C, $\theta(t)$ first increases rapidly and appears to approach a constant value. This remarkable increase in $\theta(t)$ is in contrast with the small change in light scattering intensity at 16°C mentioned above. Thus, we see that the formation and initial growth of the cholesteric phase affect only slightly the light scattering intensity but have a significant effect on the optical rotation.

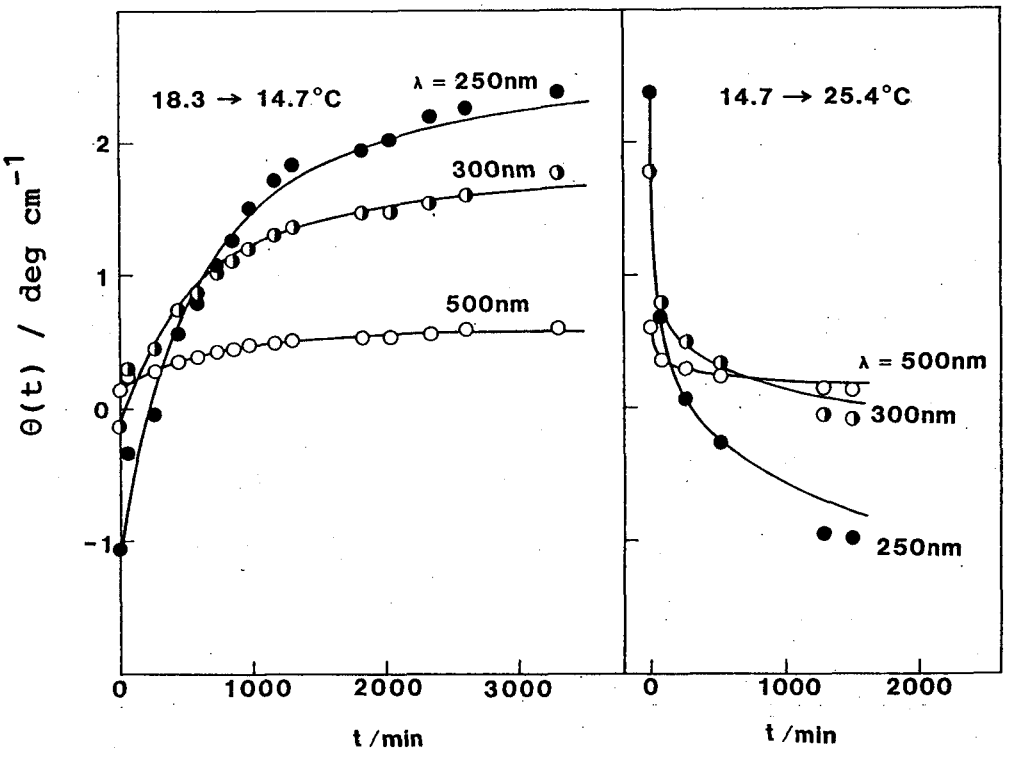

Figure 7.4 Variation in optical rotation $\theta(t)$ with the time t elapsed after the indicated temperature jumps. Filled circles, data at 250 nm; half-filled circles, at 300 nm; unfilled circles, at 500 nm. Solid curves, calculated by Eq. (7.1).

When the temperature was raised from 14.7 to 25.4°C, $\theta(t)$ first decreased rapidly and gradually reached a constant value which agreed with the value obtained at 25.6°C before the temperature change.

Similar results were obtained on different jumps.

This relatively slow relaxation process cannot be described by a single relaxation time. Indeed, it can be shown that the data in Figure 7.4 and similar ones for other conditions are represented by the following equation with two relaxation times, τ_1 and τ_2:

$$|\theta(t) - \theta(\infty)| = |\theta(0) - \theta(\infty)|[a_1 \exp(-t/\tau_1) + a_2 \exp(-t/\tau_2)] \qquad (7.1)$$

where $a_1 + a_2 = 1$. The solid curves in Figure 7.4 represent the $\theta(t)$ values calculated by this equation with appropriate values of τ_1 and τ_2; both a_1 and a_2 were nearly equal to 0.5. It was found that both τ_1 and τ_2 were independent of the starting temperature T_1. They are primarily determined by the final temperature T_2, as illustrated in Figure 7.5. Both τ_1 and τ_2 are seen to make sharp changes below 16°C, the temperature somewhat lower than T_A. These results indicate that there are two relaxation processes for the construction and destruction of the cholesteric phase.

We may suggest the following mechanism. When the temperature is raised, first the cholesteric structure

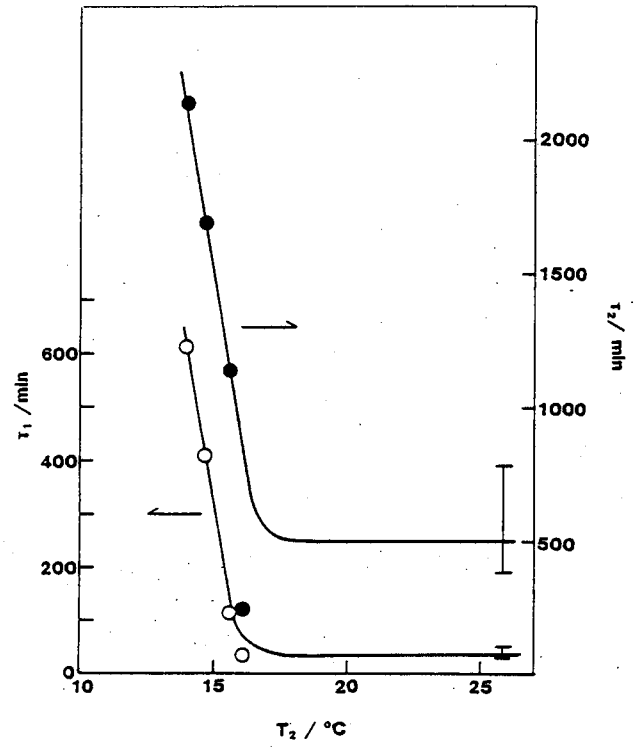

Figure 7.5 Temperature T_2 dependence of relaxation times τ_1 (unfilled circles) and τ_2 (filled circles).

relaxes microscopically in response to the new temperature; the entire system still keeps the original macroscopic structure at the initial stage. This may be a fast process corresponding to τ_1, because it involves no macroscopic rearrangement of the constituents. Then the system undergoes phase separation followed by macroscopic rearrangement of the separated phases to a

new equilibrium state. This slow process may be characterized by τ_2. A similar argument may be made when the temperature is lowered.

The experimental data so far presented indicate that aqueous schizophyllan at a temperature slightly below T_A is biphasic microscopically but that it is not in the equilibrium state but in a transient state someway between the isotropic state and completely phase separated state. This conclusion is at variance with the finding of Patel and DuPré on polypeptide solutions where they recognized some intermediate state; but our results indicate clearly the importance of the time effect, no description of which is seen in their paper. The two-state assumption may be compatible with ORD data shown in Figure 7.6, which are the values taken under the steady state condition at fixed temperatures where no further change in ORD curve was observed, i.e., $\theta(\infty)$.

It was found that there was no temperature change above 21°C; thus, the curve for 21°C is characteristic of the isotropic phase (see Figure 3.6). As the temperature is lowered, however, the optical rotation increases and the shape of the curve tends to resemble that of the cholesteric phase (see Figure 3.6). As

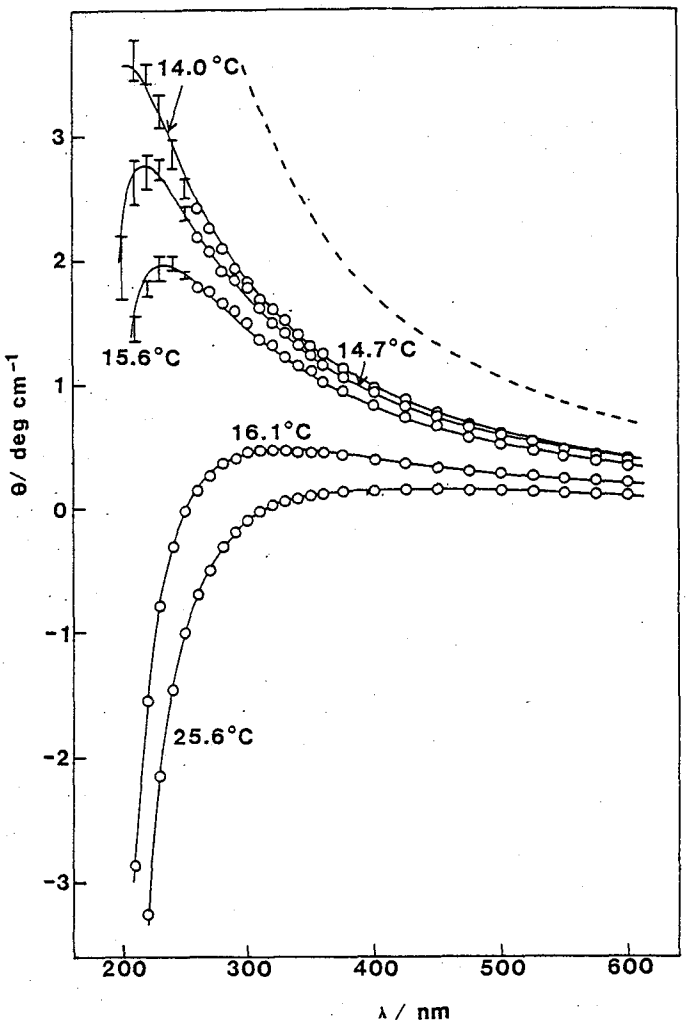

Figure 7.6 ORD curves at the indicated temperatures. Solid curves, calculated by Eq. (7.2) with the A and B values shown in Table 7.1; dashed line, calculated by Eq. (7.5) with $A_{LC} = 2.38 \times 10^{-9}$ deg cm (see the text).

Table 7.1

Values of the Numerical Constants A and B
in an Equation of the Moffitt-Yang Type (Eq. (7.2))
for an Aqueous Solution of Sample R23

T_2 / °C	A / 10^{-9} deg cm^3	-B / 10^{-19} deg cm
25.6	0.46_8	3.7_0
21.0	0.44_0	3.6_8
18.0	0.44_8	3.7_5
16.1	0.79_2	3.3_3
15.6	1.31	2.1_6
14.7	1.45	1.8_9
14.0	1.49	1.5_5

noted in Chapter 4, all these ORD curves can be represented by an equation of the Moffitt-Yang type:

$$\Theta = A/(\lambda^2 - \lambda_0{}^2) + B/(\lambda^2 - \lambda_0{}^2)^2 \qquad (7.2)$$

where λ_0 is a numerical constant. The values of the numerical constants A and B estimated are summarized in Table 7.1.

In conformity with the biphasic state mentioned above, we assume that Θ consists of two contributions,

θ_I and θ_{LC}, from the isotropic and cholesteric phases, respectively, and that θ is given by

$$\theta = \Phi\theta_I + (1 - \Phi)\theta_{LC} \qquad (7.3)$$

where Φ is the volume of the isotropic phase relative to that of the entire mixture. From the discussion given in Chapter 4, θ_I and θ_{LC} may be expressed as

$$\theta_I = A_I/(\lambda^2 - \lambda_0{}^2) + B_I/(\lambda^2 - \lambda_0{}^2)^2 \qquad (7.4)$$

$$\theta_{LC} = A_{LC}/(\lambda^2 - \lambda_0{}^2) \qquad (7.5)$$

Comparison of Eq. (7.2)-(7.5) leads to

$$A = \Phi A_I + (1 - \Phi)A_{LC} \qquad (7.6)$$

$$B = \Phi B_I \qquad (7.7)$$

The value of B_I was estimated to be -3.73×10^{-19} deg cm^3 from the data for 21°C. With this B_I value, Φ was calculated from B using Eq. (7.7). It was found that $1 - \Phi$ was relatively large, for example, $1 - \Phi$ =

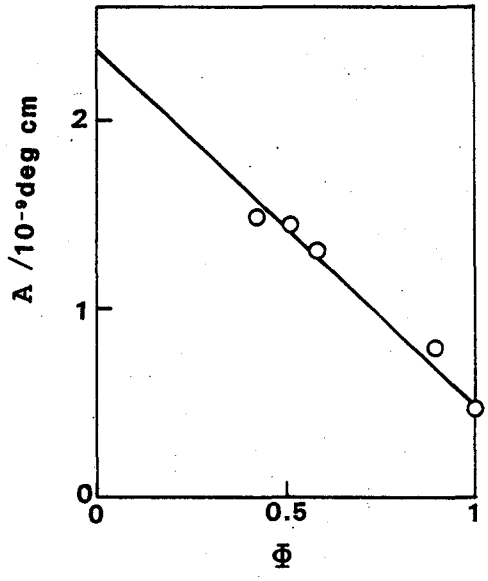

Figure 7.7 Plot of A vs. the volume Φ of the isotropic phase relative to the total solution volume.

0.58 at 14°C; the accuracy is only moderate because of the scatter of data points at lower wavelength.

Figure 7.7 shows a plot of A vs. Φ according to Eq. (7.6). Extrapolation to 1 - Φ = 1 gives 2.38×10^{-9} deg cm for A_{LC}. In Figure 7.6, the dashed line represents Θ_{LC} calculated with this A_{LC} value and the solid curves represent those calculated by Eq. (7.3) with the parameter values obtained. However, it is difficult to claim a high accuracy of the derived parameters, because the biphasic assumption for treating Θ may be of questionable validity at lower Φ range.

It can be seen that the optical rotation of the "cholesteric phase" at large wavelength is only five times as large as that of the isotropic phase. This appears to be in contradiction with the great difference in optical rotation between the isotropic phase and the cholesteric phase in planar texture, which amounts to a factor as large as 100 (see Chapter 4). Aside from the above inaccuracy, this is primarily due to the fact that the "cholesteric phase" discussed here is dispersed as spherulites in the isotropic phase, or vice versa, and refraction and reflection of light at the phase boundary might reduce the optical rotation. At the same time, however, we may not rule out the possibility that the "cholesteric phase" is not so perfectly ordered as the macroscopic one; in other words, it is still in an embryonic state with loose local ordering. More detailed information about this "cholesteric phase", e.g., its size, number, stability, etc., may be necessary to clarify what's happening on molecular level.

Chapter 8

SUMMARY AND CONCLUSIONS

This thesis has dealt with the formation of a liquid crystal in aqueous solutions of a rodlike polysaccharide schizophyllan, optical properties of the liquid crystal formed, and thermodynamic properties of concentrated schizophyllan solutions. The main results and conclusions obtained are as follows.

Formation of a Liquid Crystal

Aqueous solutions of schizophyllan were investigated by polarizing microscopy, laser light diffraction, and optical rotatory dispersion. The solutions were birefringent above a certain concentration, indicating that a liquid crystal was formed. It was concluded that this liquid crystal is cholesteric on the basis of the following observations.

(1) Examined between crossed polars, a liquid crystal solution showed fingerprint patterns with

textures characteristic of cholesteric mesophases.

(2) When confined in a thin cell, a liquid crystal solution formed a planar texture and showed a very large optical rotation.

The cholesteric pitch was of order of several μm, varying approximately with $w^{-1.9}$. The liquid crystal was optically negative, characterized by a layer birefringence between 0.0012 and 0.0018.

The results of laser diffraction and small angle X-ray scattering measurements showed that schizophyllan liquid crystals were less completely ordered than polypeptide liquid crystals.

Optical Properties

ORD measurement was made on thin films of liquid crystal solutions of schizophyllan. There was a remarkable difference in ORD curve between the isotropic and cholesteric phases; the specific rotation differed by a factor as large as 100 between the two. The ORD data at longer wavelength were consistent with the prediction by the de Vries theory for cholesterics, yielding the layer birefringence in agreement with those derived from retardation measurements.

The intrinsic birefringence of schizophyllan estimated from the layer birefringence was different from that of xanthan, and much smaller than that of crystalline cellulose. This difference was attributed to the difference in main-chain and side-chain conformations among these glucans.

Over a wider range in wavelength, the ORD data obtained for liquid crystal solutions were represented accurately by an equation of the Drude type, irrespective of the polymer molecular weight and concentration. It was concluded that such ORD behavior was not simply due to the chirality of the individual helices but characteristic of the liquid crystal.

Thermodynamic Properties

Light scattering and sedimentation equilibrium measurements were made on isotropic solutions of schizophyllan to obtain the partial derivative $[\partial\Delta\mu_0/\partial\phi]_{Mn}$ of the excess chemical potential $\Delta\mu_0$ of the solvent with respect to polymer volume fraction ϕ.

The results were analyzed by the theory of Flory and Abe[80] for rodlike polymers, yielding a non-vanishing interaction parameter χ, which was negative

and decreased with increasing ϕ. No appreciable dependence of χ on molecular weight was found. The results were compared with the theories of Onsager[72] and Cotter[77] for rodlike polymers. Both theories failed to explain the data quantitatively.

Sedimentation measurement was also made on biphasic mixtures consisting of isotropic and cholesteric phases at equilibrium to evaluate $[\partial\Delta\mu_0/\partial\phi]_{Mn}$ at the boundary between the two phases.

Integration of $[\partial\Delta\mu_0/\partial\phi]_{Mn}$ using these data and χ obtained provided $\Delta\mu_0$ as a function of ϕ. The result was compared with the Flory theory[78] for rodlike polymers with a non-vanishing χ. The agreement between theory and experiment was only qualitative for both $\Delta\mu_0$ and phase boundary concentrations.

Liquid Crystal - Isotropic Phase Equilibrium

The concentration dependence of the pitch P of the schizophyllan liquid crystal was investigated in biphasic and liquid crystal concentration regions at temperatures T between 5 and 80°C. It was found that P was a unique function of T and the weight fraction w of the polymer for a given sample.

The T - w phase diagram in the T range 5 - 80°C and in the w range 0 - 0.388 was determined for sample D40 by two new methods, which utilize the w dependence of P as a function of T and a sedimentation analysis of biphasic solutions, respectively. The phase diagram determined is characterized by a narrow, almost vertical biphasic region separating the isotropic phase from the cholesteric phase.

The molecular weight dependence of the phase boundary concentrations, the present data combined with Itou's data, was not in good agreement with theoretical predictions for athermal solutions of rodlike polymers. The discrepancy between experiment and theory cannot be accounted for by the polydispersity in molecular weight, flexibility of the triple helix, and the uncertainties associated with the axial ratio and volume fraction of the polymer. An attempt to correct the Flory theory for the non-athermality of the system failed to solve the discrepancy. The need for a further theoretical study is indicated.

Optical Properties near the A-point

When a solution of the concentration slightly higher than the A-point value was cooled in crossing the biphasic boundary, both optical rotation and intensity of scattered light began to increase at certain critical temperatures. This increase, more sensitively reflected on optical rotation than on light scattering, was due to the appearance of large anisotropic bodies, presumably spherulites of a cholesteric phase, whose number and size grew slowly. Although no macroscopic phase separation was found under the conditions tested, this differs from the pretransitional phenomenon discussed by Patel and DuPré in regard to polypeptide solutions, but involves a process eventually leading to a macroscopic phase separation.

Future Prospect

The cholesteric mesophase of aqueous schizophyllan shows an extraordinary optical rotation and a cholesteric pitch of a few microns. Both change abruptly with temperature at about $8^{\circ}C$, indicating a structural transition to occur in microscopic

as well as macroscopic scales. Since this transition accompanies a negative heat of transition, a calorimetric study of this transition is inviting.

The present study of phase equilibrium is concerned with systems containing essentially monodisperse polymers. A ternary system of two monodisperse polymers in a single solvent is of interest because of its characteristic phase behavior, as observed recently by Itou and Teramoto.[124,125]

The phase equilibrium data discussed here are concerned with schizophyllan samples of rodlike shape. It may be inviting to see what happens to the phase behavior of somewhat flexible polymers. Both theoretical and experimental studies on this problem are still on a premature stage.[126-128]

REFERENCES

1. F. Reinitzer, Beiträge zur Kenntniss des Cholestrerine, Monatschefte für Chemie, 9, 421 (1888).
2. O. Lehmann, Uber fliessende Krystalle, Z. Physik. Chem., 4, 462 (1889).
3. G. W. Gray and P. A. Winsor, in Liquid Crystals and Plastic Crystals, Vol. 1, G. W. Gray and P. A. Winsor Eds., Wiley, New York, 1974.
4. G. Friedel, Les Etats Mesomorphes de la Matiere, Ann. Physique, 18, 273 (1922).
5. W. Kast, Landolt-Börnstein Tables, Vol. 2, 6th Ed., p. 266, Springer-Verlag (1969).
6. D. Demus and H. Demus, Flussige Kristalle in Tabellen, VEB Deutscher Verlag für Grundstaffindustrie, Leipzig (1973).
7. M. Schadt and W. Helfrich, Voltage-Dependent Optical Activity of a Twisted Nematic Liquid Crystal, Appl. Phys. Lett., 18, 127 (1971).
8. I. Nakata and F. Hori, in Ekisho no Seiho to Oyo, Saiwai 2nd Ed., 1979, p 130.
9. G. W. Gray, A. Sussman, and J. P. Schroeder, in Liquid Crystals and Plastic Crystals, Vol. 1, G. W. Gray and P. W. Winsor, Eds., Wiley, New York, 1974, Chap. 7.

10. G. T. Stewart, Liquid Crystals of Lipid in Normal and Atheromatous Tissue, Nature, 183, 873 (1959).

11. G. T. Stewart, Liquid Crystals in Biological Systems, Mol. Cryst., 1, 563 (1966).

12. G. T. Stewart, in Liquid Crystals and Plastic Crystals, Vol. 1, G. W. Gray and P. W. Winsor, Eds., Wiley, New York, 1974, Chap. 6.1.

13. C. Robinson, Liquid-Crystalline Structure in Solutions of a Polypeptide, Trans. Faraday Soc., 52, 571 (1956).

14. C. Robinson, J. C. Ward, and R. B. Beevers, Liquid Crystalline Structure in Polypeptide Solutions. Part 2., Discuss. Faraday Soc., 25, 29 (1958).

15. C. Robinson, Liquid-Crystalline Structures in Polypeptide Solutions, Tetrahedron, 13, 219 (1961).

16. C. Robinson, The Cholesteric Phase in Polypeptide Solutions and Biological Structures, Mol. Cryst., 1, 467 (1966).

17. H. Freudlich, Colloidal Structures in Biology, J. Phys. Chem., 41, 1151 (1937).

18. J. D. Bernal and I. Fankuchen, X-Ray and Crystallographic Studies of Plant Virus Preparations, J. Gen. Physiol., 25, 111 (1941).

19. G. Oster, Two-Phase Formation in Solutions of Tabacco-Mossaic Virus and The Problem of Long-Range Forces, J. Gen. Physiol., 33, 445 (1950).

20. Y. Ooshima, H. Nakamura, K. Okano, Study of Liquid Crystalline Structure of Bacteriophage fd., Polym. Prep. Japan, 31, 2173 (1982).

21. W. G. Miller, C. C. Wu, E. L. Wee. G. L. Santee, J. H. Rai, and K. G. Goebel, Thermodynamics and Dynamics of Polypeptide Liquid Crystals, Pure Appl. Chem., 38, 37 (1974 b).

22. E. Iizuka, Y. Kondo, and T. Ukai, The Liquid Crystals of Sodium Salt of Poly (glutamic acid) in Aqueous Solution, Polym. J., 9, 135 (1977).

23. W. G. Miller, Stiff Chain Polymer Lyotropic Liquid Crystals, Ann. Rev. Phys. Chem., 29, 519 (1978).

24. E. L. Wee and W. G. Miller, Liquid Crystal-Isotropic Phase Equilibria in the System Poly-γ-benzyl-α,L-glutamate - Dimethylformamide, J. Phys. Chem., 75, 1446 (1971).

25. K. Kubo and K. Ogino, Thermodynamic Properties of Concentrated Poly (γ-benzyl-L-glutamate) Solutions, Polymer, 16, 629 (1975).

26. K. Kubo and K. Ogino, Comparison of Osmotic Pressures for the Poly (γ-benzyl-L-glutamate) Solutions with the Theories for a System of Hard Spherocylinders, Mol. Cryst. Liq. Cryst., 53, 207 (1979).

27. K. Kubo, Thermodynamic Properties of Poly (γ-benzyl-L-glutamate) Solutions over Entire Concentration

Range, Mol. Cryst. Liq. Cryst., 74, 71 (1981).

28. P. S. Russo and W. G. Miller, Coexistence of Liquid Crystalline Phases in Poly(γ-benzyl-α,L-glutamate) - Dimethylformamide, Macromolecules, 16, 1690 (1983).

29. P. J. Flory, Phase Changes in Proteins and Polypeptides, J. Polym. Sci., XLIX, 105 (1961).

30. S. Funada, F. Shibuya, K. Obara, and A. Teramoto, (to be published).

31. N. Mori, M. Yoshikawa, Y. Uematsu, and I. Uematsu, Liquid Crystalline Structures of Poly-γ-benzyl-L-glutamate (1) Effect of Concentration on Twisting Power, Rep. Prog. Polym. Jap., 17, 621 (1974).

32. H. Toriumi, Y. Kussumi, I. Uematsu, and Y. Uematsu, Thermally Induced Inversion of the Cholesteric Sense in Lyotropic Polypeptide Liquid Crystals, Polym. J., 11, 863 (1979).

33. H. Toriumi, S. Minakuchi, Y. Uematsu, and I. Uematsu, Helical Twisting Power of Poly(γ-benzyl-L-glutamate) Liquid Crystals in Mixed Solvents, Polym. J., 12, 431 (1980).

34. D. L. Patel and D. B. DuPré, Optical Rotatory Behavior of Polypeptide Solutions in the Liquid Crystal and Pretransition Regions, J. Chem. Phys., 72, 2515 (1980).

35. C. G. Sridhar, W. A. Hines, and E. T. Samulski, Polypeptide Liquid Crystals: Magnetic Susceptibility, Twist Elastic Constant, Rotational Viscosity Coefficient, and Poly-γ-benzyl-L-glutamate Sidechian Conformation, J. Chem. Phys., 61, 947, (1974).

36. R. W. Duke and D. B. DuPré, Twist Elastic Constant of a Cholesteric Polypeptide Liquid Crystal, J. Chem. Phys., 60, 2759 (1974).

37. D. B. DuPré and R. W. Duke, Temperature, Concentration, and Molecular Weight Dependence of the Twist Elastic Constant of Cholesteric Poly-γ-benzyl-L-glutamate, J. Chem. Phys., 63, 143 (1975).

38. D. L. Patel and D. B. DuPré, Spherulite Morphology in Liquid Crystals of Polybenzylglutamates. Optical Rotatory Power and Effect of Magnetic Field, J. Polym. Sci., Polym. Phys. Ed., 18, 1599 (1980).

39. E. Iizuka, The Effects of Magnetic Fields on the Structure of Cholesteric Liquid Crystals of Polypeptides, Polym. J., 4, 401 (1973).

40. J. Hermans, Jr., The Viscosity of Concentrated Solutions of Rigid Rodlike Molecules (Poly-γ-Benzyl-L-Glutamate in m-Cresol), J. Coll. Sci., 17, 638 (1962).

41. T. Asada, H. Muramatsu, R. Watanabe, and S. Onogi, Rheooptical Studies of Racemic Poly(γ-benzyl glutamate Liquid Crystals, Macromolecules, 13, 867 (1980).

42. W. B. Black, High-Modulus Wholly Aromatic Fibers: Introduction to the Symposium and Historical Perspective., J. Macromol. Sci. Chem., A7, 3 (1974).

43. J. Preston, W. B. Black, and W. L. Hofferbest, High-Modulus Wholly Aromatic Fibers II. Partially Ordered Polyamide-Hydrazides, J. Macromol. Sci. Chem., A7, 67 (1973).

44. W. B. Black, J. Preston, H. S. Morgan, G. Raumann, and M. R. Lilyquist, Some Physical and Mechanical Properties of Some High-Modulus Fibers Prepared from All-Para Aromatic Plyamide-Hydrazides, J. Macromol. Sci. Chem., A7, 137 (1973).

45. S. P. Papkov, V. G. Kulichikhin, V. D. Kalmykova, and A. Y. Malkin, Rheological Properties of Anisotropic Poly(para-Benzamide) Solutions, J. Polym. Sci., Polym. Phys. Ed., 12, 1753 (1974).

46. P. W. Morgan, Synthesis and Properties of Aromatic and Extended Chain Polyamides, Macromolecules, 10, 1381 (1977); T. I. Bair, P. W. Morgan, and F. L. Killian, Poly(1,4-Phenyleneterephthalamides). Polymerization and Novel Liquid-Crystalline Solutions., Macromolecules, 10, 1396 (1977).

47. S. L. Kwolek, P. W. Morgan, J. R. Schaefgen, and L. W. Gulrich, Synthesis, Anisotropic Solutions, and Fibers of Poly(1,4-benzamide), Macromolecules, 10, 1390 (1977).

48. J. L. White and J. F. Fellers, Macromolecular Liquid Crystals and Their Applications to High-Modulus and Tensile-Strength Fibers, J. Appl. Polym. Sci., Appl. Polym. Symp., 33, 137 (1978).

49. W. J. Jackson and H. F. Kubfuss, Liquid Crystal Polymre. 1. Preparation and Properties of p-Hydroxybenzoic Acid Copolyesters, J. Polym. Sci., Polym. Chem. Ed., 14, 2043 (1976).

50. G. C. Berry, Thermal-Mechanical Studies on a Heterocyclic Polymer (BBB). I. Tensile Creep and Recovery, J. Polym. Sci., Polym. Phys. Ed., 14, 451 (1976).

51. G. C. Berry, Thermal-Mechanical Studies on a Heterocyclic Polymer (BBB). II. Dynamic Mechanical Studies at Elevated Temperatures, J. Poly. Sci., Polym. Phys. Ed., 14, 1721 (1976).

52. S. M. Aharoni and E. K. Walch, Polyisocyanates and Their Liquid-Crystal Behavior, Rigid Backbone Polymers. 2., Macromolecules, 12, 94 (1979).

53. S. M. Aharoni and E. K. Walch, Rigid Backbone Polymers. 4. Solution Properties of Two Lyotropic Mesomorphic Poly(isocyanate), Macromolecules,

12, 271 (1979).

54. C. Balbi, E. Bianchi, A. Ciferri, A. Tealdi, and W. R. Krigbaum, Equilibria of Extended-Chain Polymers Exhibiting Crystalline and Liquid-Crystalline Phases, J. Polym. Sci., Polym. Phys. Ed., 18, 2037 (1980).

55. J. Bheda, J. F. Fellers, and J. L. White, Phase Behavior and Structure of Liquid Crystalline Solutions of Cellulose Derivatives, Colloid & Polymer Sci., 258, 1335 (1980).

56. S. M. Aharoni, Rigid Backbone Polymers. XXV. Solvent Effects in Phase Behavior of Solutions of Cellulose Derivatives., J. Macromol. Sci.-Phys., B21(2), 287 (1982).

57. D. L. Patel and R. D. Gilbert, Lyotropic Mesomorphic Formation of Cellulose in Trifluoroacetic Acid-Chlorinated Alkane Solvent Mixtures at Room Temperature, J. Polym. Sci., Polym. Phys. Ed., 19, 1231 (1981).

58. K. Shimamura, J. L. White, and J. F. Fellers, Hydroxy-Propylcellulose, a Thermotropic Liquid Crystal: Characteristics and Structure Development in Continuous Extrusion and Melt Spinning, J. Appl. Polym. Sci., 26, 2165 (1981).

59. R. S. Werbowyj and P. G. Gray, Liquid Crystalline Structure in Aqueous Hydroxy-Propyl Cellulose

Solutions, Mol. Cryst. Liq. Cryst., 34, 97 (1976).

60. R. S. Werbowyj and D. G. Gray, Ordered Phase Formation in Concentrated Hydroxypropyl Cellulose Solutions, Macromolecules, 13, 69 (1980).

61. T. Tsutsui and R. Tanaka, Formation of Cholesteric Mesophase in Some Hydroxypropyl Cellulose-Organic Solvent Systems, Polym. J., 12, 473 (1980).

62. G. Conio, E. Bianchi, A. Ciferri, A. Tealdi, and M. A. Aden, Mesophase Formation and Chain Rigidity in Cellulose and Derivatives. 1. (Hydroxypropyl) Cellulose in Dimethylacetamide, Macromolecules, 16, 1264 (1983).

63. T. Asada, K. Toda, and S. Onogi, Deformation and Structural Re-formation of Lyotropic Cholesteric Liquid Crystal of Hydroxypropyl Cellulose + Water System, Mol. Cryst. Liq. Cryst., 68, 231 (1981).

64. So-Lan Teng, A. Valente, and D. G. Gray, Cholesteric Liquid Crystalline Phases Based on (Acetoxypropyl) Cellulose, Macromolecules, 14, 715 (1981).

65. D. L. Patel and R. D. Gilbert, Mesomorphic Solutions of Cellulose Triacetate in Halogenated Organic Acids and Mixtures of Trifluoroacetic acid and Dichloromethane, J. Polym. Sce., Polym. Phys. Ed., 19, 1449 (1981).

66. S. N. Bhadani and D. G. Gray, Liquid Crystal Formation from the Benzoic Acid Ester of Hydroxypropylcellulose, Makromol. Chem., Rapid Commun., 3, 449 (1982).

67. G. Maret, M. Milas, and M. Rinaudo, Cholesteric Order in Aqueous Solutions of the Polysaccharide Xanthan, Polym. Bull., 4, 291 (1981).

68. H. Finkelmann, in Polymer Liquid Crystals, A. Ciferri, W. R. Krigbaum, and R. B. Meyer, Eds., Academic Press, London, 1982, p 35.

69. W. R. Krigbaum, in Polymer Liquid Crystals, A. Ciferri, W. R. Krigbaum, and R. B. Meyer, Eds., Academic Press, London, 1982, p 275.

70. T. Asada, in Polymer Liquid Crystals, A. Ciferri, W. R. Krigbaum, and R. B. Meyer, Eds., Academic Press, London, 1982, p 248.

71. S. L. Kwolek, Aromatic Polysufonamides, U.S. Patent, 3600350 (August 17, 1971); P. W. Morgan and S. L. Kwolek, Polyamides from Phenylenediamides and Aliphatic Diacids, U.S. Patent, 3819587 (June 25, 1975).

72. L. Onsager, The Effects of Shape on the Interaction of Colloidal Particles, Ann. N. Y. Acad. Sci., 51, 627 (1947).

73. A. Ishihara, Theory of Anisotropic Colloidal Solutions, J. Chem. Phys., 19, 1142 (1951).

74. M. A. Cotter and D. E. Martire, Statistical Mechanics of Rodlike Particles. I. A Scaled Particle Treatment of a Fluid of Perfectly Aligned Rigid Cylinders, J. Chem. Phys., 52, 1902 (1970); Statistical Mechanics of Rodlike Particles. II. A Scaled Particle Investigation of the Aligned-Isotropic Transition in a Fluid of Rigid Spherocylinders, J. Chem. Phys., 52, 1909 (1970); Statistical Mechanics of Rodlike Particles. III. A Fluid of Rigid Spherocylinders with Restricted Orientational Freedom, J. Chem. Phys., 53, 1902 (1970).

75. G. Lasher, Nematic Ordering of Hard Rods Derived from a Scaled Particle Treatment, J. Chem. Phys., 53, 4141 (1970).

76. M. A. Cotter, Hard-Rod Fluid: Scaled Particle Theory Revisited, Phys Rev., A10, 629 (1974).

77. M. A. Cotter, Hard Spherocylinders in an Anisotropic Mean Field: A Simple Model for a Nematic Liquid Crystal, J. Chem. Phys., 66, 1098 (1977).

78. P. J. Flory, Phase Equilibria in Solutions of Rod-like Particles, Proc. Royal Soc., Ser. A. 234, 73 (1956).

79. S. Itou, N. Nishioka, T. Norisuye, and A. Teramoto, Rodlike Nature of α-Helical Polypeptides in Solution, Macromolecules, 14, 904 (1981).

80. P. J. Flory and A. Abe, Statistical Thermodynamics of Mixtures of Rodlike Particles. 1. Theory for Polydisperse Systems, Macromolecules, 11, 1119 (1974).

81. P. J. Flory and R. S. Frost, Statistical Thermodynamics of Mixtures of Rodlike Particles. 3. The Most Probable Distribution, Macromolecules, 11, 1126 (1974).

82. R. S. Frost and P. J. Flory, Statistical Thermodynamics of Mixtures of Rodlike Particles. 4. The Poisson Distribution, Macromolecules. 11, 1134 (1974).

83. J. K. Moscicki and G. Williams, Concentrated Solutions of Polydisperse Rodlike Polymers in the Isotropic and Lyotropic Liquid-Crystalline Phases. I. The Effects of Molecular Length Distribution on Phase Behavior, J. Polym. Sci., Polym. Phys. Ed., 21, 197 (1983).

84. T. Norisuye, T. Yanaki, and H. Fujita, Triple Helix of a Schizophyllum Commune Polysaccharide in Aqueous Solution, J. Polym. Sci., Polym. Phys. Ed., 18, 547 (1980).

85. T. Yanaki, T. Norisuye, and H. Fujita, Triple Helix of Schizophyllum Commune Polysaccharide in Dilute Solution. 3. Hydrodynamic Properties in Water, Macromolecules, 13, 1462 (1980).

86. Y. Kashiwagi, T. Norisuye, and H. Fujita, Triple Helix of Schizophyllum Commune Polysaccharide in Dilute Solution. 4. Light Scattering and Viscosity in Dilute Aqueous Sodium Hydroxide, Macromolecules, 14, 1220 (1981).

87. For w = 1, n and v should be about 1.56 and 0.64, values expected for sugar[91] or cellulose.[92]

88. Gj. Dezelic and J. Vavara, Angular Dependence of the Light Scattering in Pure Liquids, Croat. Chem. Acta., 38, 35 (1976).

89. D. N. Rubingh and H. Yu, Characterization of Stiff Chain Macromolecules. Poly (n-hexyl isocyanate) in n-Hexane, Macromolecules, 9, 681 (1976).

90. R. S. Stein and J. J. Keane, The Scattering of Light from Thin Polymer Films, J. Polym. Sci., 17, 21 (1955).

91. International Critical Tables, Vol. III, 1928, p 45; Vol. VII, 1930, p 30.

92. E. Treiber, in Polymer Handbook, J. Brandrup and E. H. Immergut, Ed., Wiley-Interscience Publ., 1975, V-87.

93. P. G. de Gennes, "The Physics of Liquid Crystals," Chap. 6, Clarendon Press, Oxford, 1974.

94. S. Chandrasekhar, "Liquid Crystals," Chap. 4, Cambridge University Press, Cambridge, 1977.

95. M. Kleman, in Liquid Crystals and Plastic Crystals, G. W. Gray and P. A. Winsor, Ed., Vol. 1, 76, Wiley, New York, 1974.

96. M. Kleman and J. Friedel, Lignes de Dislocation dans les Cholesteriques, J. de Physique, 30c, 4 (1969).

97. T. Sato, T. Norisuye, and H. Fujita, Double-Stranded Helix of Xanthan in Dilute Solution: Evidence from Light Scattering, Polym. J., 16, 341 (1984).

98. H. de Vries, Rotatory Power and Other Optical Properties of Certain Liquid Crystals, Acta Cryst., 4, 219 (1951).

99. D. B. DuPrè and F.-M. Lin, Measurement of the Anisotropic Refractive Indices of Polybenzylglutamate Liquid Crystals. Molecular Factors and Despersion, Mol. Cryst. Liq. Cryst., 75, 217 (1981).

100. G. Magret et al.[67] gave 0.025 cm^3 g^{-1} for $|\Delta n|/c$, but we found a negative Δn for the liquid crystal of aqueous xanthan.

101. P. H. Hermans, "Physics and Chemistry of Cellulose Fibers," Elsevier Publ., Amsterdam, 1948, p 23.

102. K. H. Gardner and J. Blackwell, The Structure of Native Cellulose, Biopolymers, 13, 1975 (1974).

103. To better approximation, the right-hand side of Eq. (4.4) should be multiplied by a factor $(n_{//}^2 + 2)(n_{\perp}^2 + 2)(n_{\alpha} + n_{\gamma})/[(n_{\alpha}^2 + 2)(n_{\gamma}^2 + 2)(n_{//} + n_{\perp})]$ which increases very gradually with increasing ϕ and approaches unity as ϕ tends to unity. In the ϕ range of interest, it is close to 0.9.

104. M. Doi, Molecular Dynamics and Rheological Properties of Concentrated Solutions of Rodlike Polymers in Isotropic and Liquid Crystalline Phases, J. Polym. Sci., Polym. Phys. Ed., 19, 229 (1981).

105. G. Holzwarth, Molecular Weight of Xanthan Polysaccharide, Carbohydr. Res., 66, 173 (1982).

106. G. Paradossi and D. A. Brant, Light Scattering Study of a Series of Xanthan Fractions in Aqueous Solution, Macromolecules, 15, 874 (1982).

107. Y. Takahashi, private communication.

108. K. Okuyama, S. Arnott, R. Moorhouse, M. D. Walkinshow, E. D. T. Atkins, and CH. Wolf-Ullish, in Fiber Diffraction Methods, A. D. French, K. H. Gardner, Ed., American Chemical Society, Washington D. C., 1980, Chapter 26, ACS Sym. Ser., No 141, p 411.

109. B. H. Zimm, Application of the Methods of Molecular Distribution to Solutions of Large Molecules, J. Chem. Phys., 14, 164 (1946).

110. Th. G. Scholte, Determination of Thermodynamic Parameters of Polymer-Solvent Systems from Sedimentation-Diffusion Equilibrium in the Ultracentrifuge, J. Polym. Sci., A-2, 8, 841 (1970).

111. Th. G. Scholte, Determination of Thermodynamic Parameters of Polymer-Solvent Systems by Light Scattering, Europ. Polym. J., 6, 1063 (1970).

112. Z_x (x = LS, SED) refers to a given amount of the solvent. Therefore, M_0 is the molecular weight of an "equivalent solvent" corresponding to this amount and does not necessarily equal that of water.

113. This value of M_w/M_n was obtained from the observed M_z/M_w by assuming that the molecular weight distribution of each sample was of the Schulz type.

114. J. P. Straley, The Gas of Long Rods as a Model for Lyotropic Liquid Crystals, Mol. Cryst. Liq. Cryst., 22, 333 (1973).

115. H. Reiss, H. L. Frisch, and J. L. Lebowitz, Statistical Mechanics of Rigid Spheres, J. Chem. Phys., 31, 369 (1959).

116. T. Itou, M. S. Thesis Osaka University (1984).

117. T. Itou, K. Van, and A. Teramoto, Molecular Weight Dependence of the Isotropic-Cholesteric

Phase Diagram for the System Schizophyllan + Water, J. Appl. Polym. Sci., in press.

118. J. K. Moscichi and G. Williams, The Effect of a Gaussian Distribution of Chain-Lengths on the Phase-Behaviour of Model System of Rod-like Macromolecules in Solution, Polymer, 23, 558 (1982).

119. G. Conio, E. Bianchi, A. Ciferri, A. Tealdi, and W. R. Krigbaum, Composition and Fractionation within Conjugated Isotropic and Anisotropic Phases of Lyotropic Liquid Crystals, J. Polym. Sci., Polym. Phys. Ed., 18, 2037 (1980).

120. T. Yanaki, T. Norisuye, and A. Teramoto, Cholesteric Mesophase in Aqueous Solutions of a Triple Helical Polysaccharide Scleroglucan in Dilute Solution, Polym. J., 16, 165 (1984).

121. T. Yanaki and T. Norisuye, unpublished data.

122. T. Yanaki and T. Norisuye, Triple Helix and Random Coil of Scleroglucan in Dilute Solution, Polym. J., 15, 389 (1983).

123. P. J. Flory and G. Ronca, Theory of System of Rodlike Particles 1. Athermal Systems, Mol. Cryst. Liq. Cryst., 54, 289 (1979).

124. T. Itou and A. Teramoto, Triphase Equilibrium in Aqueous Soltions of a Rodlike Polysaccharide Schizophyllan, Macromolecules, 17, 1419 (1984).

125. T. Itou and A. Teramoto, Multi-Phase Equilibrium in Aqueous Solutions of a Triple-Helical Polysaccharide Schizophyllan, Polym. J. (in press)

126. G. Conio, E. Bianchi, A. Ciferri, and W. R. Krigbaum, Mesophase Formation by Semirigid Polymers: Poly(n-hexylisocyanate) in Dichloromethane and Toluene, Macromolecules, 17, 856 (1984).

127. R. R. Matheson, Jr., and P. J. Flory, Statistical Thermodynamics of Mixtures of Semirigid Macromolecules: Chains with Rodlike Sequences at Fixed Locations, Macromolecules, 14, 954 (1981).

127. A. R. Khokhlov and A. N. Semenov, Liquid-Crystalline Ordering in the Solution of Partially Flexible Macromolecules, Physica, 112A, 605 (1982).

LIST OF PUBLICATIONS

(1) K. Van, T. Norisuye, and A. Teramoto, Liquid Crystal Formation in Aqueous Solutions of a Polysaccharide Schizophyllan, Mol. Cryst. Liq. Cryst., 78, 123 (1981).

(2) K. Van and A. Teramoto, Isotropic-Liquid Crystal Phase Equilibrium in Aqueous Solutions of a Triple-Helical Polysaccharide Schizophyllan, Polym. J., 14, 999 (1982).

(3) K. Van, T. Asakawa, and A. Teramoto, Optical Rotatory Dispersion of Liquid Crystal Solutions of a Triple-Helical Polysaccharide Schizophyllan, Polym. J., 16, 61 (1984).

(4) K. Van and A. Teramoto, Light Scattering and Sedimentation Equilibrium Study on Concentrated Solutions of a Rodlike Polysaccharide Schizophyllan, Polym. J., in press.

(5) T. Itou, K. Van, and A. Teramoto, Molecular Weight Dependence of the Isotropic-Cholesteric Phase Diagram for the System Schizophyllan + Water, J. Appl. Polym. Sci., in press.